UNIVERSITY OF GENOA

POLYTECHNIC SCHOOL

DOCTOR OF PHILOSOPHY
IN CHEMICAL, MATERIALS AND PROCESS ENGINEERING
XXXVI CYCLE

# *KRAFT LIGNIN AS A FEEDSTOCK TO PRODUCE BIOFUELS AND RENEWABLE CHEMICALS*

CANDIDATE:

MATTEO BORELLA

SUPERVISORS:

GABRIELLA GARBARINO & GUIDO BUSCA

May, 2024

**Ph.D. Program in Civil, Chemical and Environmental Engineering**

**Curriculum in Chemical, Materials and Process Engineering**

Department of Civil, Chemical and Environmental Engineering

Polytechnic School, University of Genoa, Italy.

# *Kraft Lignin As A Feedstock To Produce Biofuels And Renewable Chemicals*

Matteo Borella

## *Abstract*

The utilization of biomass, obtained from organic matter like plants and wastes, is crucial in the pursuit of sustainable and renewable resources. Its importance lies in its capability to serve as a renewable energy source, leading to a diversified energy mix, while also mitigating greenhouse gas emissions. By making use of biomass, the principles of the circular economy are addressed to reducing waste and endorsing the growth of bio-based materials. Advancements in biomass utilization have led to innovative applications, revealing its potential as an energy source and a catalyst for sustainable practices. It serves as a cornerstone for the transition towards a more eco-friendly and resilient future.

Lignocellulosic biomass, particularly lignin, shows great potential for replacing fossil fuels. Despite this, its utilization remains at an early stage due to difficulties in its treatment. Nonetheless, it is imperative to develop new methodologies for exploiting lignin's potential to obtain chemicals and fuels from renewable materials, considering the limited nature of fossil resources. Kraft lignin is the most produced technical lignin in the market and its sustainable and valuable utilization holds significant implications for industry. This thesis focuses on the valorization of Kraft lignin and aims to overcome the challenges associated with its utilization.

The sulfur content of Kraft Lignin has posed a challenging issue requiring the implementation of various strategies. These have included enhancing our understanding of the production mechanism of sulfur compounds and their evolution during the pyrolysis process. We attempted to establish pathways for enhancing the value of the oil, through combining pyrolysis steps and catalytic studies. Throughout the process, we always considered the undesirable effects of sulfur on both biofuel applications and chemical production. The thesis has been developed with the previous considerations in mind and divided into different chapters as follows:

- Chapter 1: Literature Review

A literature overview is provided looking at lignocellulosic biomass composition and characteristics and focusing on lignin structure and features. Then, different extraction procedures for the separation of lignin are briefly summarized, giving more attention to the Kraft Lignoboost process, where the Kraft Lignin used in this thesis derives from. The last part of the chapter is focused on different valorization pathways for lignin, and bio-oil upgrade. Several applications for lignin derived products have been also discussed.

- Chapter 2: Materials and methods

In this chapter, the materials and all the experimental techniques used in the thesis have been reported. The fundamentals all these techniques are based on have been briefly introduced and their utilization in the valorization of Kraft lignin products has been proposed. The characterization of pyrolysis products has been performed through Fourier-Transform Infrared Spectroscopy for the qualitative characterization of unknown liquid, gaseous, and solid samples. Scanning electron microscopy was used to investigate morphology of the surfaces and the elemental composition of solid residues. Gas chromatography coupled with mass spectrometry (GC-MS) or 2D-GC provided a quali-quantitative analysis of the liquids and gas compositions. NMR gives insights on the structure and chemical bond distributions of raw materials and products obtained from pyrolysis.

- Chapter 3: A study of pyrolysis products of Kraft Lignin

A first overall study on Kraft lignin valorization through pyrolysis has been reported here. Pyrolysis yield under different operative conditions has been discussed. Several features have been investigated focusing on bio-oil production and composition. The main target was to obtain phenolic compounds from liquid aromatic pools through liquid-liquid extractions. However, gas and solid residues have been widely characterized as well, to have a complete representation of the different pyrolysis obtainable products in different reaction conditions.

- Chapter 4: Conversion of lignin into chemical intermediates

Static and dynamic temperature conditions have been investigated looking also at the impact of different lignin loading on the pyrolysis process. A study on the evolution of sulfur compounds exploring a wider range of temperatures have been performed, focusing on $H_2S$, methanethiol, and carbonyl sulfide.

- Chapter 5: Upgrading of Kraft lignin pyrolysis products: managing sulfur impurities.

The pyrolysis setup was implemented by adding an adsorption column to perform a purification of pyrolysis sulfuric gases. Four commercial activated carbons have been used for the selective adsorption of the main sulfur-containing compound in the gas phase. A study on sulfur distribution in pyrolysis products has been also performed looking at different solid residues via SEM.

- Chapter 6: Two-stage co-pyrolysis of Kraft lignin and palm oil mixture to biofuels

A co-pyrolysis study has been carried out with the aim of exploiting palm oil hydrogen content to improve the quality of derived Kraft lignin oil. A new setup was added to increase the reaction time between reagents and maximize their interaction. The oil has been characterized by focusing on its composition for biofuel application. Methyl esters formation mechanism has been further investigated, carrying out co-pyrolysis study with palmitic acid, lignin, and guaiacols.

- Chapter 7: Catalytic upgrading of bio-oil produced by Kraft lignin pyrolysis: effect of process parameters and sulfur content.

A new pyrolysis setup with a two-stage condensation has been designed and built to produce oil for catalytic upgrading. First, a proper characterization of oil fraction in terms of composition, and molecular weight distribution has been performed. Then, a catalytic study on the model compound, 4-methyl guaiacol, has been carried out to investigate the sulfur tolerance of $Cu/TiO_2$ catalyst and its activity in selective demethoxylation. Then, direct hydrodeoxygenation was performed on high-pressure reactors to upgrade the pyrolysis oil.

- Chapter 8: General discussion and conclusions.

# *Chapter 1. Literature review*

## *1.1. Introduction to the biorefinery concept*

The use of renewable materials for energy production is an ongoing challenge that must be overcome to project future developments towards a more sustainable and clean approach. Wind, water, biomass, and solar energy will play a key-role in the transition to a low-carbon economy, but current technologies are not sufficient to satisfy the energy demand for an ever-growing population [1,2]. Fossil fuels must be progressively replaced with renewable energies to lower the emissions of $CO_2$ by 2050 and reach the so-called zero-carbon society. One of the most important steps to reach this target is to improve the efficiency of the already existing processes together with developing new ones. For this reason, the valorization of wastes and renewable resources will become extremely relevant from an energetic and economic point of view, by introducing in the production chain the concept of circular economy.

Biorefineries merge all these aspects under a common concept consisting of the replacement of fossil-based with renewable carbon materials for the efficient co-production of biofuels, biochemical, and bioenergy [3]. The development of biorefinery is aimed at the use of different biomasses to produce bioproducts like biofuels (bioethanol, biogas, syngas), platform chemicals (furfural, glycerol, sugars, lipids, etc.), and other high-value products (bioplastics, polymers, fertilizers, cosmetics, and pharmaceuticals) with defined specifications for final uses, according also to the properties of the input streams. Four generations of biorefineries can be defined depending on the biomass used as a feedstock [4]. First-generation biorefineries are based on the conversion of crops rich in sugar or starch, or edible oils for the extensive production of biofuels. However, different issues emerged from the utilization of these biomasses for energy-related applications since these resources compete with their utilization as a staple food. These cultivations also require a significant amount of land for harvesting and trade-offs were needed to distribute the resources for food and energy cultivation. Another relevant problem related to harvesting first-generation biomasses involves the high use of water during irrigation and the intensive use of that enriches the water streams with biodegradable organic carbon, pesticide residues, and nutrients such as nitrogen and phosphorus responsible for the eutrophication phenomenon [5]. Therefore, the production of biofuels is justified by higher sustainability and the positive effects in terms of mitigation of climate change. However, the overall environmental impact

due to these considerations can be counterproductive and, for these reasons, second-generation biomasses were presented as the alternative to the shortage of land availability. This category comprehends non-edible and waste oils (lubricant and engine oils), industrial bio-waste (sawdust, pulp waste, sugarcane bagasse, and fruit peeling), and bioproducts like glycerol obtained as a side-product in the production of biodiesels [6]. The main advantage of this class of wastes is related to the fact that their utilization reduces bio-waste accumulation producing high-value products. Moreover, they do not interfere with the land-use distribution or alter the cost of food crops [7]. Third-generation biorefineries are mainly based on the exploitation of bacteria and microalgae, which can process alcohols and lipids to produce biodiesels thanks to their metabolism. Interestingly, their photosynthesis rate is higher than terrestrial plants, leading to faster biomass production [8]. Microalgae can be grown in wastewaters without requiring any land use and without competing with agricultural activities. Their growth needs $CO_2$ supply which can be obtained from industrial gaseous waste streams, or through direct atmospheric capture. However, the harvesting of microalgae is challenging due to their sensitivity to many parameters such as pH, and due to the low density and size of their cells. Moreover, the energy consumption is higher than the one for other biofuel production processes.

### *1.1.1. Lignocellulosic biomass valorization*

Among second-generation biomass, lignocellulosic biomasses represent one of the most promising and rich renewable feedstocks used in biorefineries [9]. Lignocellulosic biomass comprehends barley straw, coconut husk, corn stover, empty fruit bunch, rice, sugarcane bagasse, straw, sorghum stalks, wheat, and wood. These biomasses contain different amounts of lignin, hemicelluloses, and cellulose which can be processed via fractionation to produce high-value products [10]. The content of cellulose, hemicellulose, and lignin in lignocellulosic biomass is related to the type of biomass. Wang et al. reports that cellulose can reach between 40- 60 wt.%, while hemicellulose and lignin account for 15-30% and 10-25%, respectively. In addition to these three main components, lignocellulosic biomass also contains extractives and inorganic ashes, which are more present in herbaceous biomass rather than wood-derived biomasses [11].

Cellulose is a typical polycondensation polymer consisting of D-glucopyranose units covalently linked by β–1,4-glycosidic bonds [12]. Every polymeric unit has three highly reactive hydroxyl groups which influence important properties like hydrophobicity, biodegradability, and chirality, but they are also responsible for the complex hydrogen bond

network that gives cellulose a partially crystalline structure [13]. The chemical formula is often reported as $(C_6H_{10}O_5)_n$, where n represents the degree of polymerization (DP), that on average ranges in-between 9000-15000 units. The glycosidic bonds under high-temperature or acid conditions are easily cleaved, reducing the DP and contributing to the formation of furan and levoglucosan in processes like pyrolysis. The molecular arrangement of cellulose depends on its crystallinity, which directly influences physico-chemical properties. The crystalline structure, characterized by an ordered disposition of the polymer, is alternated with the amorphous structure where the monomers are non-uniformly disposed. A more crystalline and ordered structure has better thermal stability, also thanks to the hydrogen bond network which inhibits the expansion along cellulose chains [11]. Different processes altering the thermos-chemical properties of cellulose are used to refine cellulose with different degrees of crystallinity functionalizing the surface with different chemical groups. This allows the production of different cellulose-derived materials which can be applied in many industrial fields [14]. However, one of the main applications in the valorization of cellulose from lignocellulosic biomass consists in its separation from the other components of plant cell structure like lignin and hemicellulose that negatively affects the suitability for its direct hydrolysis to sugars and its further fermentation for bio-ethanol production.

Another important component of lignocellulosic biomass is hemicellulose, a plant-derived mixture of polysaccharides strongly bonded to the microfibrils of cellulose via hydrogen bond and Van der Waals interactions [15]. Hemicellulose is a heterogeneous polymer that may contain pentoses, hexoses, and uronic acids in different percentages. The most relevant hemicelluloses are glucomannans and xylans, usually present in large amounts in side-products from the pulp industry, and agriculture. In hardwoods, xyloglucans represent the major hemicellulose structure in the cell walls, responsible for the interaction with cellulose providing resistance and structural integrity to the cell [16]. Extraction and fractionation of hemicellulose from plants are performed with acid hydrolysis to hydrolyze the sugars for bio-ethanol production but also via direct hydrolysis to produce chemicals as furfural [17,18]. Concentrated acids allow not only the hydrolysis of hemicellulose but cellulose as well. These processes use acids like sulfuric acid (72%) or hydrochloric acid (41%), which have as major advantages the possibility to work in a lower temperature range reducing operational costs and limiting the formation of degraded products. However, the recovery of the acid plays a key role in the economic sustainability of the overall process, together with the higher costs for maintenance due to the acids corrosive character. Catalyzed diluted acid hydrolysis can be performed in two steps at different temperatures, with yields of 70% of

sugar recovery for sulfuric acid at 1 %. However, also in diluted acid processes the recovery of the acid is fundamental, and high amounts of wastes are produced [16].

Besides the industrial significance of cellulose and hemicellulose, recent years have witnessed an increasing focus on lignin within the research community, owing to its potential as a source of aromatic hydrocarbons. Lignin, being a natural aromatic-rich compound, stands as a valuable resource; however, the optimization of its sustainable utilization remains a critical challenge [13]. Although lignin exhibits considerable potential, its recovery and application are predominantly confined to laboratory-scale processes, with industrial exploitation largely limited to combustion for heat recovery. The chemical recalcitrance of lignin and the low selectivity in the conversion of aromatic compounds have consistently posed challenges in lignin treatments [14].

### *1.1.2. Lignin Structure: linkages and functional groups*

The intricate structure of the lignin polymer arises from the combination of phenylpropane units like p-coumaryl alcohol, coniferyl alcohol, and sinapyl alcohol (Figure 1), with their respective proportions in the final product depending on the utilized feedstocks [19]. The phenylpropane units are linked together through different linkages whose abundance and distribution can play a crucial role in lignin depolymerization. The most common linkage in lignin is the aryl-aryl ether bond, also known as the β-O-4 linkage. It connects two phenylpropane units in the lignin polymer and it is susceptible to cleavage. Other abundant bonds are represented by the carbon-carbon linkages such as the β-5, connecting the side chain of one phenylpropane unit to the aromatic ring of another, and the β-β, joining two aromatic rings directly [20–22]. Biphenyl 5–5, biphenyl ether 4-O-5, and the β-1 linkages are present as well but with less frequency and abundance.

The extraction of lignin from lignocellulosic biomass involves several processes, and various methods have been developed. Each process produces lignin with specific chemical characteristic related to the distribution of chemical functional groups. These groups define lignin physical properties. Hydroxyl -OH on aromatic and side chains are important for the formation of hydrogen bond network. Methoxy -$OCH_3$ and carboxyl -COOH groups affects lignin solubility and polarity, while ketones and aldehyde groups can be formed as well increasing lignin participation in chemical reactions. The understanding of the specific linkages and functional groups is then essential for tailoring lignin properties for further applications [23].

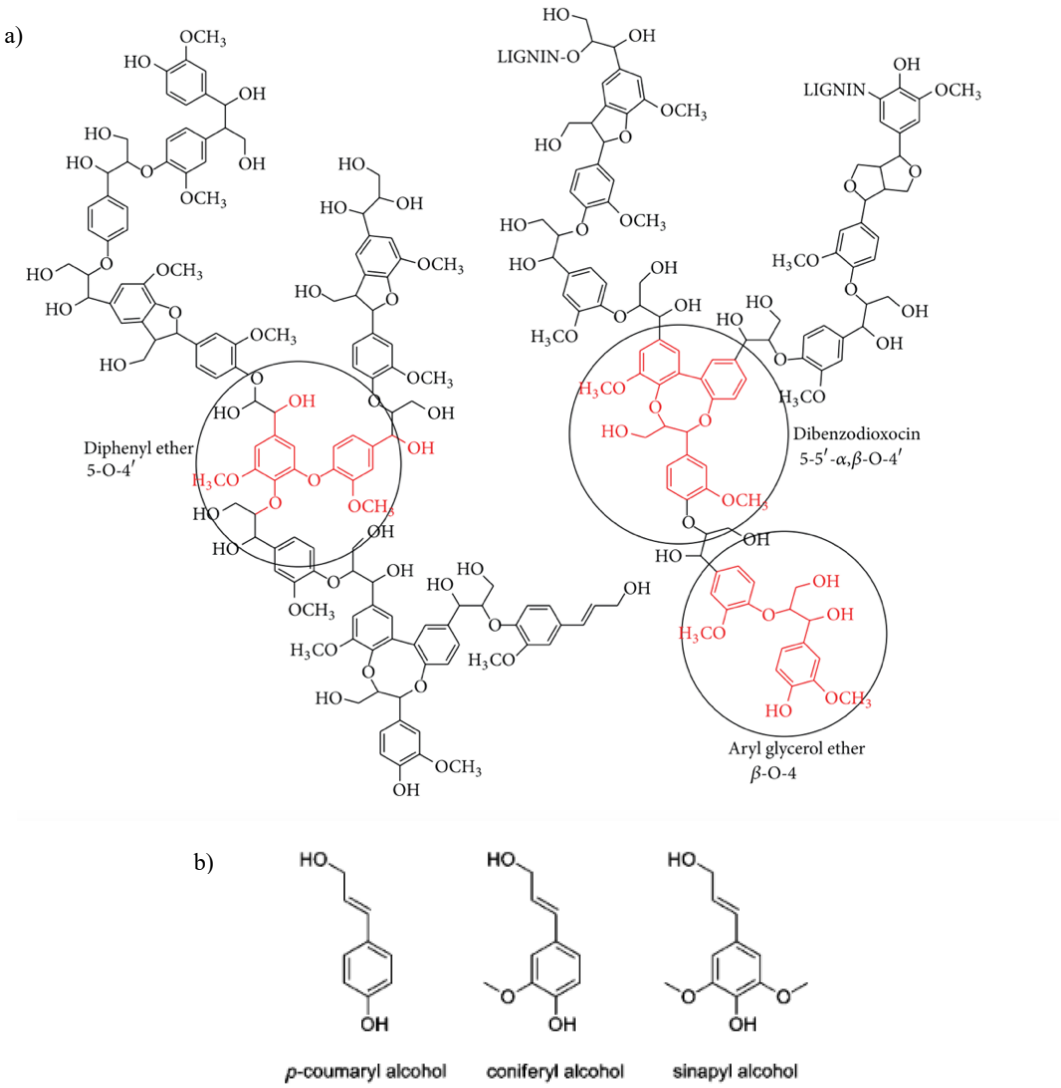


Figure 1: General structure of lignin polymer showing characteristic linkages, and functional groups (a) [24], and building blocks (b).

## *1.2. Lignin extraction and depolymerization procedures*

As said above, lignin is mostly obtained as a co-product of polysaccharide separation and utilization processes. The separation of wood components could be essentially carried out by mechanical or chemical treatments as reported in Figure 2. Chemical treatments may alter the structure of lignin and cause its partial depolymerization. However, the partially depolymerized lignin often undergoes to re-polymerization. Therefore, this residue may be the object of valorization processes as discussed in this thesis.

Several processes have been developed to separate lignin from the other components of lignocellulosic biomass.

– Physical treatments are based on the variation of parameters such as temperature, pressure, and particle size distribution to reduce the recalcitrance of the biomass and

increase lignin yield extraction. These processes are often used in combination with chemicals treatments to increase the efficiency of the extraction process without using too harsh conditions that would affect lignin structure and chemistry [25]. An alternative pretreatment is represented by steam explosion where biomass is subjected to steam at high pressure that can degrade the lignocellulosic matrix and lead to the formation of lignin-rich fractions. Steam-exploded lignin can be further used as a biofuel, but also to produce chemicals (e.g. phenols) because of the heterogeneous pool of compounds obtained [26–29].

- Biological treatment involves the use of enzymatic cocktails specialized in the hydrolysis of lignocellulosic biomasses to increase lignin extraction efficiency. For instance, cellulolytic enzyme in lignin isolation exploits enzyme activity to alter polysaccharide fractions and obtain a residue with high lignin content and a low number of impurities [20,30,31].
- Chemical treatments inevitably cause some structural modifications of the native structure of lignin. Among them, the most used are:
  - *Solvent extraction*: due to the presence of the abovementioned functional groups, it is possible to extract lignin through intensive chemical treatment with solvents fractionating the native lignin into smaller soluble fragments. It is important though, to find a trade-off between the lignin extraction and the effective modifications to its structure that can be monitored by looking at the stability of the β-O-4 linkages. Extraction with organic solvent at room temperature is possible and allows the recovery of lignin with fewer structural modifications but with a low overall efficiency [32]. Physical pretreatments such as ball milling can break cleavable bonds reducing the particle size and the recalcitrance of the biomass, improving the extraction efficiency [33,34]. Organosolv extraction stands as an alternative to the pulping processes. The use of solvents such as ethanol, and methanol, among others, coupled with acid or basic catalysts allows the recovery of lignin with high β-aryl ether content and limited amount of carbohydrates, ash and other impurities [35–37]. In this process, alcohols are essential because they are incorporated in the β-aryl ether units, trapping reactive cations formed during acid pre-treatments and preventing unwanted recondensations.
  - *Acid hydrolysis*: lignocellulosic biomass can be treated with strong acids to hydrolyze the hemicellulose and break the linkages between lignin and cellulose. This results in the extraction of lignin in soluble form but with higher grade of structural changes.

Sulfuric acid and hydrochloric acid are two of the most adopted acids found in literature [38,39].

- *Ionic liquids*: the use of ionic liquid for lignin extraction is an emerging alternative to the before mentioned processes, which proved to have high lignin extraction efficiency. Ionic liquids are a class of compounds known also as liquid salts obtained via acid-based neutralization which are competitive also for their competitive cost and their potential reusability [41–44].

The different range of process conditions, employed in the mentioned lignin extraction technologies, gives rise to variations in the chemical structure and properties of the obtained lignin. Consequently, the categorization of lignin becomes quite intricate. One of the prominent classification schemes proposed in the literature is based on the sulfur content as shown in Figure 2.

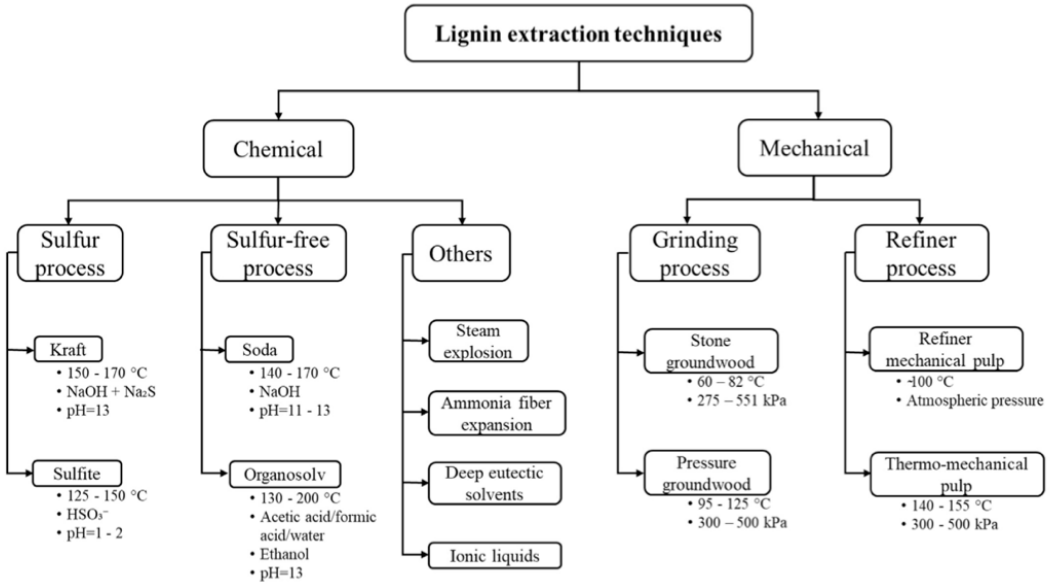


Figure 2:A scheme for the possible classifications of lignin extraction techniques. Mechanical methods are often used to improve the yields of chemical treatments. Chemical treatments involve sulfur-free processes, sulfur-based processes, and alternative techniques that are based on innovative solutions and solvents [40].

### *1.2.1. Sulfur-free lignin*

The soda-based delignification process is an interesting alternative to the traditional pulping methods. Based on the same process conditions and principles, soda pulping is compatible with existing kraft pulping technology, but is a sulfur-free process. Sodium hydroxide (NaOH) is the main chemical used in the soda pulping. Soda lignin is distinguished from kraft lignin and lignosulphonates by the absence of sulfur and the different content in vinyl

ethers. This process has limited use for easily pulped materials such as straws and some hardwoods, but it is not a major process. Additives such as anthraquinones may be used as a pulping additive to decrease carbohydrate degradation. A more recent development foresees the use of oxygen in the soda pulping process. However, oxygen bleaching is not very specific to the delignification process compared to other pulping methods. It has been utilized in the production of phenolic resins, and dispersants, and for polymer synthesis. It can also be used in areas such as animal nutrition due to its sulfur-free properties. However, due to its low pulp yield performance, the use of the soda pulping process in pulp mills is becoming increasingly rare.

An alternative is represented by the organosolv delignification process which utilizes organic solvents to dissolve lignin, to effectively separate it from carbohydrates in lignocellulosic biomass. This method provides several advantages for various bioproduct applications, offering the potential for sulfur-free processes depending on the solvents employed. The resulting lignin can exhibit high purity, chemical reactivity, and non-toxic characteristics. However, the quality of the extracted lignin is contingent upon the specific pretreatment conditions employed. The obtained lignin has a homogeneous structure with a low molecular weight and polydispersity. Increasing the severity of organosolv process conditions leads to a notable reduction in the molar mass of extracted lignin compared to untreated lignin. Additionally, a decrease in aliphatic hydroxyl group content and an increase in syringyl phenolic units and condensed phenolic structures can be obtained. Due to its hydrophobic nature, organosolv lignin exhibits high solubility in organic solvents and minimal solubility in water. To recover organosolv lignin from the solvent, a precipitation step is necessary, involving adjustments to concentration, pH, and temperature [41,42].

### *1.2.2. Sulfur-rich lignin*

Many technical lignins are already available and produced on the market. In fact, it is estimated that more than 80% of the worldwide production of lignin derives from Kraft and lignosulfonate pulping methods which are sulfur-based processes and consequently result in sulfur-rich lignin [19,25,42,43].

Sulphite pulping is a chemical pulping process using mixtures of sulfuric acid and/or its alkali salts ($Na^+$, $NH_4^+$, $Mg^{2+}$, $K^+$ or $Ca^{2+}$) to dissolve lignin by forming sulphonate functionalities and cleaving existing lignin bonds. During the sulphite process, lignin is broken down into a sulfonated compounds with various functional groups that provide unique colloidal properties. The sulphite pulping process, which used to be dominant, now

accounts for less than 10% of pulp production in this country, partly due to environmental concerns. Sulphite pulping offers several advantages, including bright and easily bleached pulps, as well as higher yields compared to kraft pulping [41]. Lignosulfonates have a variety of uses, including as colloidal suspensions, stabilizers, dispersants, binders, detergents, adhesives, components of feed, surfactants, and additives for cements.

#### *1.2.2.1. Kraft Lignoboost Process*

The Kraft Lignoboost process begins with the cooking stage where lignocellulosic biomass (usually wood chips) is treated in the evaporation train with a mixture of sodium hydroxide (NaOH) and sodium sulfide ($Na_2S$) under high temperature and pressure. In the presence of heat and chemicals, lignin undergoes a series of chemical reactions. Sodium hydroxide (NaOH) breaks down the ester linkages, leading to the dissolution of lignin in the cooking liquor. Sodium sulfide ($Na_2S$) aids in preventing the formation of undesirable by-products. Then the so-called black liquor consisting in dissolved lignin and solid content of 30-45% is drained from the evaporator and cooled down. Lignin deriving from Kraft cooking is soluble for pH>10, therefore an acidification is performed to precipitate lignin. Phenolic OH groups are weakly acidic, and their protonation increase with the decreasing of the pH. $H_2SO_4$ and $CO_2$ are commonly used as acidifying agents because they do not alter the black liquor matrix. After lignin precipitation, the resulting slurry is filtered leading to the formation of a filtered cake of precipitated lignin and a filtrate which is recirculated to the liquor cycle and resent to the evaporator. The filtrate is then redispersed in sulfuric acid at pH=2-4 ensuring the complete precipitation of lignin. In this process, lignin is separated as a side-products, and it is used as fuel for the recovery boiler and the production of steam. However, the real potential of lignin as a renewable source of biofuels and biochemicals is well known, and therefore it is important to study more efficient pathways for its valorization.

Depending on acidification and delignification conditions, lignin can have different sulfur content that goes from 1.5 to 8 wt.%, but on average it is around 2-3 wt.% [44]. This is mainly due to the cooking process in Kraft pulping where 20-50% of sodium sulfide used is wasted. The distribution of sulfur in lignin and its form has always under debate. At the initial stage of Kraft cooking, lignin has a relevant amount of sulfur around 5 wt.% that then is dissolved at high temperature when alkaline hydrolysis occurs. Several authors suggested that in sulfur-containing lignin, sulfur may be present in the forms of thiols, thiirane and sulfide groups, but no organic disulfide, polysulfide, thiocarbonyl and dialkyl sulfide groups are present [45–47]. However, mercaptans undergoes oxidation during the Kraft cooking

and form disulfides and sulfonic acids [48]. The presence of sulfur in Kraft Lignin (KL) limits its industrial potential because it releases sulfur-containing gas compounds into the environment and reduces bio-oil yields during pyrolysis, standing as one of the most remarkable parameters to monitor for KL valorization [46]. The lignin that has been used as raw material for this thesis derives from Kraft Lignoboost pulping process, therefore, it was important to understand its chemical features, being Kraft lignin valorization the aim of this work.

## *1.3. Lignin depolymerization approaches*

As already mentioned, lignin residue obtained from the pulping industry is a solid residue and it is used as a source of energy and valorized through combustion. A proper valorization of lignin can be obtained also preserving its molecular structure for instance in the preparation of lignin-derived polymers, or the production of equipments for energy storage applications. However, besides new emerging valorization approaches, depolymerization pathways to exploit lignin polymer as a source of chemical monomers remain of major interest due to the wide network of reactions, and potential products obtainable by its degradation. Therefore, chemical depolymerization of lignin stands as the main focus of this chapter. Several depolymerization methods have been developed, in the last decades, to attempt an efficient and target-related cleavage of the chemical linkages of lignin polymer.
Breaking lignin linkages with high selectivity is achievable only using catalysts with different physicochemical properties. The range of different catalysts that have been investigated is wide and strictly dependent on the target product that must be obtained and its specific requirements. Catalysts act on a chemical level lowering the energy required for the fractionation of lignin into smaller fragments. Depolymerization catalysis can be divided into different groups of catalysts according to their activity:

- *Acid-catalyzed:* the use of acids has been adopted since the mid-twentieth century for the cleavage of β-O-4 linkages. Acid protons allow the break of ether bonds leading to the formation of the phenolic monomers, and the mechanism has been proposed and shown by Roy et al. [49]. Many researchers studied the influence of different solvent-acid ratios in lignin fractionation [50–52]. This process is generally performed at high temperatures (> 200°C [50]) and pressures, using solvents like ethanol or ethylene glycol mixed with acids to allow a separation between a water-soluble and water-insoluble lignin products.

- *Base-catalyzed:* to extract phenolic monomers from lignin, excellent catalytic performances were observed using bases such as KOH, NaOH, and $Ca(OH)_2$ [53,54]. Also in this case, the main target is the of β-O-4 linkage. The depolymerization rate increase with the increasing of the strength of the base, however, many weak bases have been used as well, even if with a remarkably high char formation during the process [55]. Moreover, base-catalyzed depolymerization does not occur with diluted bases in water, therefore, many organic solvents are commonly used [56]. According to Karagöz et al., the production of carboxylic acid during the depolymerization can influence the pH and, consequently, the monomer production [57]. The process conditions are harsh, with high temperatures and pressures, making the entire process poorly sustainable from the economic point of view.
- *Metal catalyzed:* the utilization of metallic catalysts allow to operate at milder conditions with higher selectivity than those of previously mentioned processes [58,59]. The activity of Ni catalysts in lignin depolymerization were extensively investigated, to selectively break down the ether bonds and produce chemicals. Bimetallic alloys were employed to increase the reactivity and selectivity under mild conditions. Noble metal and their alloys (Ru, Pd, Pt, Ti) showed good performances in lignin conversion to chemicals, but also limitations due to the high cost and the over-hydrogenation of aromatics rings [60–67]. Non-noble metals such as Cu, Fe, Al, Zn, Co, and Mo have been also proposed as a cheap and more environmental friendly alternatives for lignin depolymerization [59,68–70].

Lignin degradation can occur also on biocatalysts such as fungi[71–73]. As an example, white-rot *basidiomycetes* are fungi responsible for natural lignin degradation due to their high oxidizing potential. Beside lignin oxidation they are responsible of demethylation and the cleavage of C-C side chain linkages and β-O-4 bonds. [74]. Enzymes are proteins produced during fungi metabolism, which can act as biocatalysts and can be active in the degradation of lignin. Lignin-degrading enzymes can be classified as Lignin-Modifying Enzymes (LME), if they represent the direct responsible for lignin degradation, or Lignin-degrading Auxiliary Enzymes (LAE) which assist the depolymerization by $H_2O_2$ generation [75]. Milder operational conditions and increased yields of uncondensed lignin can be attained through the utilization of oxidative ligninolytic enzymes. Enzymes such as *lignin peroxidases*, *manganese peroxidases*, versatile *peroxidases*, and *laccases* have demonstrated so far the ability to effectively depolymerize native lignin, as reported in the cited reviews [76–78].

### *1.3.1. Thermochemical methods for isolated lignin valorization*

A wide range of thermochemical methods has been adopted in the depolymerization process exploring deep sets of process conditions [79–83]. These methods involve lignin treatments to high temperatures (250-800°C) and, in some cases, elevated pressures (from 2 to 30 MPa), inducing transformative processes that break down the complex lignin polymer, as reported in Figure 3, where it is observable, at a glance, the operation range of more common thermochemical processes. Thermochemical techniques include solvolysis, hydrothermal liquefaction, gasification, and pyrolysis, each offering unique pathways for lignin conversion.

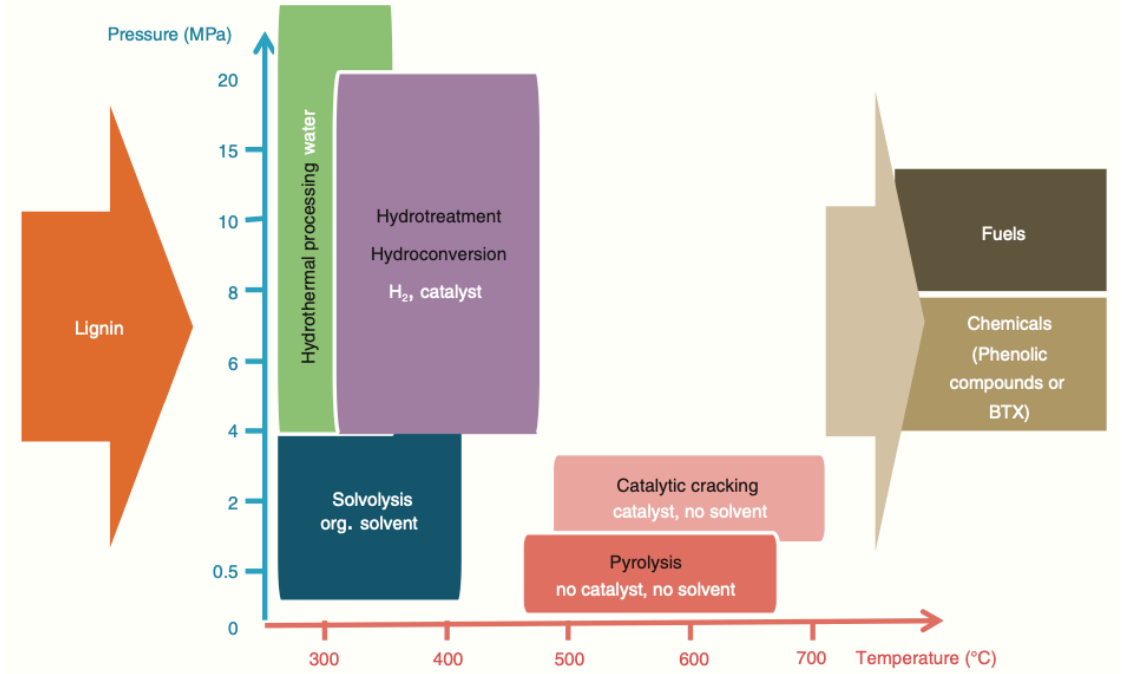


Figure 3:A classification of thermochemical methods used for lignin valorization. Several applications are reported depending on the process temperature and pressure being biofuels and chemicals the main target [84].

Solvolysis consists in the conversion of lignin using organic solvents able to act as H-donor to improve the hydrogenation rate and liquid product yield. Solvents like tetralin, ethanol and glycerol have been often used due to their hydrogenation capability, low cost, and low environmental impact [84].

Hydrothermal liquefaction processes work at higher temperatures and pressures, using water as a solvent in sub- and supercritical conditions. Under these conditions the cleavage of ether linkages, but also dealkylation and demethoxylation occur. The limitation of this technique is related to the high specific heat of water; an optimized recovery of the heat then can play a crucial role in the economical sustainability of the process. Alkali salts, phenolics, or other

organics have a positive effect in the increase of the oil yields, reducing the repolymerization of reactive fragments [85].

Biomass gasification is a thermochemical procedure that employs a restricted amount of gasifying agent to convert solid biomass into useful gases, including methane ($CH_4$), carbon dioxide ($CO_2$), carbon monoxide (CO), hydrogen ($H_2$), and a solid residue known as char. The gases can be processed further via the F-T method or utilized as heat and energy for the generation of power units. The gasifying agent is generally targeted accounted for the final syngas use and air, oxygen, or supercritical water (SCW) are generally chosen. Air is frequently used as a gasifying medium due to its accessibility and cost-effectiveness, even though dilution of obtained syngas is the main drawback. Nevertheless, when steam is utilized as a gasifying medium, the product gas comprises a higher H/C ratio. Tar formation presents a significant challenge during the gasification process. It is problematic to purify and has a negative impact on the yield of $H_2$ [86–88]. Several reviews and paper can be found in literature reporting different reactor configurations and operative conditions for biomass gasifiers [89–91].

#### *1.3.1.1. Lignin pyrolysis*

Pyrolysis represents one of the most powerful methods used for the depolymerization of biomasses since it consists of the thermal decomposition of materials in an oxygen-free environment. Avoiding combustion, pyrolysis products are mainly formed by the thermal cracking of molecules at high temperatures. In many cases, the main target of lignin pyrolysis is the bio-oil rich in aromatic compounds, even if further treatments are generally required due to the high content of oxygenated compounds. Other products of pyrolytic processes consist of a gas, and a solid residue, referred to as biochar, produced in different ratios depending on process parameters such as temperature, reaction time, pressure, particle size distribution, and chemical composition of the feedstocks, among others.

Fast pyrolysis involves processes with high heating rate, and many technologies such as bubbling fluidized bed, transported bed, and circulating fluidized bed, have been developed and studied in the past decades [92,93]. Pyrolysis of lignin exploits the high reactivity of the oxygenated functional groups. Methoxy groups can decompose in smaller radicals and act as a stabilizer for high molecular weight fragments produced during lignin cracking preventing further polymerization and char formation. Hydroxyl groups can decompose as well from side chains through dehydration, favoring the formation of unsaturated side chain compounds such as propenyl-guaiacol and vinyl-guaiacol [11]. Therefore, the chemical

structure of the lignin treated, and the distribution of functional groups have a huge impact on pyrolysis products distribution, and their chemical composition. Gaseous products often include carbon monoxide, carbon dioxide, methane, and hydrogen, but depending on the process condition they can be further treated to produce syngas and contribute to the energy balance being mostly burned for energy recovery.

Lignin degradation *via pyrolysis* occurs through a wide range of temperatures. Lower temperatures between 150-400°C, allow the cleavage of the weak bonds such as β-O-4 linkages, and non-phenolic ether bonds. Without hydrogen external supply, the hydrogen produced is not enough to stabilize monomers fragments that tend to repolymerize into dimers or oligomers. Above 400°C, many linkages break, leading to the production of vanillin, and guaiacol-units. At temperatures higher than 550°C, aromatic rings start to decompose, and the production of non-condensable gases is favored. Moreover, also the content of polycyclic aromatic hydrocarbons (PAH) and coke formation increase significantly. Methyl and methoxy groups are one of the major responsible for coke formation, but a higher heating rate can partially suppress char production. Many catalytic approaches have been developed to assist the demethoxylation and demethylation, limiting the recondensation of monomers [56]. Zeolites are well-known catalysts and they have been used to increase the aromatic yields during lignin depolymerization. However, their pore structure favors the recondensation of monomers, and coke formation, caused by the high content of alkylated guaiacols and phenols in lignin [94]. Different metals have been adopted as well to convert lignin into specific monomers with high selectivity, making pyrolysis an efficient but not selective process.

## *1.4. Lignin-derived bio-oils*

Bio-oil often represents the most valuable pyrolysis product, constituting a complex mixture of organic condensable compounds, including sugars, ketones, aldehydes, acids, aromatic and phenolic compounds, among others. Its composition strongly depends on the chemical makeup of the biomass used for its production, as well as other factors such as biomass pretreatment (moisture, ash content, and particle size) and pyrolysis conditions (temperature, heating rate, reaction time, pressure). Consequently, bio-oils produced under different conditions may exhibit variations in composition and physico-chemical properties [95]. In its raw state, pyrolysis bio-oil may have high water content, viscosity, and a wide molecular weight distribution due to the presence of recondensed compounds. Therefore, its direct

application as biofuel is not feasible, requiring further upgrades to enhance its properties and broaden its spectrum of applications. This significantly impacts the cost and sustainability of the bio-oil industry, given the challenges associated with processing bio-oil. The presence of water from biomass condensation is notably higher compared to crude oil from refineries, potentially compromising engine ignition processes and reducing the fuel's energy content. Furthermore, the high oxygen content negatively affects solubility for fuel blending, increasing acidity and corrosiveness. Indeed, bio-oils produced via non-catalytic pyrolysis often necessitate additional upgrading processes to be suitable for use as biofuels or sources of chemical intermediates [96,97].

Emulsification of bio-oils with poor stability can be achieved by blending them with more stable biodiesels or polar solvents to reduce viscosity. However, these enhancements merely mitigate the low-quality features of some properties rather than constitute a proper upgrade of the oil. Upgrading techniques irreversibly alter the chemical structure of the oil, transforming bio-oil components into mixtures with improved physico-chemical properties [98].

### *1.4.1. Upgrading bio-oil approaches*

Steam reforming, catalytic cracking, supercritical fluid treatments, and hydrotreatment are some of the most relevant approaches adopted for bio-oil upgrades. Steam reforming is a well-known process that treats hydrocarbons with high-temperature steam to produce mainly CO and $H_2$. The temperature range is around 700-1000°C, where other parallel reactions such as water gas shift are shifted to the formation of CO, $H_2O$, and coke. In bio-oil steam reforming the reaction network is wide and complex, and for this reason, studies on phenolic and oxygenated model compounds have been performed to develop a kinetic study for this application [99]. Generally, Ni-based catalysts are used for steam reforming of hydrocarbons, however, at high temperatures, carbon deposition is favored through the Boudouard reaction, CO reduction, hydrocarbon decomposition, and pyrolytic coke formation, leading to fast catalyst deactivation. Moreover, pretreatments such as hydrodesulfurization are required to avoid sulfur poisoning, and thus increasing operational cost of the process. The suitability of this process for bio-oil upgrading is related to the feedstock properties and to the target to obtain. Therefore, Kraft lignin pyrolysis oil may not be a suitable feedstock for steam reforming due to its sulfur content [100].

Catalytic cracking is an alternative technique used for bio-oil upgrade to remove heteroatoms such as oxygen, producing $H_2O$, $CO_2$, and CO. Different reactor configurations like

fluidized-bed or fixed-bed have been used at relatively high temperature and high pressures. Acid catalyst such as zeolites (HZSM-5, H-Y, H-mordenite, SAPO-11, MgAPO-36, ZnHZSM-5, etc.) are commonly used catalyst to break oxygenated compound into hydrocarbon mixtures despite their possible deactivation due to coke formation [101]. Supercritical fluids, including supercritical water, ethanol, and methanol, have been explored for the upgrading of bio-oil. This exploration is driven by the distinctive characteristics exhibited by solvents under supercritical conditions, such as liquid-like density, gas-like diffusivity and viscosity, and exceptional efficiency in mass and heat transfer [102]. The use of supercritical solvent allows the enhancement of the energy content of the oil reducing heteroatoms, and viscosity. However, high-cost solvents and harsh conditions represent a challenge for their industrial implementation [98].

#### *1.4.1.1. Hydrotreatment of bio-oil*

One of the most well-established methods for oil upgrade is hydrotreatment, which consists in the removal of heteroatoms using high pressure of hydrogen and is generally applied in the refinery with a hydrotreatment section that includes hydrodesulfurization, hydrodemetalation, and hydrodenitrification of topping-cuts in severe process conditions. However, looking at bio-oil case, hydrotreatment should account for an extra unit. Hydrodeoxygenation (HDO) involves the removal of oxygen through water formation and other heteroatoms such as N and S, if present, in the form of $NH_3$ and $H_2S$. Moderate temperature conditions in the range between 200-400°C are commonly adopted in the hydrotreatment process due to the exothermic character of the hydrogenation reaction which is not favored at high temperatures and enhances cracking and coke formation reactions. High hydrogen pressure in the range of 10-30 MPa ensures good efficiency promoting the stabilization of high molecular weight reactants, limiting the carbon deposition, and preserving the catalyst from deactivation. However, high pressures influence operational costs and may lead to safety issues. Notably, good HDO efficiency has also been obtained with low/atmospheric $H_2$ pressures as reported in several studies in the literature [103–106]. The correct selection of catalysts is of fundamental importance to achieve good results in the upgrading process. To limit deactivation mechanisms due to poisoning, sintering, coking, and blocking of active sites, parameters such as conversion and selectivity under severe conditions and catalyst stability must be monitored. Hydrodesulfurization (HDS) catalysts such as $NiMo/Al_2O_3$ and $CoMo/Al_2O_3$ [63,107,108], supported noble metal catalysts such as Pd/C, Pt/C and Ru/C [70,104,109,110] and other non-noble metal catalysts such as Ni-

based catalysts have been extensively investigated in the upgrading processes of pyrolysis oil [64,69]. At the industrial level HDO process is carried out for example in the UOP-ENI Ecofining process [111]. Ecofining process is constituted by a first stage for the hydrotreatment of triglycerides, followed by a second stage of hydroisomerization to improve the cold flow properties of diesel fuel. From the catalysis point of view, in the first reactor classical hydrotreatment formulation are generally used, while in the second stage, bimetallic supported catalysts are generally preferred. A schematic of the discussed process is reported in Figure 4.

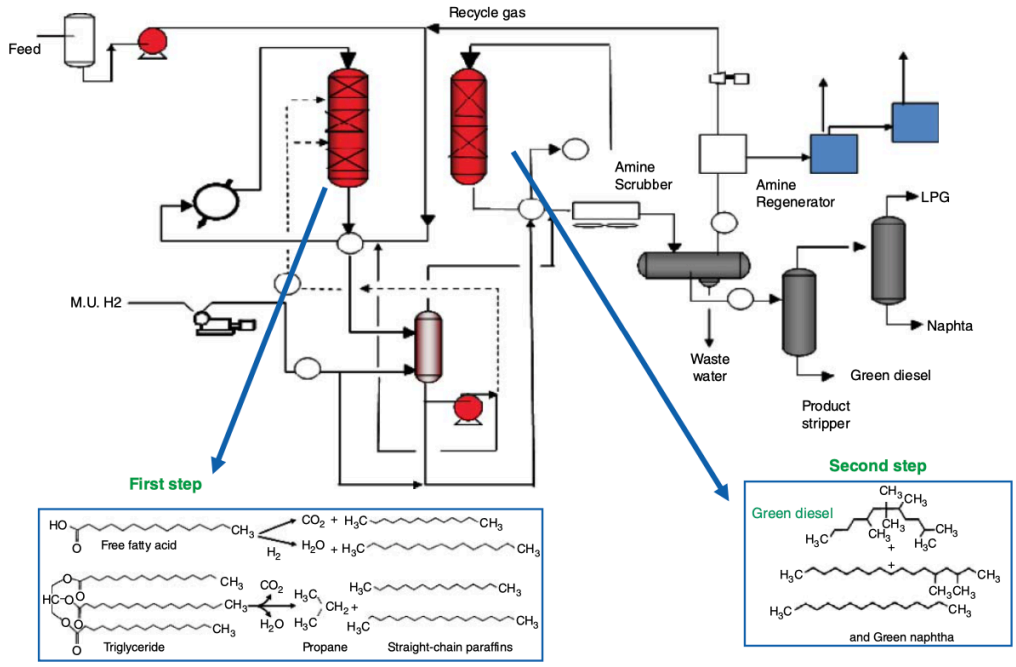


Figure 4:A scheme of UOP-ENI Ecofining$^{TM}$ process

### *1.4.1.2. Selective demethoxylation*

Due to the wide spectrum of compounds present in pyrolysis-derived bio-oils and the related complex network of chemical reaction involved in upgrading processes, model compound studies have been performed to isolate and study specific reactions or pathways. Lignin-derived monomers often have methoxy substituents that enrich the oxygen content of the bio-oil. Selective demethoxylation is therefore an attractive route for their conversion to alkyl-substituted phenolics [65,105,112,113]. Guaiacols are well-known model compounds used in catalytic demethoxylation studies to address the production of biobased phenolics, however, the removal of the methoxy group is not trivial. The energy needed to break the C-O bond that connects the aromatic ring and the methoxy group is very similar to the energy

required to remove the phenolic OH, and it is higher than the energy needed for the demethylation. Standard temperatures vary from 240 to 400°C, with hydrogen pressures ranging from 0.1 to 4 MPa. The application of valuable metal catalysts, such as Pt, Pd/C, and $Au/TiO_2$, has produced high guaiacol conversions and excellent selectivities. When 4-n-propylguaiacol was used as the starting material, $Au/TiO_2$ achieved a yield of up to 84% for demethoxylated phenols [105]

Environmental issues related to the use of noble metals and high costs lead researchers to find attractive alternative using less-precious catalysts such as Ni, Fe, and Mo. Mo-based catalysts have been extensively studied by Yang et al., where the main products were demethoxylated phenols, together with parent phenol, cresols, xylenols, and aromatics such as benzene and xylenes. Product selectivity depends on the amount of Mo used. Lower Mo loadings yield the highest amounts of low molecular weight demethoxylated products, with 5% Mo being the ideal amount. The use of 5% $MoO_3/TiO_2$ resulted in a 97% conversion of guaiacol and an 82% selectivity for demethoxylated phenolics [105]. A reaction mechanism is also proposed, as reported in Figure 5.

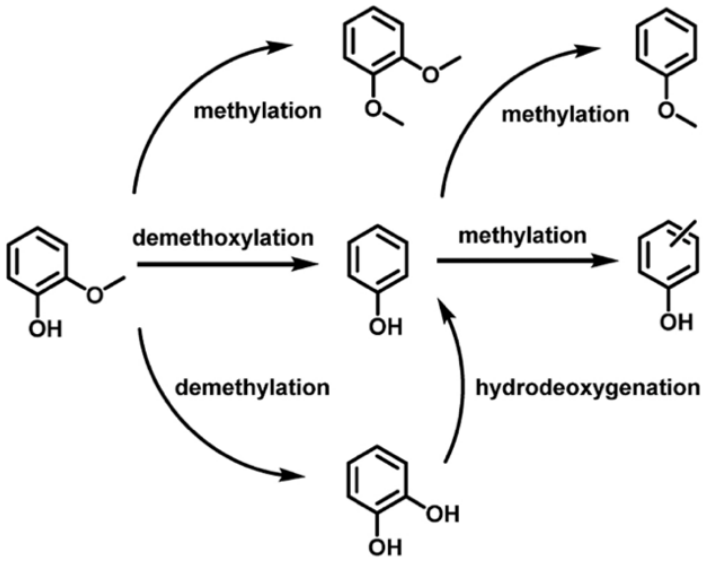


Figure 5: A reaction scheme is proposed for the selective demethoxylation of guaiacols using $MoO_3/TiO_2$ catalyst, explaining the most relevant products obtained and the reactions involved in their formation [65]

Being phenols and methylated phenols the main products, demethoxylation can occur directly by the removing of the methoxy group of guaiacols, or it can be the results of a demethylation of guaiacols to catechols followed by a dehydroxygenation to phenols. Similar studies have been reported in literature focusing on Cu activity on different inorganic

supports such as $TiO_2$ in various forms. Among them $TiO_2$-P25 shown the best results in term of activity, guaiacol conversion, and selectivity to alkylated phenols [65].

## *1.5. End use and applications*

As previously mentioned, the processing of lignin opens a wide range of possible applications, spanning from the production of renewable materials, heat and power energy, biofuels, to chemical intermediates (Figure 6). Nowadays, the combustion of lignin in the Kraft process constitutes nearly 98% of the total lignin produced, notwithstanding its moderate heat value of 25 MJ/kg [114]. The combustion step is pivotal for enhancing the energy efficiency of the entire Kraft process and mitigating the environmental impact in terms of $CO_2$ emissions. However, alternative pathways for utilizing lignin-derived products include the production of syngas for methanol and dimethyl ether production, as well as green diesel via the Fischer-Tropsch process [88,115]. Water-soluble lignin finds applications as a binder in water-based paintings [116], and as an additive to enhance the strength of cements [117]. Despite these established applications, emerging technologies are harnessing lignin as a polyelectrolytic and polymeric material, where it contributes to the development of macromolecules like carbon fibers due to its naturally carbon-rich structure [118]. Lignin proved to be a promising green carbon precursor, transformable into various carbonaceous materials, including activated carbon nanofibers and hierarchical porous carbons (HPCs). These materials exhibit well-defined porous structures and have been employed in the preparation of electrodes for lithium-ion batteries (LIBs) and supercapacitors[119,120].

The primary and significant application of lignin remains in the production of valuable intermediates, a market traditionally dominated by petrochemistry and predominantly reliant on fossil resources. Shifting from non-renewable resources to lignin as the starting point for chemical intermediates, without altering the underlying chemistry, could have a substantial industrial impact. Various oxidized products, including vanillin, vanillic acid, cyclohexane, and dimethyl sulfoxide (DMSO), can be obtained as valuable intermediates. Vanillin, utilized as a flavoring agent in food, beverages, and pharmaceuticals, illustrates this transition, with approximately 20% of market-available vanillin being lignin-derived, in contrast to the majority sourced from crude oil [121]. Similarly, DMSO, another potential lignin-derived product, is renowned for its commercial solvent applications. Notably,

DMSO is the outcome of the oxidation of dimethyl sulfide, itself a byproduct of Kraft pulping [122]

Phenolic compounds, esteemed for their stability and established market value, have become a focal point of research owing to their reactivity and acidic characteristics. Traditionally derived from petroleum-based benzene through the cumene process [114] , these compounds hold significant versatility. Their applications span diverse industries, finding utility in cosmetics, food products, as well as the manufacturing of adhesives and phenolic resins [123–125]. The current reliance on petroleum sources prompts a reevaluation of sustainable alternatives, and understanding the potential for the synthesis of phenolic compounds from renewable resources offers a promising avenue for both economic and environmental considerations. Researchers are actively exploring innovative methods to harness these compounds from bio-based feedstocks, and lignin stands as one of the most promising.

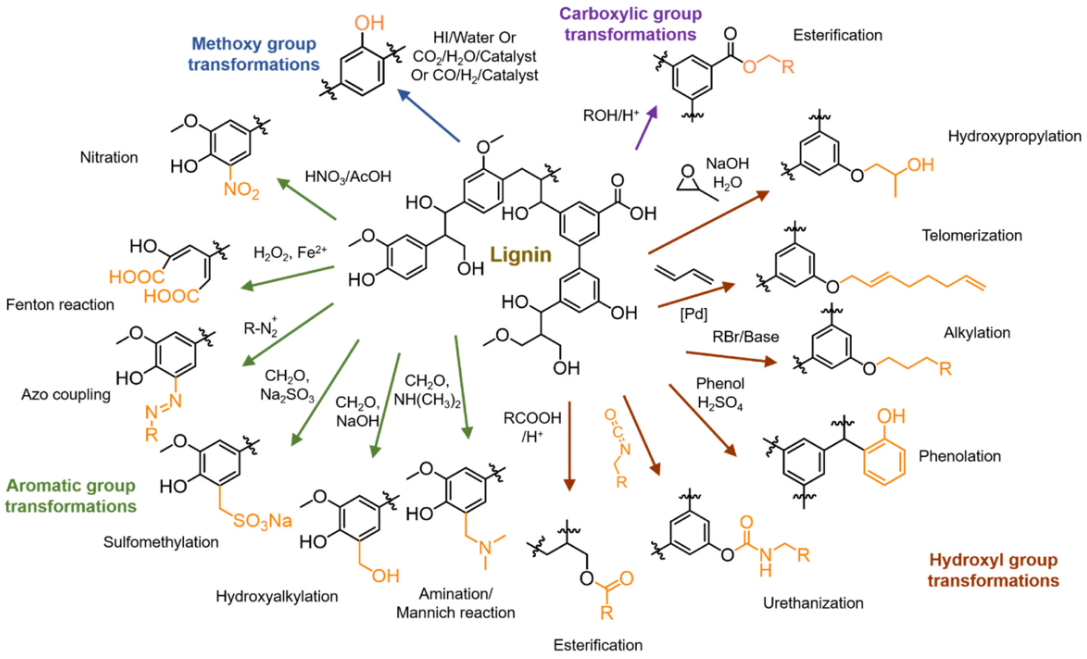


Figure 6: A scheme of the possible valorization pathways and the most relevant product obtainable from its depolymerization [126].

# *Chapter 2. Materials and methods*

## *2.1. Materials*

The commercial Kraft lignin (denoted as KL in the following) used in this work has been provided by StoraEnso® (Lineo™ Classic Lignin, Kotka, Finland), and its chemical characteristics are available at the supplier website (https://www.storaenso.com/en/products/lignin/lineo). Lignin was characterized in terms of moisture and ash content. For liquid extractions, ethanol (assay 99.8%, Sigma Aldrich, St. Louis, Mo., USA) and NaOH (assay 99.7%, Sigma Aldrich, St. Louis, Mo., USA) were used to obtain the desired EtOH/$H_2O$ (1:1 *v*/*v*) and NaOH/$H_2O$ (0.1 M) mixtures. Chloroform (assay 99.9 %, Carlo Erba reagents, Milan, Italy) was used to dilute reaction liquids for gas-chromatographic analysis. KBr (Carlo Erba reagents, Milan, Italy) was adopted to perform FT-IR analysis of the samples.

Four different commercial activated carbons from Comelt PCA1120 have been used: Carbosorb MA 1,5, Carbosorb 360 C3, Carbosorb 53, Carbosorb 73, denoted from a to d, respectively, in chapter 4. Palm oil was retrieved from A&A Fratelli Parodi Spa, while palmitic acid and guaiacol were purchased from Sigma Aldrich (assay 98%) and they have been used in co-pyrolysis study reported in Chapter 6.

Copper nitrate trihydrate (99-104%), $TiO_2$-P25 (>99.5%), SiC (>97.5%) were used for the Cu/$TiO_2$ preparation. n-dodecane (> 99.0%) and decane (> 99.0%) have been used as external standards, thiophene (>99%) used as external sulfur source and 4-methyl guaiacol (>98%) as model compound in the catalytic upgrade of the oil. DMSO (>99.9%) were used as solvent for NMR analysis. Acetone was used for the bio-oil collection from the pyrolysis setup. All these materials have been purchased from Sigma Aldrich. Toluene used as a solvent in the catalytic upgrade, and tetrahydrofuran (THF) stabilized with butylated hydroxytoluene (BHT) utilized for the analysis have been purchased from Boom B.V.

## *2.2. Methods-Experimental techniques*

In this section, all the techniques used to characterize the raw materials and all the pyrolysis products will be discussed, giving an overview on the fundamentals of each technique, and explaining the reasons for their utilization in relation to the target. In the first section, the characterization of raw materials and solid pyrolysis residues will be discussed. Then, all the techniques adopted for liquids and gas characterization will be presented.

### *2.2.1. Scanning Electron Microscopy (SEM)*

**Fundamentals**:

SEM stands as a powerful method to investigate the surface of probes with the production of high-resolution images. Electron microscopy uses accelerated electron beams with short wavelength which are responsible of diffraction effects able to resolve atomic features at very small scale ranging from nanometer to micrometer scale. The high-energy electron beam invests the sample, and the analysis of the outcoming electrons provide information about the topography, morphology, composition, grain orientation, and crystallography of the sample. Sample's shape and size, but also surface characteristics like roughness and texture can be investigated using this technique.

To perform SEM analysis, an electrical conductivity of the sample is needed to avoid overcharging of the surface that would result in poor-quality images. The electrons of the source provide energy to the electrons of the sample. Due to this energy boost, the electrons of the specimen (the so-called secondary electrons) can be released and then interact with the near-surface generating several types of signals. These signals can be due not only to the secondary electrons, but also to the back-scattered electrons and X-rays (Figure 7). Back-scattered electrons are those reflected through the elastic scattering by the atoms of the sample. The area involved by the scattering depends on the characteristic of the sample atoms, but also on the energy of the beam source. The collection of all the recorded signals is performed by a detector that process the data and provide a high-resolution image of the specimen surface. X-rays are used in energy-dispersive X-ray analysis (EDX), they are emitted when the electrons go back to the lower energy level after their excitement by the electron beam. X-rays have a specific wavelength depending on the difference in the energy level of the elements present in the sample. Therefore, the sample elemental composition can be obtained due to the characteristic x-ray emission of each element [127].

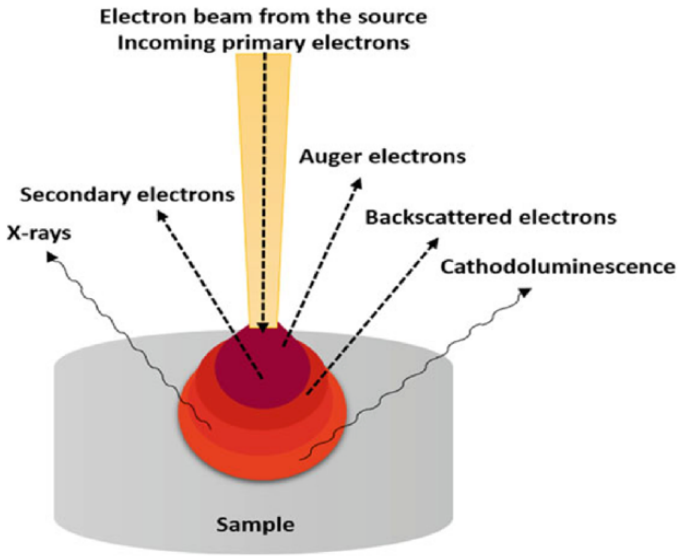


Figure 7: A graphic representation of the specimen invested by the electron beam in the SEM technique. All the different types of electrons reflected and collected to reproduce a high-resolution image of the sample are reported [127].

Sample morphology, at the nanometer scale, have been investigated through SEM technique on the carbonaceous residues obtained from pyrolysis. Shape, roughness, and elemental composition of the sample have been evaluated with SEM-EDX, studying different site of interest focusing on the sulfur distribution over the surface.

### *2.2.2. CHNS Elemental analysis*

**Fundamentals**:

CHNS analysis represents a fast approach to determine the elemental composition of materials in terms of hydrogen, nitrogen, carbon, and sulfur content. The basic principle of this technique is the sample combustion in a furnace using pure oxygen. Pure oxygen is usually required to limit the contribution of nitrogen present in the air during the combustion. In the combustion chamber carbon will be converted to $CO_2$, hydrogen to water, nitrogen to nitrogen oxides ($NO_x$) and sulfur to sulfur oxides. These gases will be then sent by an inert gas out of the combustion chamber and pass over high purity copper to ensure the complete oxygen removal and the conversion of nitrogen oxides to nitrogen.

Before reaching the detector, where different quantitative techniques can be applied, gases pass through an adsorbent trap that allow only the passage of $CO_2$, water, $N_2$ and $SO_2$ [128].

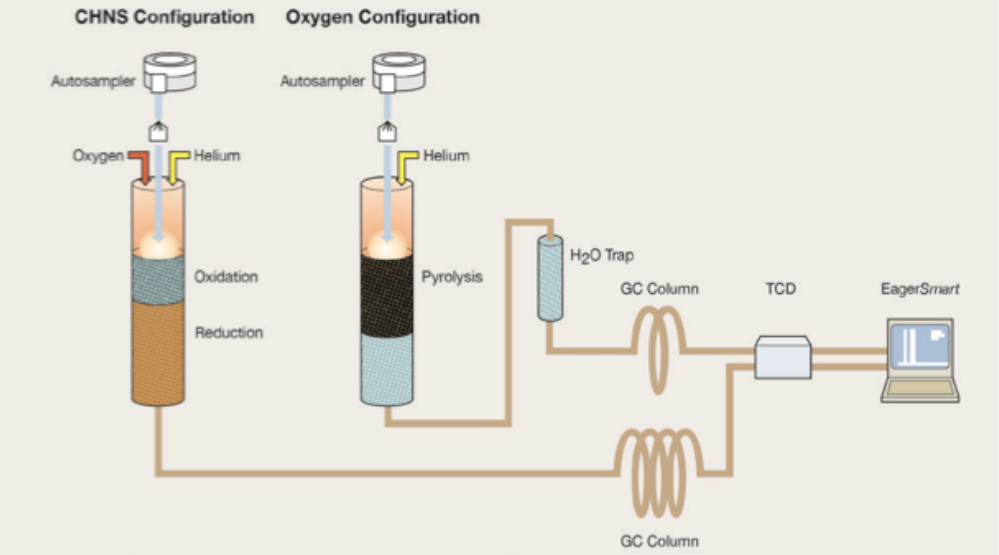


Figure 8: Graphical representation of the CHNS analysis procedure [129]

Figure 8 shows the schematic of CHNS instrument. CHNS technique have been used for the elemental characterization of pyrolysis residues and bio-oils produced during the pyrolysis experiments.

### *2.2.3. Fourier-Transform Infrared Spectroscopy*

**Fundamentals**:

Infrared spectroscopy is one of the most valuable analytical techniques. It can be used to study samples in any state, including liquids, pastes, powders, films, fibers, gases, and surfaces, by using the appropriate sampling technique.

A molecule to exhibit infrared absorptions, must possess a change in the electric dipole moment. The interaction between infrared radiation and matter is related to the change in molecular dipoles, which are associated to vibrations and rotations of the molecular bonds. A molecule can only absorb radiations when the incoming infrared radiation has the same frequency of one of the molecule fundamental modes vibrations. Vibrations can involve either a change in bond length (stretching) or bond angle (bending). Some bonds can stretch in-phase (symmetrical stretching) or out-of-phase (asymmetric stretching). Overtone bands in an infrared spectrum are multiples of the fundamental absorption frequency. Combination bands occur when two fundamental bands simultaneously absorb energy at different wavenumbers and the resulting band appears as the sum of the individual wavenumbers, making the spectra interpretation difficult for complex and unknown samples [130].

Fourier-Transform Infrared Spectroscopy (FTIR) is based on the interference of radiation between two beams that results in an interferogram, a signal produced by the change in their pathlength. Fourier-transformation methods allow to convert the distance in frequency. The radiation emitted by the beam source is passed first through an interferometer and then to the sample with the resulting signal collected by a detector (Figure 9). The produced spectra usually have a decreasing wavenumber from left to right and can be divided in *far-infrared* (<400 $cm^{-1}$), *mid-infrared* (4000-400 $cm^{-1}$), and *near-infrared* (>4000 $cm^{-1}$).

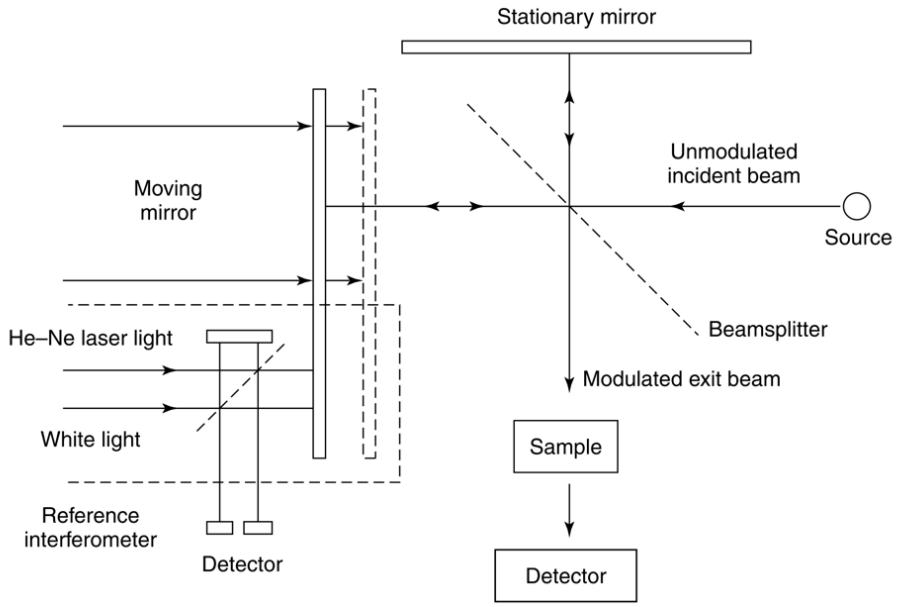


Figure 9: A general scheme of the main components of FT-IR spectrometer[130].

FT-IR analysis have been performed to have a better understanding of the composition of the raw materials, and the recorded spectra are reported in the different chapters. Moreover, this technique was used for the pyrolysis products characterization to have a qualitative idea of the products composition. This technique can give a suggestion on the possible different reaction pathways occurring during pyrolysis reaction.

### *2.2.4. Gas Chromatography-Mass Spectrometry (GC-MS)*

**Fundamentals:**

Gas chromatography-mass spectrometry (GC-MS) (Figure 10) is an important technique adopted for the identification and quantification of unknown mixture of liquid and gaseous compounds. The importance of this technique relies on the combination of gas chromatography for the separation of volatile and semi volatile mixtures, and mass

spectrometry for the identification of the compounds. In fact, GC can separate compounds but not properly identify them, while mass spectrometry identifies compounds without being able to separate them. Therefore, their coupling allowed to achieve good results filling the leakages of each technique.

In chromatography the liquid sample is dissolved in a solvent and then vaporized to separate the analytes [131]. Then, it is pushed by an inert carrier (mobile phase), through a stationary phase which can consist of solid adsorbents (gas-solid chromatography (GSC)), or liquids on inert supports (gas-liquid chromatography (GLC)). In general, the molecules separation occurs in a chromatographic column which can present different diameter size and length [132].

One of the main problems related to GC and MS coupling is related to operative pressures, since GC works almost at atmospheric pressure while mass spectrometry requires vacuum conditions. For this reason, an interface is necessary to direct the gas from GC to the MS, such as gas carrier spitters or gas carrier separators. The gas exiting from the GC column is sent to an ionization chamber where the sample is hit by high-energy electron beam. These electrons remove valence electron and convert molecules in molecular ions. An important parameter is related to the ratio between the mass and the charge of the ion (M/z). The mass analyzer separates the ions based on their M/z ratio and produce a mass spectrum which consist in an M/z ratio distribution graph. M/z ratio is often related to the molecular weight distribution of the molecule. Therefore, thanks to the mass spectrum is possible to identify the compounds present in an unknown sample.

Quantitative analysis can be performed by GC-MS analysis. Quantitation can be made analyzing the peak area of a compound on the mass chromatograms and compared in with the total area [133–136]. Multidimensional chromatography has been developed using different chromatography columns (mainly two) in series. Different configurations have been implemented and they have been classified into two categories: heartcutting 2D-GC or comprehensive two-dimensional gas chromatography (GC×GC). The latter has been used in thesis work and consists of two columns in series in which the interphase between them is a modulator. The sample exiting the first column is sent to the second one in the form of a pulsation, at a precise time intervals. This allows a first separation of single-column GC, while secondary separations are fast isothermal analyses conducted in series with a progressive temperature increase. The result is reported in a two-dimensional graph that allows a much higher resolution and separation of the analyzed mixture [137].

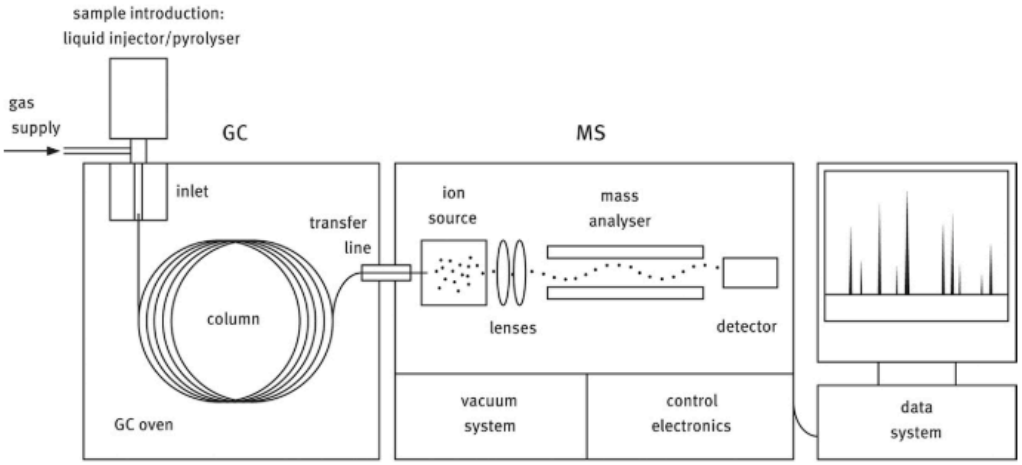


Figure 10: A scheme of the main components of GC-MS [138]

In this thesis, GC-MS instrument was used for the quantitation of the compounds present in the produced pyrolysis oils and gas. Due to the complexity of depolymerized products mixture multidimensional analysis have been performed as well on the hydrotreated oil obtained after catalytic upgrade.

### *2.2.5. Gel Permeation Chromatography (GPC)*

Gel permeation chromatography (GPC) (Figure 11) is one of the most used techniques adopted for the characterization of polymers molecular weight distribution. This process, also mentioned as size-exclusion chromatography (SEC), consist of a separation of the analytes in an unknown mixture through their effective dimensions. The separation of the analytes occurs merely from the mechanical point of view. Organic molecules are separated passing through a packed column with a specific and controlled pore size dimension. The molecules bigger than the pore-size are excluded while the smaller ones diffuse in and out the pores. As a main result, bigger molecules elute faster than smaller ones. Then, a proper separation occurs for the molecules that can penetrate through the column. Number average molecular mass ($M_n$), mass average molecular mass ($M_w$), peak molecular mass ($M_p$) and polydispersity ($M_w/M_n$) can be obtained with GPC analysis. Solubility can be a limiting factor for the analysis of organic molecules , however, the use of powerful solvent such as tetrahydrofuran can extend the applicability of this technique [139,140].

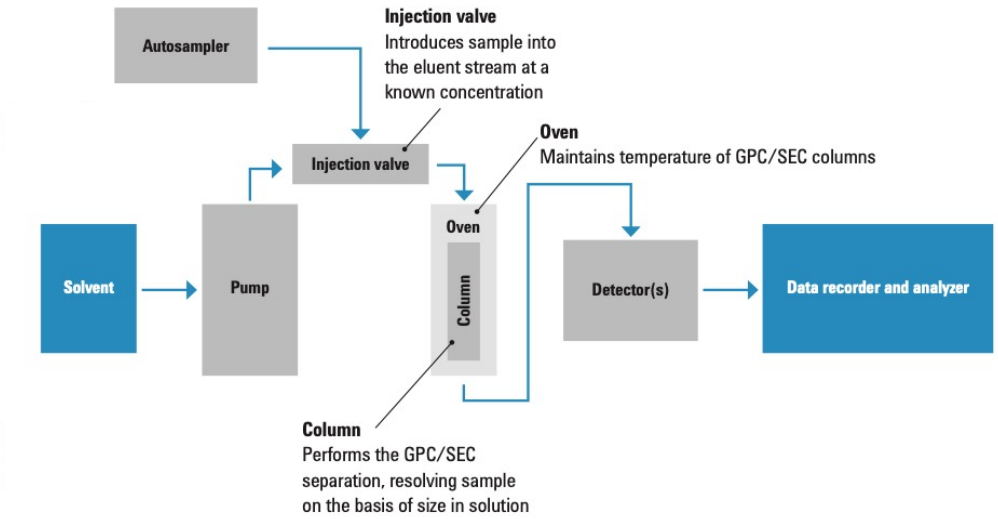


Figure 11: Representation of the main components of GPC analysis process, taken from Agilent Technologies Inc. [141]

Molecular weight distribution of different pyrolysis oil fractions obtained in the different tests have been evaluated to understand the effect of temperature. Moreover, the molecular weight distribution allows the monitoring of the lignin depolymerization, and to understand the efficiency of pyrolysis and hydrotreatment processes.

### *2.2.6. Nuclear Magnetic Resounance (NMR)*

Nuclear magnetic resonance spectroscopy is an important analytic technique giving information on molecule structures by observing the behavior of atomic nuclei immerged in a magnetic field (Figure 12). The interaction between the molecule and the magnetic field is obtained measuring the absorbance of radio-frequency magnetic radiation that stimulate a nuclear spin transition. The resulting NMR spectra contain information about atomic structure according to the position, intensity, and the peak splitting of resonance peaks. The molecular environment of nuclei influences the absorption of the radiation by each nucleus when immerged in a magnetic field. Therefore, each nucleus of a specific molecule generates its own spectral pattern.

Nuclear spin transitions are observable only in nuclei that have a spin nuclear magnetic moment different from zero such as $^{1}H$, $^{13}C$, $^{15}N$, $^{19}F$ and $^{31}P$. Most of the common isotope of carbon ($^{12}C$) for instance do not have a nuclear spin, thus, they cannot be detected with NMR analysis [142]. Protons are the most studied nuclei with NMR thanks to their abundance in organic and biological molecules. Therefore, $^{1}H$-NMR has a high sensitivity since $^{1}H$ protons are easily detectable. Other nuclei such as $^{13}C$ are also present in organic

matter, despite its abundance in nature is only around 1% of the $^{12}C$ isotope. The sensitivity of $^{13}C$ resonance is lower than the $^{1}H$ proton, and it can result in less peaks overlapping due to a wider frequency range for each signal [143].

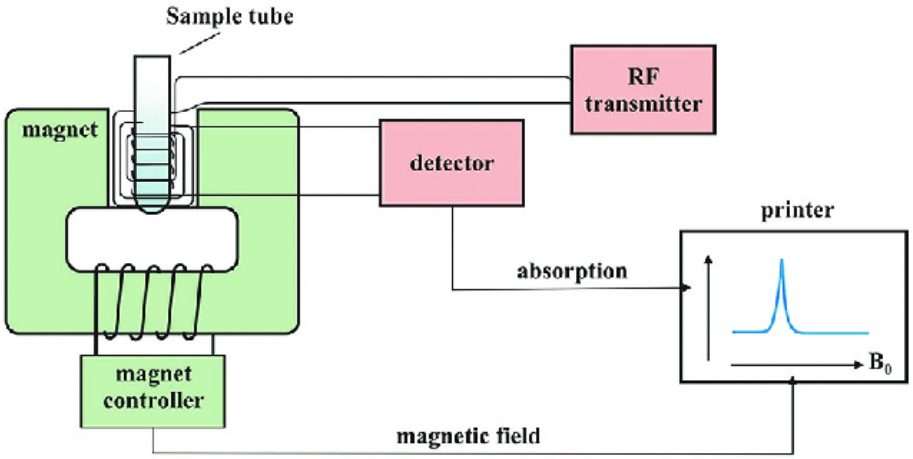


Figure 12:A graphic representation of NMR components. The sample is immerged in the magnetic fields generated by a magnet. The detector converts the absorbance of the radiofrequency into a spectrum characterizing the structure of the sample [144]

NMR technique was adopted to investigate the structure of the obtained pyrolysis oils. Moreover, it was also used to investigate the structural changes of the pyrolytic oil due to the hydrotreatment. In particular, $^{13}C$-NMR analysis was performed.

# *Chapter 3. Pyrolysis of Kraft Lignin: optimization of reaction temperature and product analysis procedures*

Data reported in this chapter has been already published:
Borella,M.; Casazza,A.A.; Garbarino,G.; Riani,P.; Busca,G., A Study of the Pyrolysis Products of Kraft Lignin, Energies, 2022, 15, 991. https://doi.org/10.3390/en15030991, [145]

In this paper, commercial Kraft lignin has been pyrolyzed at different process conditions in the absence of a catalyst. The resulting products have been separated and quantified to give a better understanding of the chemical distribution of the cracked compounds. In addition, the chemical composition of the liquid fraction has been studied. Liquid–liquid extractions have been performed with the aim to extract aromatic compounds to evaluate the feasibility of separation processes and the identification of valuable molecules.

## *3.1. Materials and methods*

### *3.1.1. Materials*

Sample morphology and elemental compositions were investigated by means of a Zeiss Evo 40 equipped with a Pentafet Link Energy Dispersive X-ray Spectroscopy system managed by the INCA Energy software (Oxford Instruments, Analytical Ltd., Bucks, UK).

### *3.1.2. Fresh Lignin Characterization Procedures*

Fresh Kraft Lignin (KL) was characterized by focusing on ash and moisture content, elemental composition, and morphology. Moisture and ash content were measured in agreement with AOAC methods [146]. Morphology was investigated by scanning electron microscopy (SEM), while the elemental composition of KL was determined through energy-dispersive X-ray spectroscopy (EDX). These analyses were performed on fresh KL and on pyrolytic residues to evidence the influence of the reaction temperature on morphological properties. EDX focused on the composition in terms of C, Na, S, and O content, describing how their distribution varies with the reaction conditions.

### *3.1.3. Pyrolysis Setup*

The reactions were carried out following the scheme reported in Figure 13. The reaction system consists of a quartz tubular reactor (2 in Figure 13) charged with 5 g of KL (3) and collocated in an oven (1, Carbolite, MTF 10/25/130, Pocklington, UK). A nitrogen purge was needed to guarantee oxygen removal and to avoid a combustion reaction. Three temperatures, 350, 450, and 550 °C were investigated and kept for a reaction time of 3 h. The reactor was connected to a Liebig condenser (5) that allows the condensation of low boiling compounds. The liquid condensate (L) was recovered in a flask (7) while non-condensable gases (G) were collected in a latex balloon (6). The condensed liquid fraction shows two phases: an aqueous light phase observed on top and an organic heavy phase in the bottom part of the flask. At the reaction end, a solid was still present in the reactor as biochar, and it is referred to as a solid residue (SR). Data reproducibility was evaluated by running each experiment three times, allowing us to assess good data consistency.

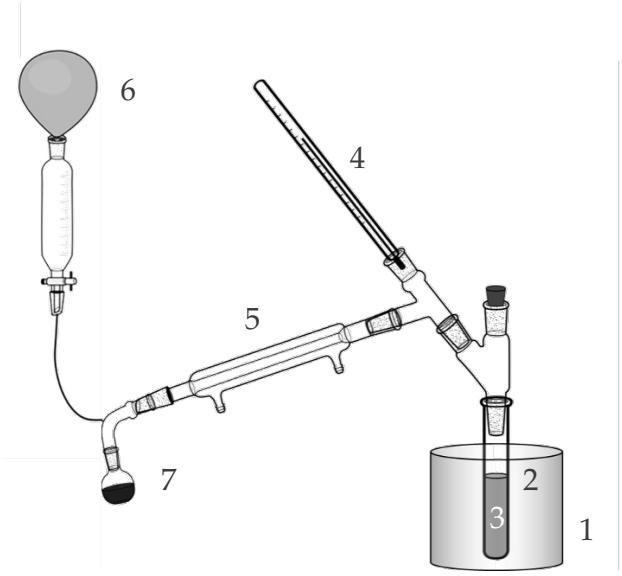


Figure 13: The experiment setup used for the pyrolysis reaction. The Kraft lignin (3) is positioned inside the oven (3). A condenser (5) allows the separation of the oil(7)and a gas (6). The residue remains in the tubular reactor (2).

### *3.1.4. Extraction Procedures*

As stated above, the qualitative analysis of liquid fraction L was performed by means of L–L extractions. An amount of 1.0 mL of chloroform ($CHCl_3$) was used to dissolve the L fraction and characterize it with GC-MS. Even though L is constituted by two separated phases, the aqueous fraction represents a negligible part of the total liquid. Moreover, the GC-MS analysis was performed only on the chloroform soluble fraction which was

separated from the water phase by means of a centrifuge step. Two different liquid extractions were then performed on the chloroform-diluted L products: one with EtOH/$H_2O$ (1:1 *v*/*v*) and a second with alkaline $H_2O$ 0.1 M. Then, the extraction solution was agitated and centrifuged using a centrifuge set to 7500 rpm for 10 min. In both cases, the resulting solution separated into two phases: a heavy phase (HL) consisting of bio-oil diluted in chloroform and a lighter phase (LL) with the compounds extracted from the solutions. LL was then analyzed using FT-IR spectroscopy while HL was analyzed by means of GC-MS. To individuate all the species in the HL, all the relevant peaks of the resulting chromatogram were integrated manually.

### *3.1.5. Equipment and Characterization Procedures*

Both KL and pyrolysis products (L, SR, G) were analyzed using Fourier transform infrared spectroscopy (FT-IR) by means of a Nicolet 380 instrument (Thermo Scientific, Madison, WA, USA). Reaction liquids were characterized by spreading a drop of sample on a KBr disk (disk weight 1000 g) of powdered KBr. The solid residue was analyzed using a pressed disk of KBr mixed with samples (1:100, *w*/*w*) while gaseous products were imposed to pass in an IR glass cell with KBr windows. For both liquid and gaseous products, additional analyses were performed in a gas chromatography–mass spectrometer (GC–MS) Focus-ISQ equipped with a single quadrupole detector (Thermo Scientific, Milan, Italy) using a TG-SQC column (15 m × 0.25 mm × 0.25 μm). Helium (>99.99) was used as a gas carrier (1 mL/min) and the injection temperature was set at 230 °C. The oven temperature changed according to the following conditions: 70 °C for 5 min, then the temperature was increased from 70 to 270 °C, at 5 °C/min, from 270 °C to 320 °C at 25 °C/min, and finally left at 320 °C for 25 min. A quantitative analysis was carried out by injecting 100 μL of reaction gas into the GC-MS. For each test, four injections were performed in total, one every 45 min of reaction time, to monitor the changes in gas composition over the reaction time. The areas of the resulting peaks related to the individual species detected were normalized with the area of the total injection to quantify the relative amount of the different species in the sampled gas.

Reaction liquids and extraction bio-oils were analyzed with an analogous procedure, diluting the liquid sample with 1 mL of $CHCl_3$ up to a ratio of 1:10 (*v*/*v*). A Scanning Electron Microscope (SEM) was used to investigate the commercial Kraft lignin and biochar residues morphology.

## 3.2. Results and discussion

### 3.2.1. Characterization of Fresh Lignin

The fresh lignin was characterized by measuring its ash content (~1 wt.%) and humidity content (~3 wt.%). An SEM analysis at low magnification (Figure 14) shows the presence of particles/aggregates whose maximum size is around 20 μm or less. Simultaneously realized EDX analysis is reported in Table 1. It must be remembered that this analysis does not detect hydrogen. The measured O/C ratio is 0.47. The EDX analyses are in rough agreement with the elemental analyses reported for Kraft lignin samples [147]. In particular, the EDX elemental analysis revealed the presence of sulfur and of sodium, in accordance with Latham et al. [148], which is related to lignin pretreatment with white liquor, a solution of NaOH and $Na_2S$, performed to isolate lignin from the other components of wood in the Kraft process [148].

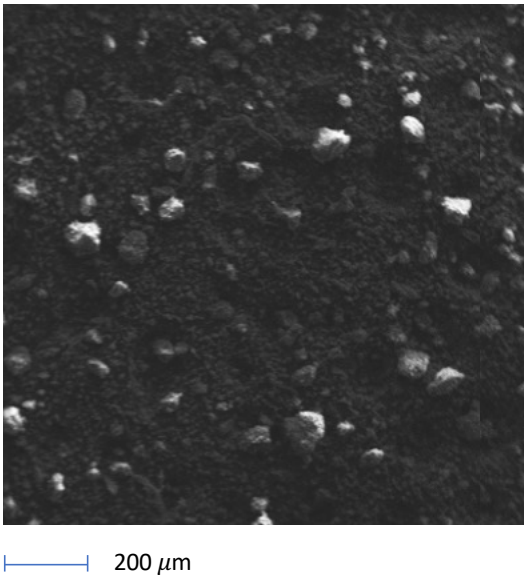


Figure 14: SEM analysis of fresh Kraft lignin.

Table 1: SEM-EDX analysis of fresh lignin and reaction residues at different temperatures.

| Pyrolysis Temperature | C (%) | O (%) | Na (%) | S (%) |
|---|---|---|---|---|
| As received | 67.1 | 31.6 | 0.2 | 1.1 |
| 300 °C | 70.2 | 28.6 | 0.5 | 0.7 |
| 350 °C | 73.7 | 24.6 | 0.5 | 1.3 |
| 450 °C | 82.0 | 16.2 | 0.5 | 1.3 |
| 550 °C | 89.8 | 7.7 | 0.7 | 1.9 |

The FT-IR spectrum of KL is shown in Figure 15. The strong band centered at 3418 $cm^{-1}$ is due to the OH stretchings of phenolic and alcoholic (polysaccharidic) groups together with water. Aromatic and aliphatic $CH_x$ stretching bands are evident in the region of 3100–2800 $cm^{-1}$. The band at 1705 $cm^{-1}$, with a shoulder around 1740 $cm^{-1}$, is due to the C=O stretchings of carbonyl and carboxyl (ester) groups. The stretchings of C-C bonds in aromatic rings can be related to the peaks at 1597, 1513, 1453, and 1426 $cm^{-1}$, while the peak at 1463 $cm^{-1}$ is likely mainly due to $CH_2$ deformation (scissoring) modes. In this region, OH deformation modes of cellulosic units are also present. The peak at 1362 $cm^{-1}$ is usually assigned to phenolic OH in-plane deformation modes, while the many peaks in the range of 1300–1000 $cm^{-1}$ are due to C-C and C-O coupled stretchings in different structural units. The region below 1000 $cm^{-1}$ is mainly associated with out-of-plane CH and OH bonds. The spectrum is fully consistent with those reported for Kraft lignin by different authors [149,150].

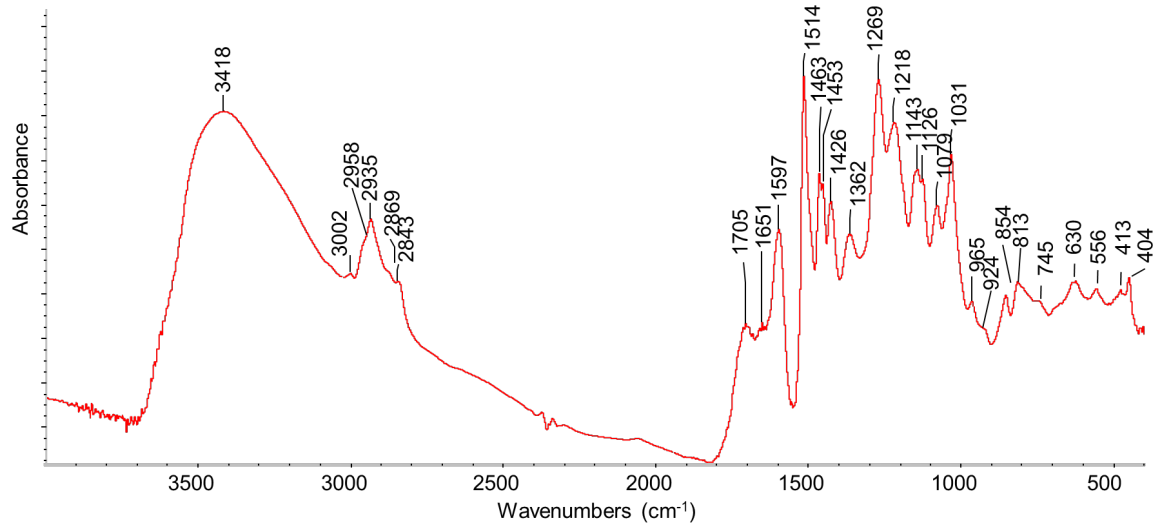


Figure 15: FT-IR spectrum of fresh Kraft lignin.

### *3.2.2. Effect of Reaction Temperature on Product Distribution*

The effect of reaction temperature on product distribution is shown in Figure 16. The yields were evaluated via gravimetric measurements on liquid and biochar after the reaction. The amount of gas has instead been calculated from mass balance. The amount of solid residue (SR) tends to decrease with increasing reaction temperature. Indeed, the SR at 350 °C is 72 wt.% while at 550 °C it is lowered to 42.7 wt.%. The gas production (G) remains almost

constant during all the tests with a slight increase at high temperatures. Interestingly, the amount of liquid (L) is strongly affected by the reaction temperature. At 350 °C the L production is negligible while the highest yield is obtained at 550 °C, where it reaches 28.7 wt.%. Indeed, product yields in biomass pyrolysis are strongly affected by both feedstock characteristics and reaction conditions, and, for this reason, different values can be found in the literature. Setter et al. [151], for example, studied the influence of different percentages of Kraft lignin on the bio-oil obtained from sugarcane bagasse pyrolysis resulted in a maximum yield in bio-oil between 400 and 550°C and a decreasing trend in biochar production with increase of the temperature, in agreement with our data.

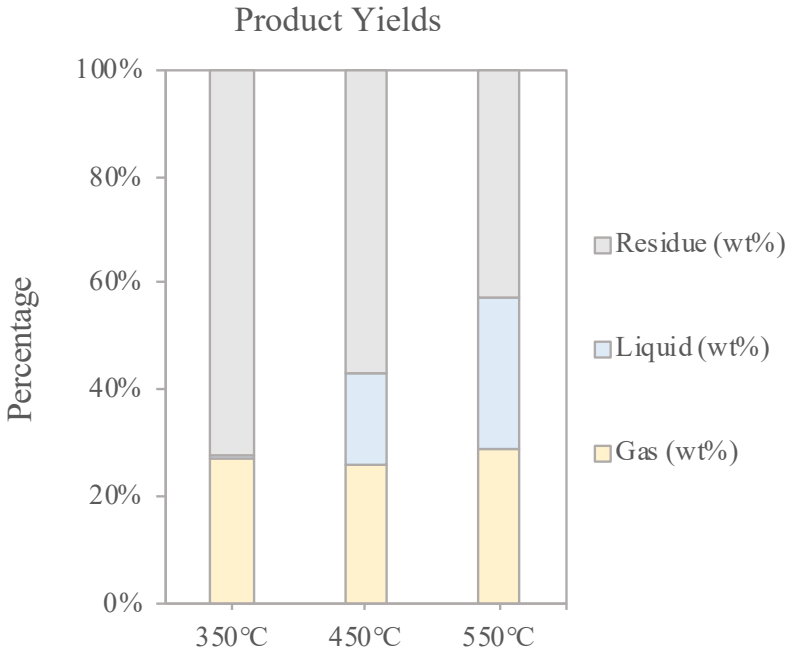


Figure 16: Pyrolysis product yields distribution at 350, 450, and 550 °C.

### *3.2.3. Solid Residue (Biochar) Characterization*

The solid residue (SR) that remains at the bottom of the reactor after the pyrolysis reaction is usually denoted as biochar. In general, it is essentially a carbon residue, and when it has high porosity, it may have interesting applications as an activated carbon [152,153]. In our case, SEM images (Figure 17) show that in the case of the sample treated at 300 °C the observed particles or aggregates had already grown significantly in size with respect to the original lignin particles, up to a predominant size of around 0.2 mm. Further heat treatments gave rise to further increases, at least of part of particles/aggregates, up to >0.5 mm. The elemental analysis data (EDX) of SRs are reported in Table 1 and compared with data for fresh lignin. The carbon content increases with increasing pyrolysis temperature, starting

from 67 wt.% in fresh lignin up to 89.76 wt.% in the sample obtained at 550 °C. Na wt.% content in the solid grows with pyrolysis temperature, showing that it does not participate in volatile or liquid products. The behavior of sulfur is more complex, showing that it decreases significantly at low pyrolysis temperatures, while its wt.% increases at the highest temperatures. This indicates that sulfur is in part released in the form of volatile or liquid compounds at low temperatures, while it in part forms non-volatile compounds still strongly bonded to biochar at higher temperatures. The amount of oxygen exhibits a percentage drop which can be attributed to the formation of highly oxygenated gases and vapors which are in part collected as bio-oil after their cooling in the condenser.

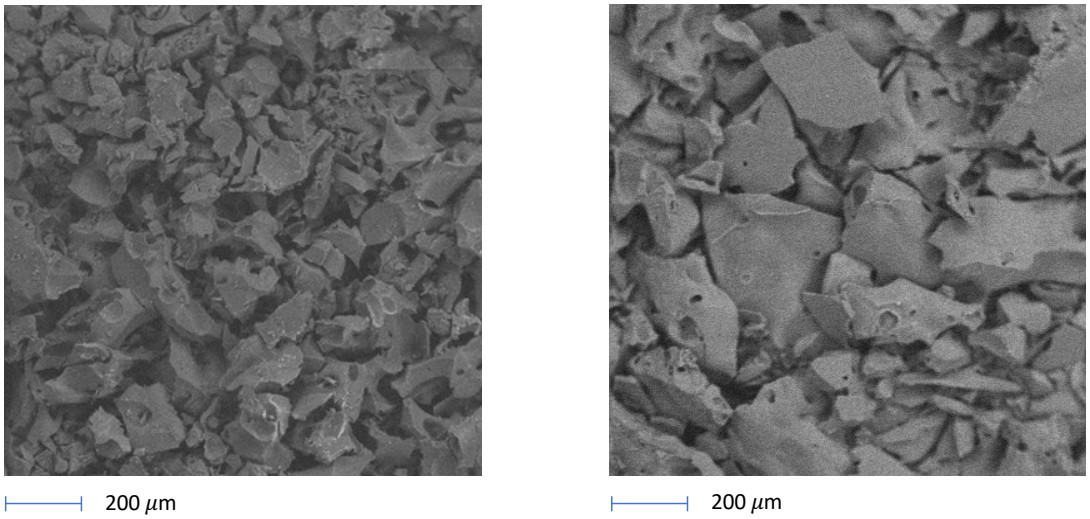


Figure 17: SEM pictures of biochar materials after pyrolysis reactions at (a) 300 °C and (b) 550 °C, respectively.

The FT-IR spectra of the samples produced at the different pyrolysis temperatures (Figure 18) show a relatively high absorption baseline and, together with absorptions of some water (3445 and 1614 $cm^{-1}$), a few weak bands in the C-H stretching region (3100-2800 $cm^{-1}$) as well as in the region below 1700 $cm^{-1}$, where CH deformations and the stretching of double and single CC and CO bonds fall. Interestingly, the absorption in the region of C=O double bond stretchings appears to be fully disappeared. This spectrum is typical of highly carbonaceous solids, with few residual functional groups. The comparison of this spectrum with that of the starting lignin sample shows that lignin is largely decomposed and carbonized, in agreement with the EDX data. However, it is possible that carbonized matter, which strongly absorbs the IR radiation, masks the permanence of the features of still incompletely converted lignin.

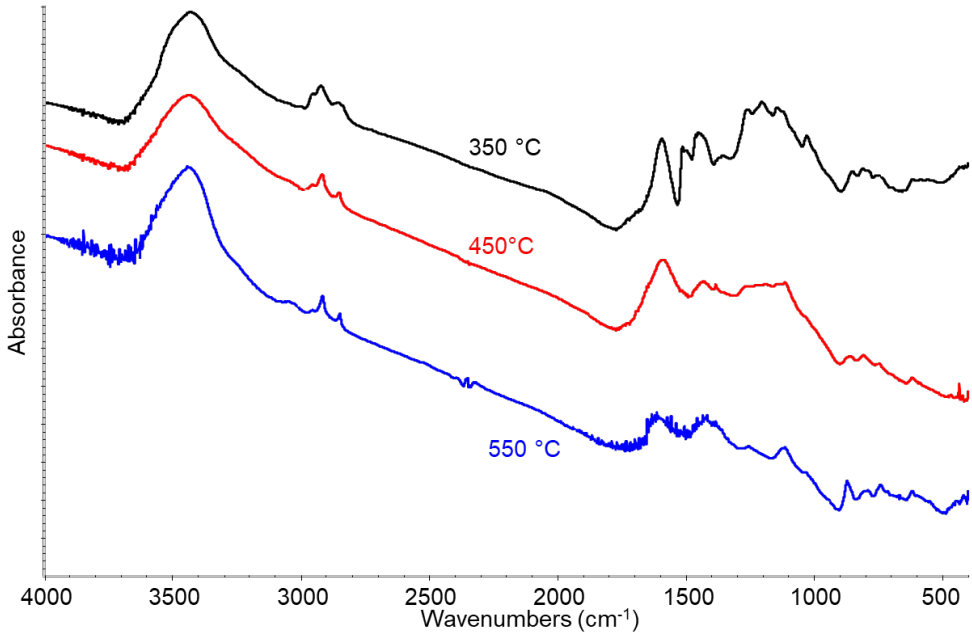


Figure 18: FT-IR analysis of SR at 350, 450, and 550 °C.

### *3.2.4. Gas Products Characterization*

In Figure 19, the IR spectra of gases obtained by lignin pyrolysis are reported. All the spectra show the presence of rotovibrational bands centered at 3715, 3612, 2345, and 667 $cm^{-1}$ due to carbon dioxide (combination modes, asymmetric stretching, and deformation modes, respectively), at 3011 and 1304 $cm^{-1}$ due to $CH_4$ (stretching and deformation modes), at 2140 $cm^{-1}$ due to the stretching mode of carbon monoxide, and at 2062 $cm^{-1}$ due to carbonyl sulfide (COS asymmetric stretching). Moreover, the expansion of the spectra after treatments at higher temperatures show the presence of ethylene associated with the peak at 949 $cm^{-1}$ (c) and of propylene (band at 911 $cm^{-1}$), while the rotovibrational C-O stretching band of gaseous methanol centered at 1032 $cm^{-1}$ is evident in particular in the spectrum of the gas obtained by pyrolysis at 450 °C. Casazza et al. [154] investigated, at the same temperatures used in this study, the pyrolysis of grape marc, where lignin is present in significant amounts. They did not observe the formation of COS and other sulfur compounds in the resulting gas, where instead nitrogen-containing molecules were found due to the decomposition of protein compounds.

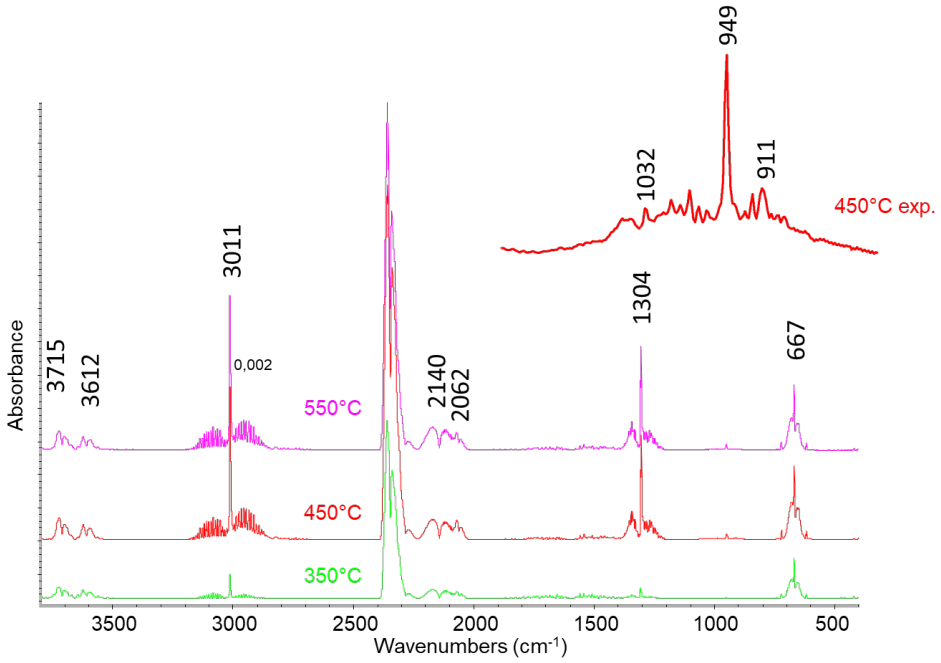


Figure 19: FT-IR analysis of pyrolysis gas at 350, 450, and 550 °C.

GC-MS analysis of gases detects all the products observed by IR with additional components, which are not detected or detectable in the IR spectrum or have a low concentration in the composition of the pyrolysis gas. Together with small amounts of some light hydrocarbon and oxygenated compounds (i.e., ethanol), in particular, the GC-MS results revealed the presence of other sulfur compounds in G such as $CH_3SH$, $CH_3$-S-$CH_3$, $SO_2$, $H_2S$, and $CS_2$. The evolution of the sulfur-containing species during the reaction time was monitored using a relative abundancy parameter, R, calculated as the ratio between the areas underlying the peak of the considered sulfur species in the chromatogram and the areas of the total compounds in the injection in GC-MS. Figure 20 represents the time–temperature evolution of these compounds, where each histogram represents every GC-MS injection performed during each test. The pyrolysis temperature influences the quantity of sulfur-containing compounds produced, but it does not affect their time evolution. Since gas is mainly produced in the first part of the reaction experiment at each temperature, the R parameter tends to remain constant during the 3 h of the reaction time. However, there are some exceptions: dimethyl sulfide ($CH_3$-S-$CH_3$) and methyl mercaptan ($CH_3SH$) have a drop in the concentration through the reaction time, while the concentration of hydrogen sulfide ($H_2S$) slightly increases. The changes in the $H_2S$ content are barely detectable since it is by far the most relevant compound in the gas mixture and its relative abundance parameter is one order of magnitude greater than that of the other compounds. Our data are different from those of Yan et al., who performed a thermogravimetric analysis on Kraft lignin showing

hydrogen sulfide as the only relevant sulfur compound detectable, whose production is restricted to a temperature range between 300 and 450 °C [155].

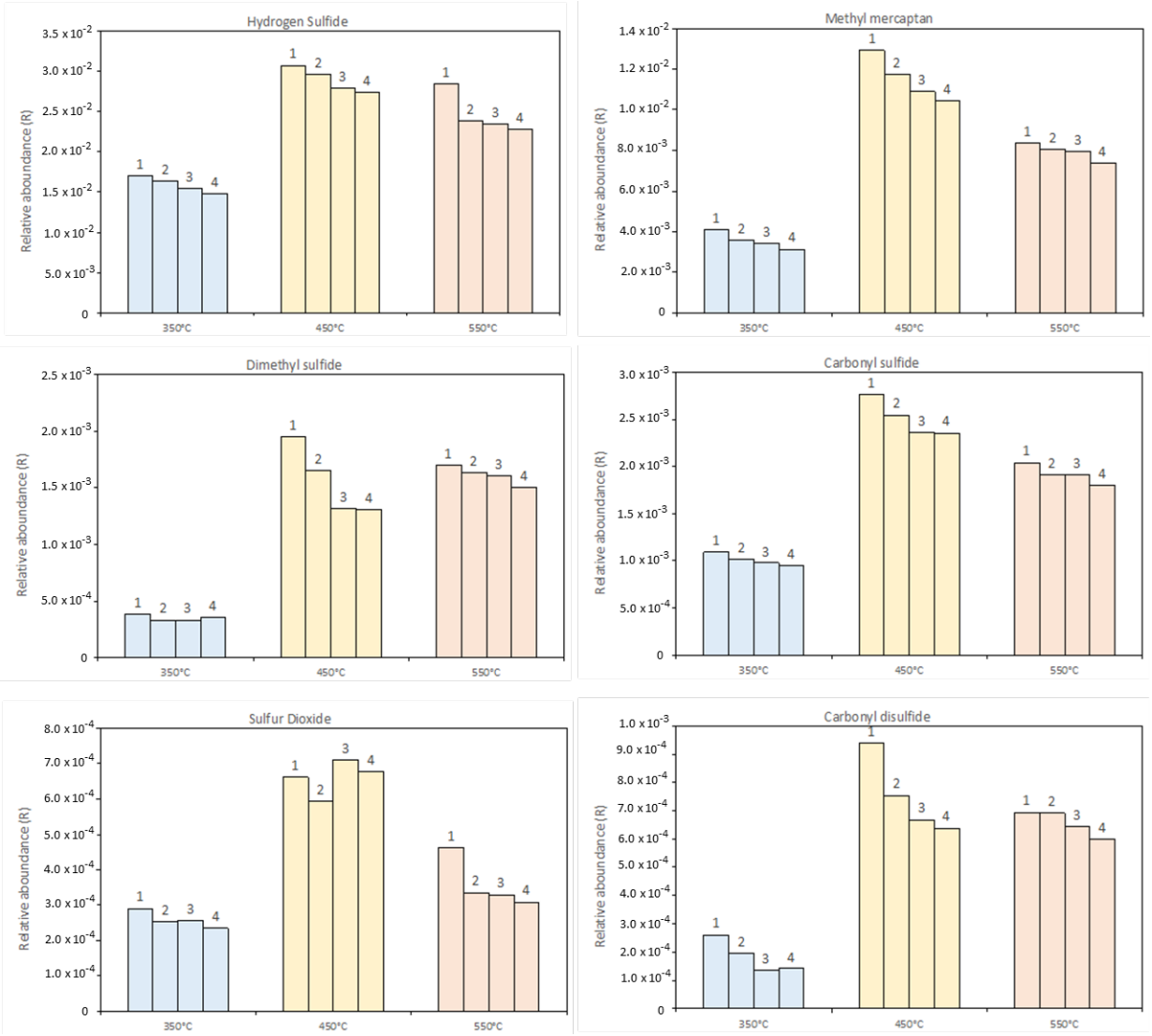


Figure 20: Evolution of sulfur-containing compounds during the reaction. GC-MS analysis after (1) 45 min, (2) 90 min, (3) 135 min, and (4) 180 min of reaction time.

### *3.2.5. Liquid Products Characterization*

FT-IR analysis was performed on the L fractions, usually denoted as “bio-oils”, as shown in Figure 21. After pyrolysis at 350 °C the spectrum of the liquid is dominated by the features of water (OH stretchings at around 3400 $cm^{-1}$, the scissoring mode at around 1620 $cm^{-1}$, broad “vibrational” modes around 600 $cm^{-1}$), although some weak features indicate that organic molecules are also present, dissolved in it. An expansion of the spectrum reveals its similarity with that of water glucose or mixed sugars solution (in particular, the doublet at

1049, 1032 $cm^{-1}$) [156]. This suggests that in these conditions some dehydration process occurs together with the hydrolysis/dissolution of polysaccharide residuals. After higher temperature pyrolysis, the spectrum of the resulting bio-oil, much more abundant, shows the presence of a wide range of compounds. Indeed, the spectra of the bio-oils produced at 450 and 550 °C are essentially the same and are closely similar to that of the starting solid lignin. This suggests that the liquid produced is constituted by "monomeric" or less polymerized species, retaining the same functional groups of lignin. The most evident differences between the spectra of lignin and bio-oils are that the band at 1079 $cm^{-1}$, well evident in the lignin spectrum, is not evident in the spectrum of bio-oils, while in the CH stretching region, peaks at 3054 and 2959 $cm^{-1}$ are relatively stronger. Moreover, the bands at 791 and 747 $cm^{-1}$ are much stronger, relatively, in the spectrum of bio-oils than in that of lignin. These spectral modifications could be associated with the reduced number of methoxy groups associated with methanol evolution in the gas phase.

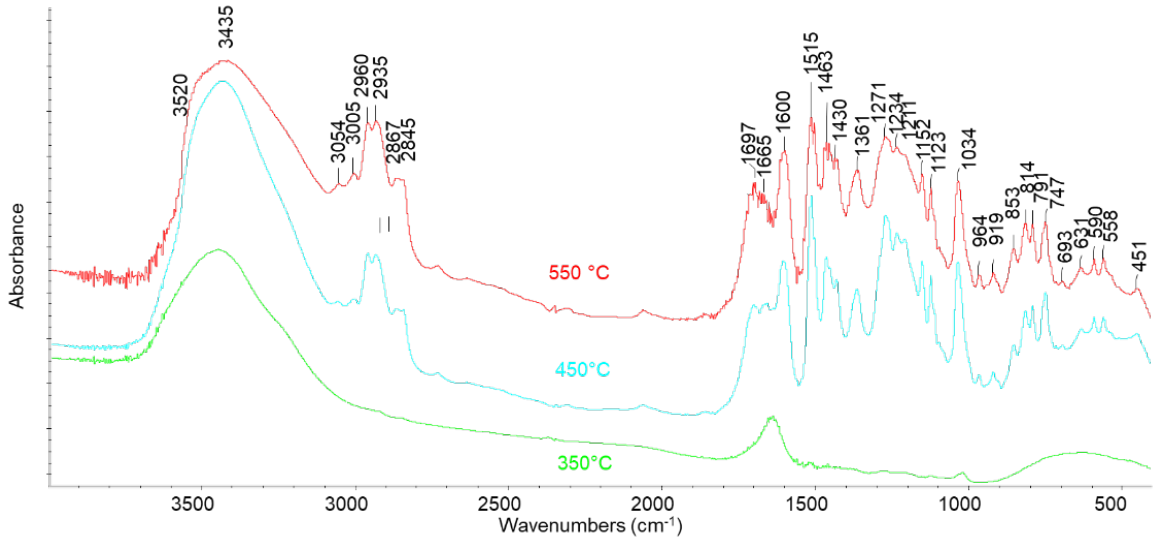


Figure 21: FT-IR spectra of L pyrolysis fraction at 350, 450, and 550 °C.

L characterization with GC-MS was realized after an extraction/dilution step with $CHCl_3$. The liquid produced during the pyrolysis process consists of two separated phases: a bottom-heavy oily phase and an aqueous top phase. Despite the aqueous phase being clearly visible, it represents a negligible percentage of the total liquid mass. Thus, the extraction with $CHCl_3$ previous to the GC-MS analysis was performed on the total L produced. The $CHCl_3$-soluble fraction was separated from the aqueous phase by means of a centrifuge step, and then it was analyzed in the GC-MS (Table 2). The characterization was only performed on liquids produced in the tests at 450 °C and 550 °C, due to the low liquid yield at 350 °C (~1 wt.%).

Table 2: List of most relevant compounds detected from the GC-MS analysis of bio-oil reported as area percentage (%).

| | 450 °C | | | 550 °C | |
|---|---|---|---|---|---|
| **Compound Name** | **$CHCl_3$** | **Ethanol/$H_2O$** | **NaOH/ $H_2O$** | **$CHCl_3$** | **NaOH/ $H_2O$** |
| Furfural | 0.57 | 0.36 | 3.11 | 0.32 | 3.35 |
| Ethylbenzene | 0.18 | 0.16 | 1.33 | 0.16 | 1.81 |
| o-Xylene, Benzene, p-Xylene | 0.10 | 0.11 | 1.15 | 0.16 | 2.25 |
| styrene | 0.09 | – | 1.32 | 0.09 | 1.23 |
| propanal 3 methyl thiol | 0.11 | – | 1.40 | 0.10 | 1.06 |
| Phenol 2-methoxy or 4-methoxy | 19.35 | 11.43 | 2.08 | 8.66 | 1.50 |
| disulfide, methyl (methyl thio) methyl | 0.39 | 0.27 | 4.73 | 0.01 | 2.88 |
| 2 methoxy-6-methyl Phenol | 1.21 | 1.11 | 2.18 | 0.94 | 1.57 |
| 3 methoxy-5-methyl Phenol | 34.05 | 23.70 | 13.43 | 16.57 | 8.72 |
| 1-2 Benzenediol | 2.11 | 1.72 | – | 2.65 | 0.67 |
| 3,4 dimethoxy Toluene | 0.24 | 0.31 | 4.05 | 0.52 | 3.31 |
| 2 ethoxy methyl phenol | 1.02 | 1.59 | – | 1.55 | 0.94 |
| Phenol 4 ethyl 2-methoxy | 14.41 | 10.59 | 23.10 | 8.84 | 17.92 |
| 1-2 Benzenediol 4-methyl | 1.30 | 1.94 | – | 3.58 | – |
| 2-methoxy-4-vinilphenol | 0.85 | 1.81 | – | 2.51 | – |
| benzene 4 ethyl 1-2 di methoxy | 0.17 | 0.36 | 1.34 | 0.28 | 0.88 |
| Eugenol | 0.99 | 1.62 | 3.81 | 1.13 | 1.76 |
| Benzene, 4-ethyl-1,2-dimethoxy- | 0.41 | 0.77 | 5.57 | 0.78 | 33.87 |
| phenol 2-methoxy-4-propyl | 1.15 | 2.38 | 9.74 | 1.88 | 7.19 |
| 4-ethyl catechol | 0.56 | 0.97 | – | 1.66 | – |
| vanillin | 1.18 | 1.85 | – | 1.40 | – |
| phenol 2 methoxy-4-propenyl | 0.59 | 1.47 | 1.51 | 1.45 | 1.05 |
| 1,4-benzenediol, 2,3,5, trimethyl | – | – | 1.49 | 0.29 | – |
| phenol 2 methoxy-4-propenyl | 4.05 | 6.51 | 5.19 | 5.04 | 3.71 |
| Ethanone (1-3 hydroxy-4-methoxyphenyl) | 1.29 | 2.60 | – | 3.22 | – |
| 1-2 dimethoxy 4 n propyl benzene | 0.11 | 0.27 | 1.07 | 0.58 | – |
| 2-propanone (1-3 hydroxy-4-methoxyphenyl) | 0.29 | 1.99 | – | 1.88 | – |
| 3 ethoxy 4 methoxy benzaldehyde | 0.58 | 1.18 | – | 1.27 | – |
| 4-(3-methoxy phenyl) propyl cyanide | – | – | 2.45 | – | – |
| methyl 2-hydroxy-3-ethoxyBenzylEther | 1.50 | 3.25 | – | 3.65 | – |
| L-4-Hydroxy-3-methoxyphenylalanine | 0.11 | 0.22 | 1.30 | 0.24 | – |
| 2-isopropyl-10-methyphenantrene | 0.24 | 0.49 | 1.38 | 1.71 | 1.36 |
| 1,1′-Biphenyl, 2,2′-dimethyl-6,6′-dinitro- | 0.43 | 0.68 | – | 2.34 | – |
| Phenol, 2-methoxy-4-propyl- | 1.38 | 4.56 | – | 4.31 | – |
| Phenanthrene carboxylic acid | 0.33 | 0.72 | 3.07 | 1.01 | 0.94 |
| Phenol, 2-methoxy-4-propyl- | 0.37 | 1.22 | – | 0.98 | – |
| 4 diethyl amino phenyl isothiocyanate | 0.58 | 1.70 | – | 1.81 | – |
| Phenanthrene carboxylic acid | 0.37 | 0.82 | – | 2.12 | – |
| Phenol, 2-methoxy-4-Propyl- | 0.27 | 0.83 | – | 1.01 | – |

The GC-MS analysis of the liquid extracted after pyrolysis at 450 °C, in agreement with the IR analysis, shows the presence of many oxygenated aromatic compounds, with a large predominance of alkyl- and alkoxy-phenols (Figure 22). Alkyl phenols have been considered

as a separated class of compounds since their importance as high-value intermediates can influence the economic feasibility of the process. In the other oxygenated compound fractions, alcohols, ketones, ethers, carboxylic acids, methoxy alkanes, aromatics, aldehydes, and esters have been included. Among them, benzenediols, i.e., catechol, resorcinol, hydroquinone, and some alkyl-derivatives are present. However, sulfur is also present in a few non-aromatic compounds. A small amount of hydrocarbons is also observed. In this fraction, alkyl benzenes, xylenes, and styrene are present. In particular, the main peak corresponds to 3 methoxy-5-methyl-phenol, while strong peaks are also those corresponding to the two isomeric compounds 2-methoxy-phenol (guaiacol) and 4-methoxy-phenol and to 4-ethyl-2-methoxy-phenol. The peaks of these four compounds correspond to more than 65% of all GC spectra in the liquid obtained by pyrolysis at 450 °C, as shown in Figure 23, where the chromatograms obtained from the GC-MS analysis of the $CHCl_3$-diluted bio-oil are reported. The same compounds are also the most abundant after pyrolysis at 550 °C but their amount decreases significantly at this temperature. The reaction liquid composition is completely different from that obtained from the pyrolysis of vegetable oils. Phung et al. [157] studied the conversion of palm oil at 450 °C, and the produced liquid was mainly composed of C8-C16 hydrocarbons. Furthermore, the thermal treatment of plastics (PET, PU, PVC, etc.) led to liquids with different compositions in the function of the used polymer [158].

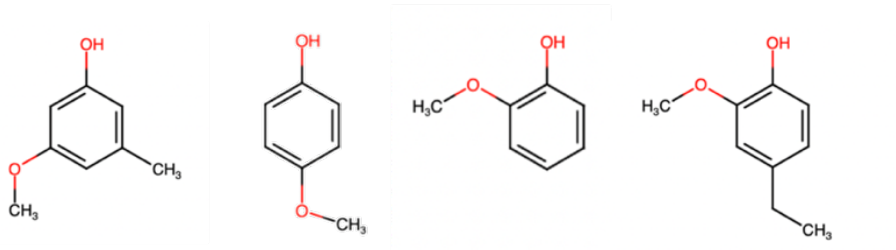


Figure 22: Structures of the most abundant compounds in liquid pyrolysis products.

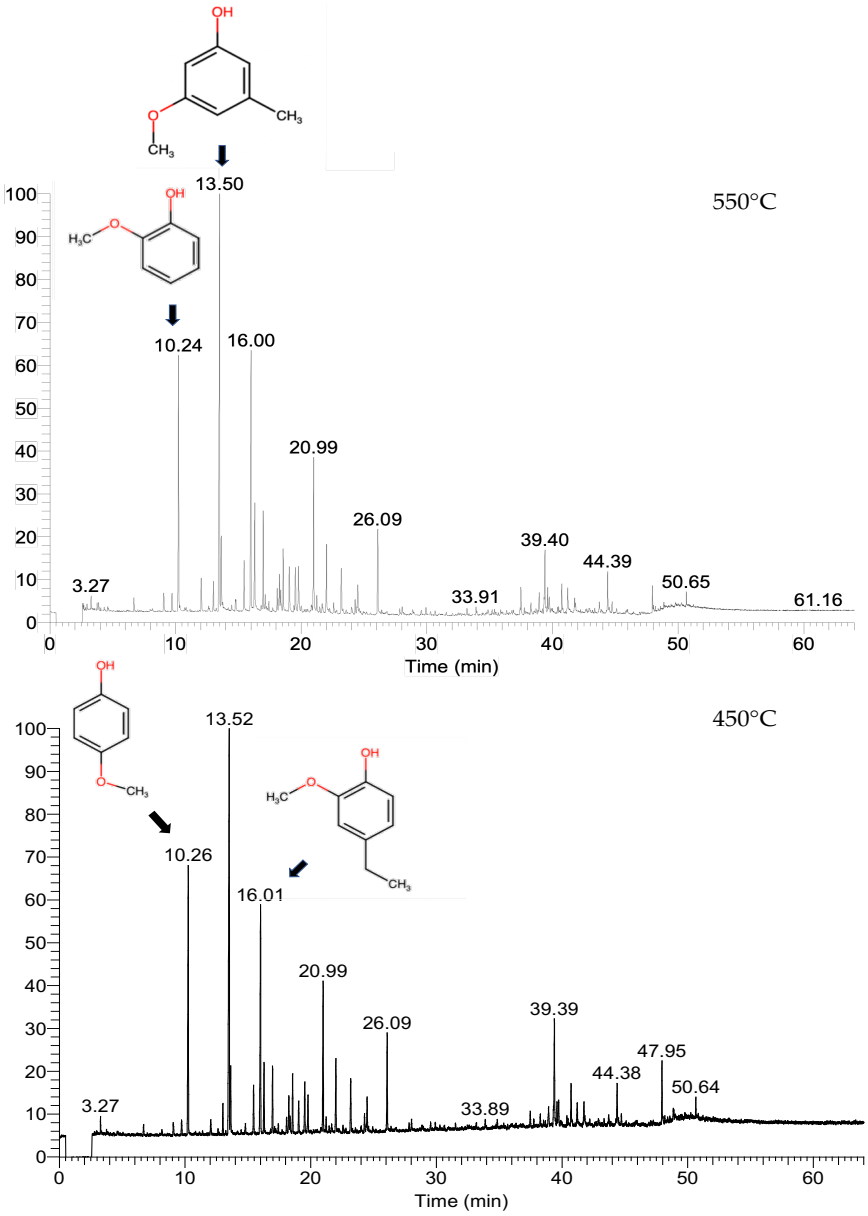


Figure 23: GC-MS chromatograms of the $CHCl_3$-diluted bio-oil produced at 450 and 550 °C.

Once the composition of the L fraction was determined, two different extractions were made with the main objective of extracting phenolic-like compounds from the liquid. The solvents that were used in this process are ethanol/water and NaOH/water solutions, as described in the methods section. Figure 24a shows the changes in the composition of the bio-oil obtained. The phenolic fraction decreased by 13 and 30% in the raffinate bio-oils obtained by extracting with ethanol/water and NaOH/water solutions, on the L produced at 450 °C, respectively. The higher extraction power of the alkaline solution is due to the acid behavior of phenols in solution, and for this reason, only the NaOH/water solution was added to the L produced at 550 °C. In this case, a 31% reduction was also obtained, as shown in Figure 24b. After extraction with the ethanol/water solution, the resulting re-fined bio-oil also had

a lower amount of sulfur compared to the one obtained with NaOH/water, even if the extracted fraction of phenols was smaller. This suggests that sulfur compounds were also extracted. In contrast, alkaline water solution allows the better extraction of alkyl phenols but the percentage of sulfur in the bio-oil increases together with hydrocarbon and oxygenated compound fractions. Similar behavior can be noticed for the extractions performed at 550 °C.

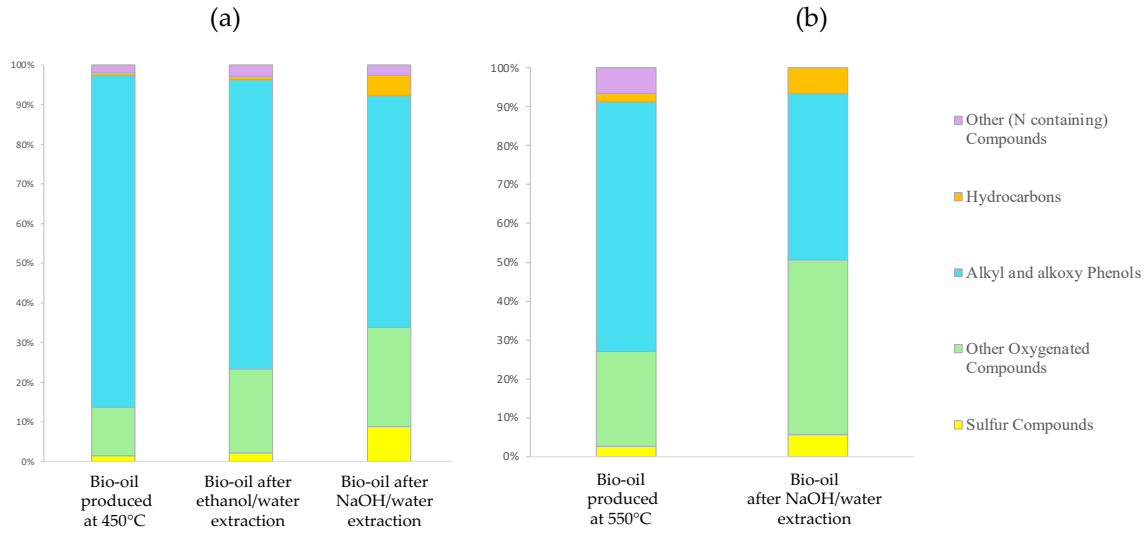


Figure 24: (**a**) Extractions on the L produced at 450 °C. (**b**) Extraction on L produced at 550 °C.

Interestingly, sulfur compounds can be found in liquid as dimethyl sulfide, thiols, and thiophenes. Even though these compounds represent a small percentage of L, their presence is still remarkable due to the implication of sulfur in the eventual bio-oil application as a fuel. In fact, sulfur in liquid can be corrosive, can lead to the formation of gaseous sulfur compounds such as $SO_2$ and $H_2S$ (which are toxic), and can also poison the catalysts [107,108,159–161].

## *3.3. Conclusions*

In this study, the behavior of a commercial Kraft lignin in different isothermal conditions was investigated. The distribution of the products of the pyrolysis reaction was studied and characterized.

Biochar is mainly a carbonaceous material, with the presence of a low quantity of sodium and sulfur. Pyrolysis temperature affects the elemental composition of biochar. The carbon content increases as the temperature increases, up to almost 90 wt.% in samples produced at 550 °C. In contrast, the amount of oxygen in the pyrolytic residues follows an opposite trend,

showing a drop from 31 wt.% in fresh lignin to 7 wt.% for samples treated at 550 °C. The produced reaction gas contains carbon oxides, light hydrocarbons (methane, ethylene, propene), and oxygenated compounds (methanol, ethanol). However, it also presents a relevant amount of S-containing compounds, which affect the gas quality. Their evolution and production depend on the reaction temperature. Hydrogen sulfide is by far the most-produced S-compound in the gas product.

The composition of bio-oil produced in the test performed at 450 and 550 °C changes with the temperature, even if the most remarkable class of compounds in the L fraction is always represented by alkyl and alkoxy-phenols, present together with alkyl-dihydroxy-benzenes, oxygenated compounds, a few hydrocarbons, and sulfur compounds. From extractions performed on the pyrolysis liquid, it can be evinced that the phenol extraction power of the NaOH/water solution is higher than the ethanol/water solution. However, in the conditions adopted, the extraction of alkyl-alkoxy phenols is still far from complete. On the other hand, most of the sulfur compounds are not extracted under these conditions.

# *Chapter 4. Pyrolysis of Kraft Lignin: Effects of process parameters*

Data reported in this chapter has been already published:

**Borella M**.; A.A. Casazza, G. Garbarino, P. Riani, G. Busca, Conversion of Lignin to Chemical Intermediates: a Study of Pyrolysis of Kraft Lignin, Chem Eng Trans 92 (2022) 631–636. https ://doi.org/10.3303/CET2292106.

Experiments of pyrolysis of commercial Kraft lignin have been realized in the 250-550 °C range. Product analyses have been performed by FT-IR, GC-MS, SEM-EDX analyses. The main goal of the work is to optimize the experiments in terms of liquid yield, reduction of oxygen content in the resulting biochar, and removal of sulfur, found mainly in the gas phase. It has been concluded that the amount of the starting lignin charged in the reactor must be limited to be fully positioned in the heating chamber also during high temperature treatment. Sulfur may be partially removed in the gas phase as $H_2S$ and $CH_3SH$ mainly, by a pre-treatment at 250 °C. The maximum amount of liquid product, mainly constituted by methoxy- and alkyl-methoxy-phenols, and the maximum solid deoxygenation are both obtained at 550 °C.

## *4.1. Materials and methods*

### *4.1.1. Lignin characterization*

Fresh Kraft lignin (KL) characterization has been carried out with a particular focus on the morphology, elemental composition, ash, and moisture content. The latter has been measured according to Spennati et al.[162]. KL morphologies have been studied with scanning electron microscopy (SEM) whereas energy-dispersive X-ray spectroscopy (EDX) analysis was performed to assess the chemical elemental composition. To better understand the influence of the temperature on SR composition and morphological properties, EDX analyses have been performed both on fresh lignin and pyrolytic residues, focusing on the content of C, Na, S, and O in the samples.

### *4.1.2. Test procedures*

In this work, tests have been performed experimenting different temperature ranges in order to understand which is the influence of process conditions on the reaction products. In particular, the first series of tests have been carried out comparing the behavior of KL at isothermal conditions in the same reactor configuration charged with 10 and 5 grams of KL, respectively. This parameter may have a remarkable impact on product yields due to the variation of the encumbrance of the reacted lignin inside the reactor and possibly different fluid dynamic conditions in terms of contact in between the gas, liquid, and solid phase. These tests have been performed at 350, 450, and 550°C and maintained at the set temperature for 3 hours, using the same setup described in the previous chapter.

Then, a wider range of temperature has been investigated in tests carried out starting from 250 °C with a progressive increase of temperature up to 550 °C. The temperatures that have been investigated are 250, 300, 350, 400, 450, and 550°C. During each step, the reaction takes place for 90 minutes allowing two measurements of the gas phase with GC-MS, one every 45 minutes. After the second GC-MS measure, a nitrogen purging has been performed in order to remove all the gas produced. After gas purging, the temperature has been increased up to the next reaction step. This procedure allowed to perform GC-MS analysis only on the gas produced at the set temperature and to separate its contribution from the gas produced at lower temperatures.

### *4.1.3. Equipment and characterization procedures*

Both reaction products (SR, G, L) and fresh lignin have been characterized using Fourier transform infrared spectroscopy (FT-IR) using a Nicolet 380 instrument (Thermo Scientific, Madison, WA, USA). KBr pressed disks (disk weight 1.000g) have been prepared for the FT-IR analysis of liquid and solid products. Liquids have been analyzed spreading on the KBr disk surface while solids have been analyzed using a pressed disk made of samples mixed with the KBr powder (1:100, w/w). Gaseous products were analyzed by forcing them to flow in a glass IR cell equipped with KBr windows.

Gas chromatography-mass spectrometer (GC-MS) analysis was performed on liquid and gaseous products using a Focus-ISQ instrument (Thermo Scientific, Milan, Italy). $10^{-4}$ L injections have been performed every 45 minutes of the reaction time for the GC-MS quantitative analysis of pyrolytic gas. Areas beneath peaks in the chromatogram have been normalized with the total area, in order to obtain a relative abundance parameter (R) showing a quantitative measure of the relative amount of the species detected in the sample.

Using a similar procedure, liquid products have been analyzed diluting the sample in $CHCl_3$ (1:10, v/v) and performing a $10^{-6}$ L injection in the GC-MS.

## *4.2. Results and discussion*

### *4.2.1. Products distribution and characterization*

In Figure 25 the yields in gas, liquid, and solid products obtained by heating KL, as a function of reaction temperature and amount of lignin charged to the reactor, are reported. The amount of liquid and gas products increases significantly both by increasing the reaction temperature, and by decreasing the reactant amount charged. Obviously, the amount of the produced biochar is reduced at higher temperature and when less lignin is treated.

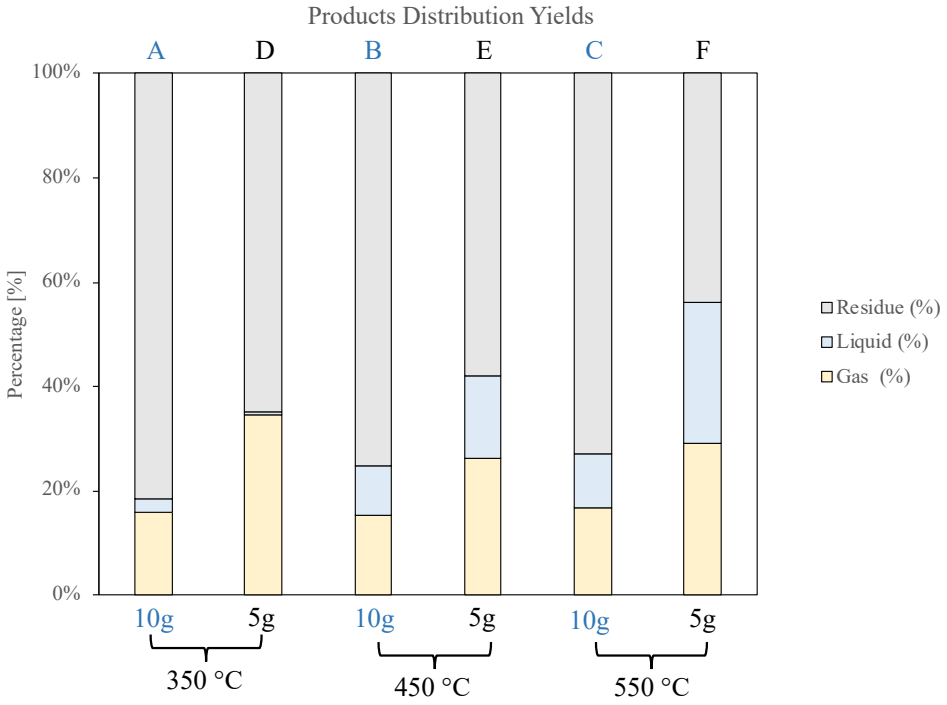


Figure 25: Product yields in pyrolysis experiments at different temperatures 350,450, and 550°C, and using different loading of lignin.

In Table 3, the carbon and oxygen content in the resulting biochar is reported, as analyzed by EDX for the same experiments. It is evident that pyrolysis results in solid deoxygenation. However, such deoxygenation is more abundant at higher temperatures and with smaller lignin charged on the reactor. EDX analysis cannot reveal hydrogen: it shows the presence of small amounts of sulfur and sodium impurities in the biochar. The wt.% amount of sodium as expected tends to increase with lignin conversion, due to the likely non-volatility or poor volatility of sodium compounds in this temperature range. The wt.% amount of sulfur in the

resulting biochar has a more complex behavior. This suggests that part of sulfur is released in the liquid and gaseous phases, upon experiments D and E, i.e. at 350-450 °C using 5 g of lignin in the reactor. However, part of sulfur is certainly strongly retained in the biochar, even after pyrolysis at 550°C.

Table 3: EDX analysis on biochar materials.

| Name | Lignin Charge [g] | Pyrolysis temperature [°C] | C (wt.%) | O (wt.%) | Na (wt.%) | S (wt.%) |
|---|---|---|---|---|---|---|
| ----- | --------- | Lignin as received | 67.1 | 31.6 | 0.2 | 1.1 |
| A | 10 g | 350 | 74.0 | 24.7 | 0.3 | 1.0 |
| B | | 450 | 76.3 | 22.0 | 0.5 | 1.2 |
| C | | 550 | 79.0 | 19.5 | 0.5 | 1.0 |
| D | 5 g | 350 | 72.6 | 26.6 | 0.3 | 0.5 |
| E | | 450 | 81.5 | 17,0 | 0.5 | 1.0 |
| F | | 550 | 89.7 | 7.7 | 0.7 | 1.9 |

### *4.2.2. FT-IR characterization of pyrolysis residues*

The FT-IR spectra of the obtained biochar samples are reported in Figure 26, where they are compared with the spectrum of the as-received Kraft lignin sample. The spectrum of Kraft lignin closely corresponds to that reported in the literature [163]. The absorption bands are those typical of aromatic rings, methoxy groups, and phenolic compounds, as discussed already in the previous chapter. The spectra of the residues from experiments A to C are essentially the same, although the intensities of the bands are decreased in intensity. This agrees with the occurred limited conversion during these experiments. In contrast, the spectra of the samples resulting from experiments D to F are much different, showing the quite complete disappearance of the bands. This agrees with the likely formation of carbon-rich matter and the loss of oxygen-containing functional groups.

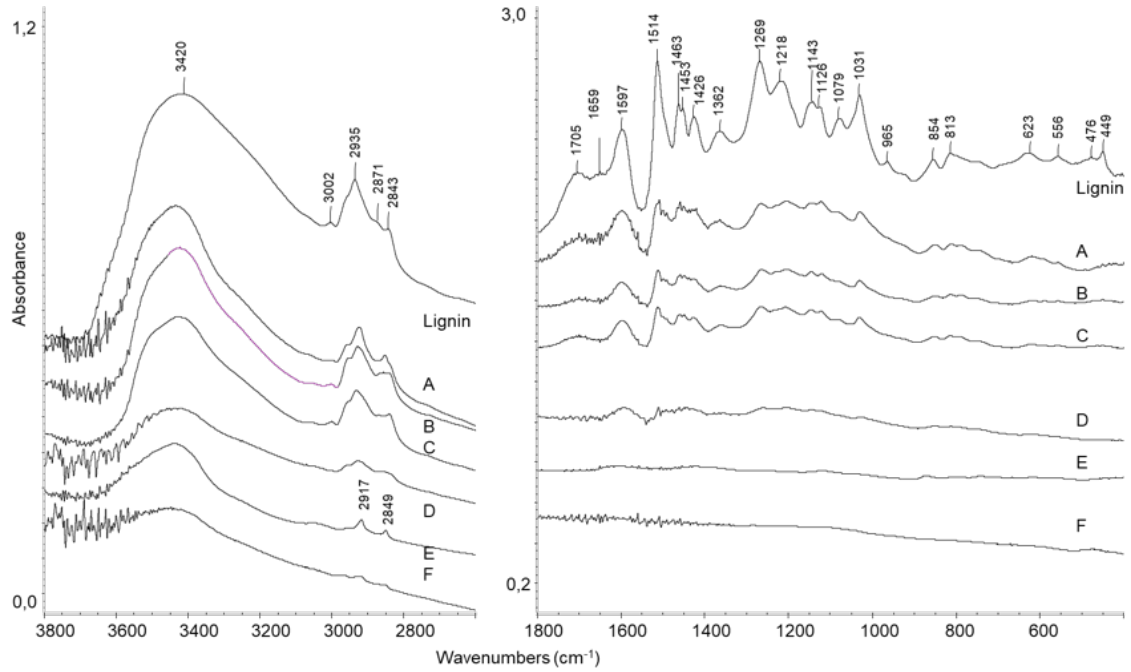


Figure 26: FT-IR spectra of as-received Kraft lignin and pyrolysis residues (biochars).

The analysis of liquid products, realized by GC-MS, shows that the most abundant components are those reported in previous chapter in Figure 22. In particular, the main peak corresponds to 3 methoxy-5-methyl-phenol, while strong peaks are also those corresponding to the two isomeric compounds 2-methoxy-phenol (guaiacol) and 4-methoxy-phenol and to 4-ethyl-2-methoxy-phenol. The peaks of these four compounds correspond to more than 65% of all GC spectrum in the liquid obtained by pyrolysis at 450°C and 550°C, 5 g (experiments E and F). In any case, several sulfur compounds have been observed in the liquid products, in particular thiols, sulfides and polysulfides.

### *4.2.1. Sulfur products evolution*

The produced gases have been analyzed using FT-IR and GCMS techniques. The main observed products are $CO_2$, CO, methane, ethylene, propylene, and several sulfur compounds, in particular hydrogen sulfide, $H_2S$, methanethiol, $CH_3SH$, dimethyl sulfide $(CH_3)_2S$, and carbonyl sulfide, COS. To go deeper into the behavior of sulfur impurities in Kraft lignin, sequential pyrolysis experiments have been performed at 250, 300, 350, 400, 450, and 550°C, analyzing the evolved gas in each single step, as reported in the methods section.

From the data reported in Figure 27, it results that the different sulfur compounds behave in a partially different way. Taking into account the experiments realized with 5 g of starting lignin (deep colors), which correspond to higher lignin conversion, gaseous sulfur

compounds, in particular $H_2S$ and $CH_3SH$ which are the most abundant, are predominantly emitted at the lower temperatures, starting already at 250 °C. Instead, with experiments performed with 10 g of starting lignin, where lignin conversion is lower, the maximum emission of the sulfur compounds is slightly shifted to a higher temperature (mainly 300-350 °C). This might be related to the fact that upon pyrolysis the expansion of the reaction medium for the evolution of gas and liquids produces a different temperature gradient in the reactor itself, suggesting that pyrolysis reaction might occur with a more complex situation far from full isothermicity.

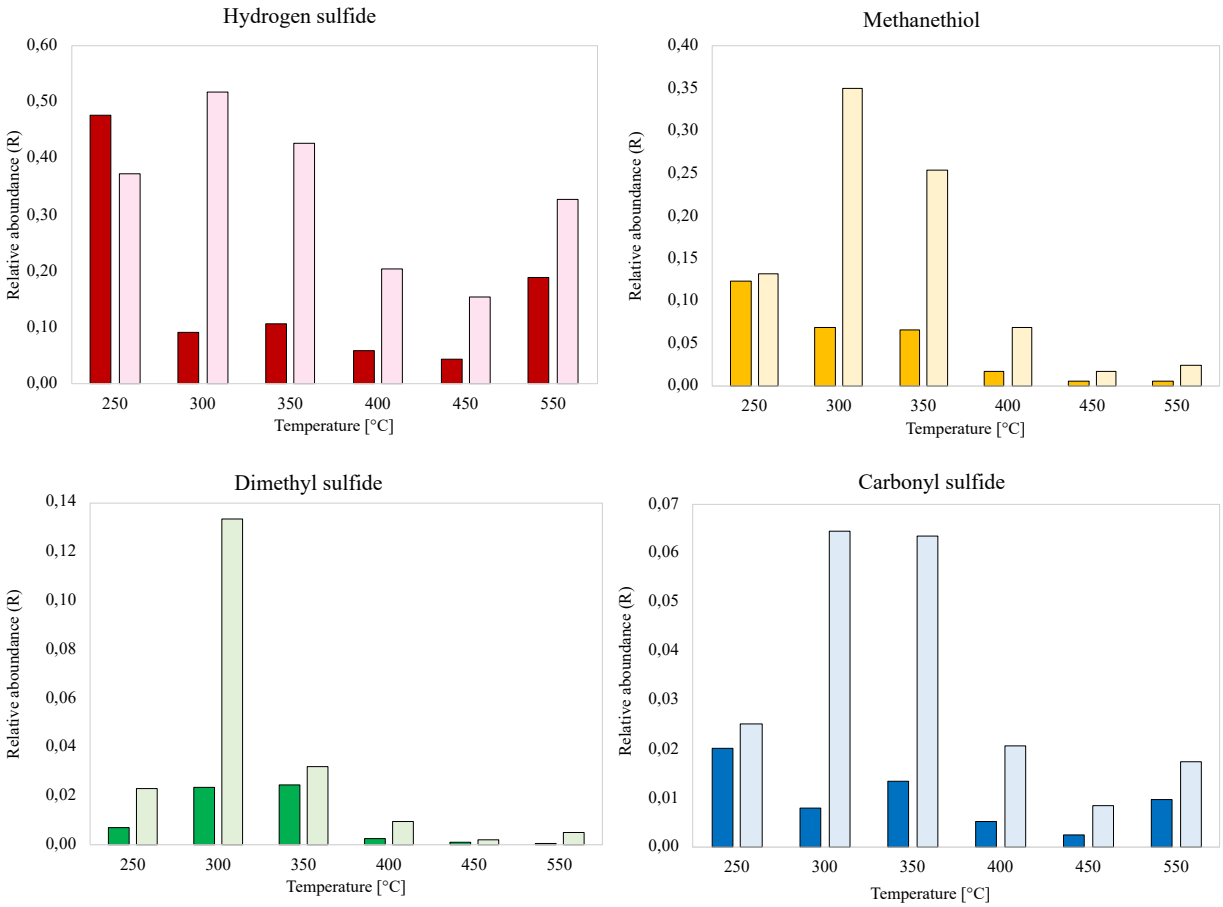


Figure 27: Relative abundance (% of GC area) of sulfur compounds in the gases evolved in sequential pyrolysis experiments. Deep colors: 5 g. Light colors: 10 g of starting lignin.

## *4.3. Conclusions*

From the present work, we concluded that experiments realized with 5g starting lignin in our reactor allow higher conversion, probably because the solid matter is better positioned in the heating region of the reactor. The pyrolysis allows very large solid deoxygenation if treated at 550 °C for 3 h. The maximum liquid product yield obtained in our experiments is 28.7 %,

with methoxy-, methoxy-methyl- and methoxy-ethyl phenols as the main liquid components. The obtained char in these conditions still retains a limited oxygen content (7.6 %) and appears to be largely carbonized. The sulfur impurities typical of Kraft lignin distribute between gaseous, liquid, and solid products. However, it seems that a previous step of treating at 250 °C could allow the release in the gas phase of a large part of sulfur as $H_2S$ and $CH_3SH$. Further experiments are programmed to release sulfur in the gas phase as much as possible in a previous pyrolysis pre-treatment step, and to later increase the liquid yields by a second higher temperature pyrolysis step.

# *Chapter 5. Pyrolysis of Kraft lignin: upgrading of products managing sulfur impurities*

Data reported in this chapter is under finalization for submission at the time of writing the present thesis:

**M. Borella**, A.A. Casazza, G. Garbarino, P. Riani, G. Busca, Upgrading of Kraft lignin pyrolysis products: managing sulfur impurities.

Pyrolysis of Kraft lignin and the sulfur evolution in pyrolysis products have been already investigated in our previous studies[145,164]. In this work, an upgrading of the setup has been reported adding an adsorbent bed of activated carbon for gas purification. Moreover, a biochar characterization has been performed to study the influence of the adsorption on the sulfur distribution in products. This further development can be an important step to improve the quality of the gas and its calorific value, also obtaining a bio-oil rich in phenolic compounds and with a low amount of sulfur.

## *5.1. Materials and methods*

### *5.1.1. Pyrolysis setup and experimental procedure*

The pyrolysis setup used in this work has been already reported in previous chapters with the addition of a purification column (5) as shown in Figure 28. Pyrolysis gas (G) has been collected in a latex balloon after its adsorption on a bed of four different commercial activated carbon with different pore dimensions and sizes. The adsorption step is needed to remove sulfur-containing compounds that are known to be present in pyrolysis products of kraft lignin as reported in previous works. A carbonaceous solid residue material remains inside the reactor after pyrolysis, and it will be referred to as biochar (SR). The system is purged with nitrogen for 10 minutes before every test to guarantee an oxygen-free environment. Tests have been performed at 500°C for a reaction time of 3 hours.

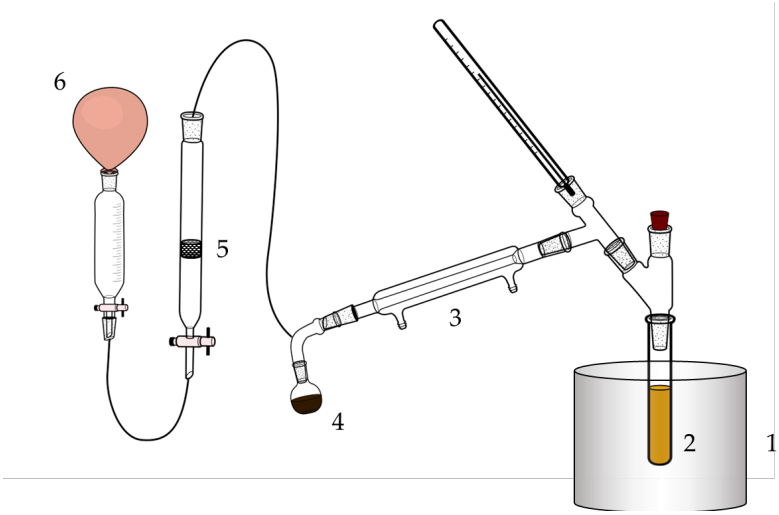


Figure 28: Graphic representation of pyrolysis setup. In figure are reported: 1) pyrolysis furnace; 2) reactor; 3) condensation unit; 4) flask for bio-oil collection; 5) Adsorption bed of activated carbons; 6) latex balloon for gas collection.

## *5.2. Results and discussion*

### *5.2.1. Biochar characterization*

Fresh lignin characterization in terms of moisture and ash content has been already discussed in our previous works [145,165]. The elemental composition obtained through SEM-EDX of the raw lignin and all the biochar materials produced after the different experiments are reported in Table 4. Raw Kraft lignin has a small amount of Na whose presence is due to white liquor composition during the isolation process of lignin [166]. At 550 °C Na concentrates up to values around 0.7 wt. % in all the tests performed because of the low volatility of Na compounds which remains in the residue upon the pyrolysis. The SEM images show a wide particle size distribution. The O/C ratio in the fresh lignin is 0.47, while after pyrolysis at high temperature it strongly decreases down to 0,1, due to the formation of oxygen-rich bio-oil and pyrolysis gas. The behavior of sulfur distribution is more complex. Different types of surface morphologies have been considered to evaluate a potential connection between roughness and sulfur deposition. Despite some regions in the biochar surface have presented a local higher content in S, no particular morphologies have been directly connected to the accumulation of S. No differences in the average sulfur distribution in biochar can be noticed, however, a decrease in S content can be observed if compared to the tests performed without activated carbon (Figure 29, a-Carbosorb MA 1.5, b-Carbosorb 360 C3, c-Carbosorb 53, d-Carbosorb 73). This can be related to the adsorption of sulfur species in the gas phase, and manifest that the presence of activated carbon can affect the equilibria in all the other phases even if with a small contribution. Han et al. (2018), studied

the evolution of sulfur from fast pyrolysis of sulfonated Kraft Lignin which from elemental analysis showed a higher O/C ratio due to higher oxygen content and lower carbon content. Moreover, sulfonated lignin has a higher sulfur content (4.8 wt.%) compared to the lignin used in this paper [167].

Table 4: Elemental composition in terms of C, O, Na, and S of fresh lignin as received, biochar obtained in tests performed without the adsorption bed and biochars obtained with different activated carbons (a-Carbosorb MA 1.5, b-Carbosorb 360 C3, c-Carbosorb 53, d-Carbosorb 73)

| Pyrolysis Temperature | Activated Carbon | C (wt.%) | O (wt.%) | Na (wt.%) | S (wt.%) |
|---|---|---|---|---|---|
| As Recieved | - | 67.1 | 31.6 | 0.2 | 1.1 |
| 550°C | - | 90.0 | 7.7 | 0.7 | 1.5 |
| 550°C | a | 89.4 | 8.5 | 0.7 | 1.4 |
| 550°C | b | 89.5 | 8.6 | 0.7 | 1.3 |
| 550°C | c | 88.8 | 9.3 | 0.6 | 1.3 |
| 550°C | d | 89.5 | 8.6 | 0.6 | 1.3 |

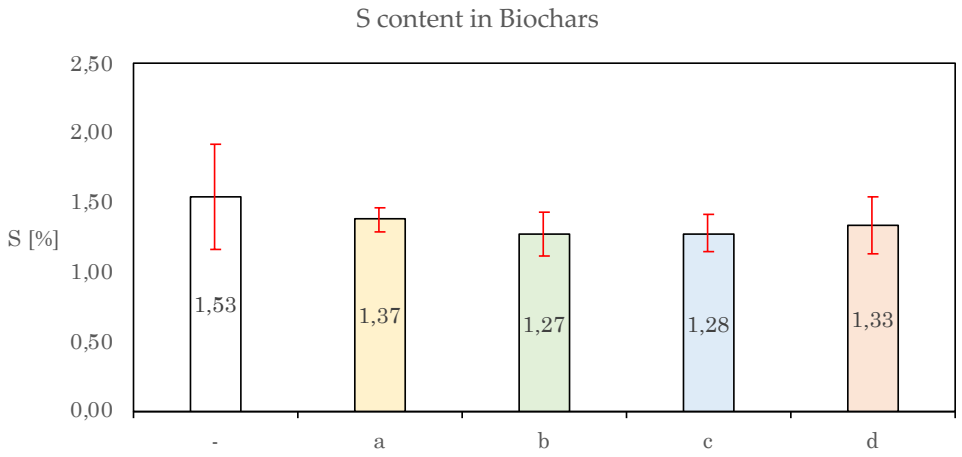


Figure 29: S distribution (wt.%) in Biochar with the adsorption section with different activated carbons (a-Carbosorb MA 1.5, b-Carbosorb 360 C3, c-Carbosorb 53, d-Carbosorb 73) and without the activated carbon bed

### *5.2.2. Product yields distribution*

Product yields at the temperature of 500°C are in agreement with our previous works [145,165]. Yields have been evaluated via gravimetric measurement: the solid residue retained at the bottom of the reactor and the liquid product has been evaluated by weight difference. However, due to the high viscosity of the resulting product part of the liquid remained attached to the walls of the plant, this fraction has been washed with chloroform and then weighted after the evaporation of the solvent. Gas fraction has been then calculated

by weight difference closing the mass balance. The presence of the activated carbon bed, as expected, did not affect the product yields that are reported in Figure 30.

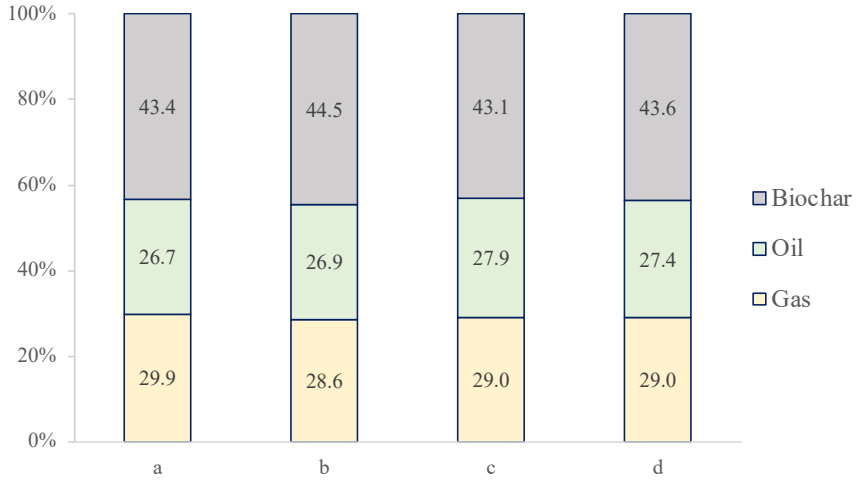


Figure 30: Yields distribution of pyrolysis tests using different activated carbons (a-Carbosorb MA 1.5, b-Carbosorb 360 C3, c-Carbosorb 53, d-Carbosorb 73).

### *5.2.3. Gas products characterization*

Gas products have been characterized using FT-IR spectroscopy. In previous studies, the pyrolysis gas of Kraft lignin has been obtained without the adsorption bed of activated carbon using the same setup and process conditions. This spectrum (Figure 31) has been used as a reference to study the influence of the adsorption bed on gas composition. From a qualitative point of view, no significant changes could be detected by FT-IR spectra comparison, except for the peak at 2062 $cm^{-1}$ attributed to the asymmetric stretching of COS that is not detected in the other tests. Apart from that, the main composition remains characterized by CO, $CO_2$, and $CH_4$. However, the ratio between the intensities of $CO_2$ and $CH_4$ at 2293 $cm^{-1}$ and 3093 $cm^{-1}$ changes using different activated carbons. Since these carbons have a good selectivity toward the adsorption of $H_2S$, competitive adsorption of $CO_2$ may occur explaining the variation of $CO_2/CH_4$ ratio.

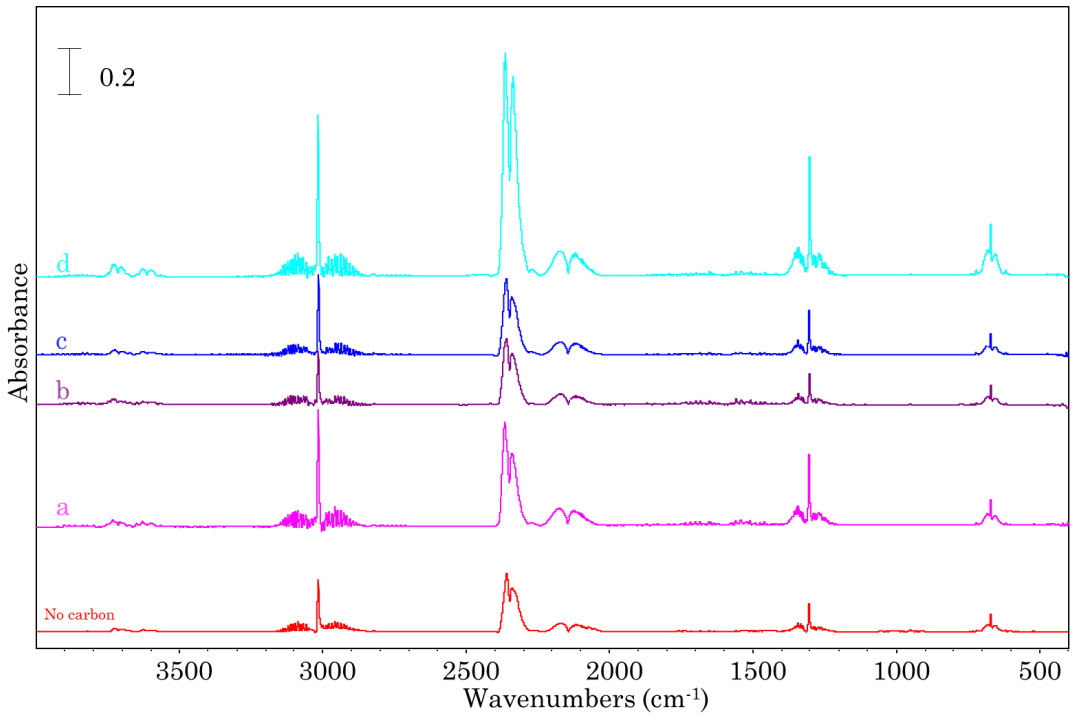


Figure 31: FT-IR spectra of the pyrolysis gas obtained without adsorption bed of activated carbon, and with four different activated carbons bed (a-Carbosorb MA 1.5, b-Carbosorb 360 C3, c-Carbosorb 53, d-Carbosorb 73).

Quantitative analysis of pyrolytic gas has been performed using GC-MS, to identify all the chemical species which are present in the gas phase but cannot be clearly observed with FT-IR or which concentration is too low to be detectable. The presence of several sulfur compounds such as $CH_3SH$, COS, $CH_3$-S-$CH_3$, $SO_2$, $H_2S$, and their evolution profile during the pyrolysis test has been already discussed in other papers [145,165] . In this work, GC-MS analysis has been performed on gas samples after the adsorption on the activated carbon bed, focusing on the most abundant compounds which are carbonyl sulfide, methanethiol, and hydrogen sulfide. Han et al. worked on stepwise pyrolysis tests on Kraft lignin, and they showed that sulfur dioxide represents the most relevant compounds at low temperatures (i.e. 250 and 350 °C), whose content strongly decrease with the increasing temperature. The relative content of $SO_2$ is around 20% at 550°C. However, in this work, the evolution of $SO_2$ was limited if compared to the other sulfur containing compounds. They suggest that the form in which sulfur is present in the biomass influences the formation of specific compounds. Then, sulfur in the form of sulfide lead preferably to the formation of $H_2S$, $CH_3SH$, and $CH_3SCH_3$ while in the form of sulfites lead to $SO_2$ formation [167]. In fact, also Dondi et al. (2014) reports a list of sulfur containing compound presents in the pyrolytic gas of Kraft lignin where $SO_2$ is not detected for temperature higher than 500°C [45], supporting our results. In Figure 32 data have been reported comparing the relative abundance of these

compounds with the test performed without the adsorption bed , to evaluate the adsorption efficiency of the carbons and to purify the pyrolytic gas. For each test, four injections have been performed to establish the values of concentration of different S species, during the reaction time. The parameter R has been calculated as the ratio between the area of the sulfur compound considered and the area of the total injection. All the activated carbons show good adsorption of sulfur compounds improving the quality of the gas. Moreover, during the entire reaction time, the value of the R parameter does not undergo significant changes due to the fact that the sulfur produced is not enough to saturate the bed of carbons and reduce the adsorption efficiency of the bed. Moreover, most of the products are produced in the first part of the reaction time. Hydrogen sulfide abundance in gas has lowered by one order of magnitude, from more than 2.5 % up to less than 0.3 %. Even though almost all the carbons have the same efficiency in the removal of S-containing compounds, COS adsorption on carbon b exhibits the worst performance reducing COS content in gas from 0.2 % to 0.1%. Several factors can influence the adsorption process, and depending on activated carbon structural and chemical features different yields can be achieved. For instance, Yan et al., (2002), showed that for some activated carbons adsorption capacity towards $H_2S$ is influenced by moisture content resulting in higher adsorption efficiency. In other cases, humidification of activated carbons did not produce the same results [168].

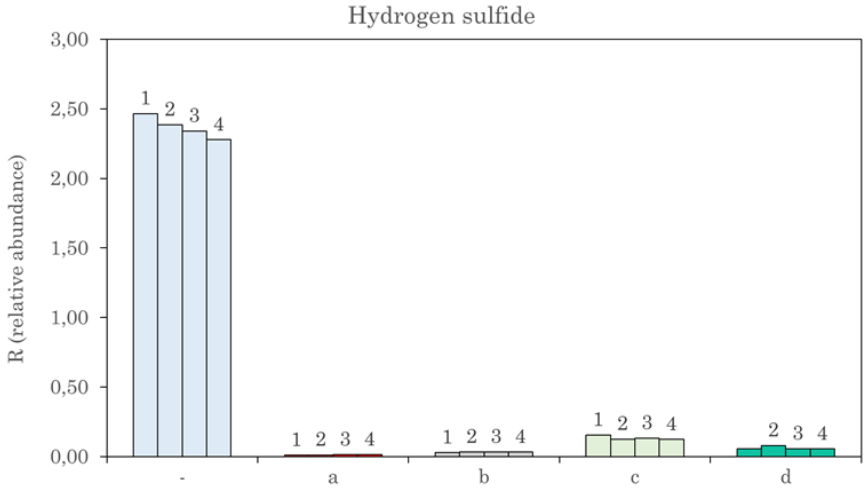

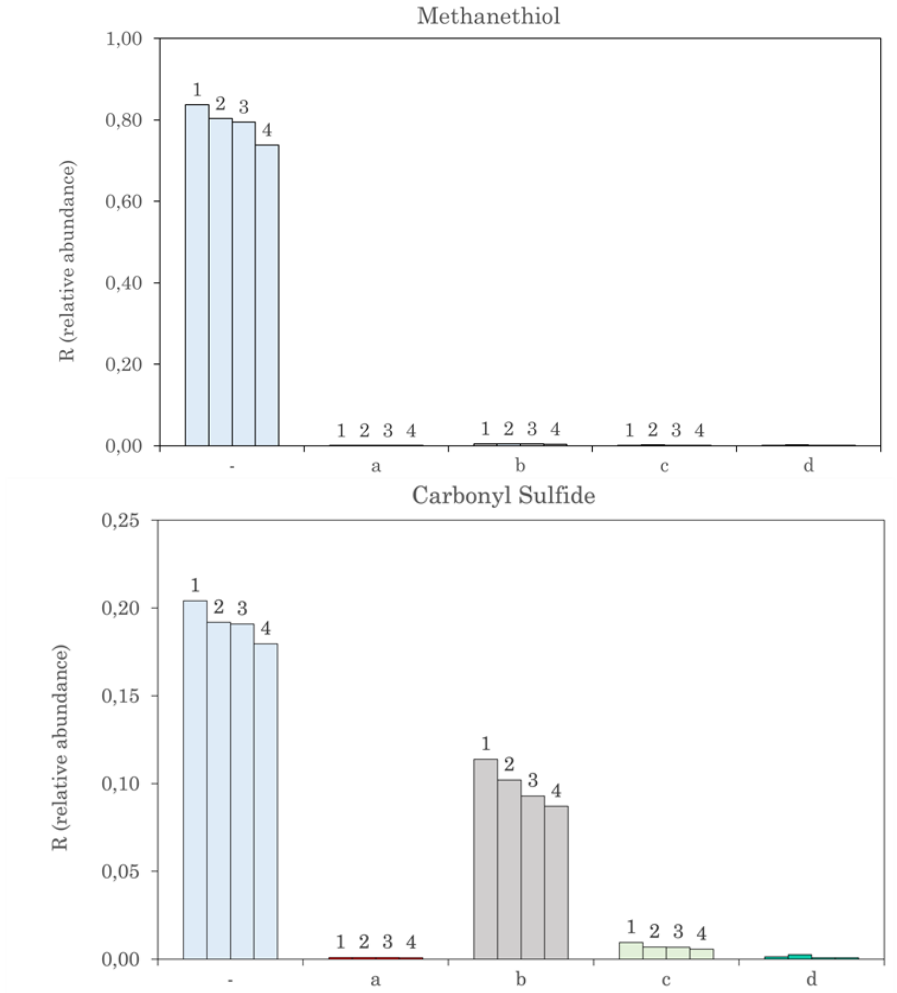


Figure 32: GC-MS for quantitative analysis of Hydrogen sulfide, methanethiol and carbonyl sulfide present in the pyrolytic gas. Each histogram represents a different injection in GC-MS (four each test). Data reported are related to average values obtained without adsorption bed and to values obtained after the adsorption on four different activated carbons (a-Carbosorb MA 1.5, b-Carbosorb 360 C3, c-Carbosorb 53, d-Carbosorb 73).

### *5.2.4. Liquid Characterization*

During pyrolysis, a small amount of water is produced and collected with the bio-oil. A dilution with chloroform is needed to enhance the separation between the hydrophobic and hydrophilic phases. After a centrifuge step, the bio-oil has been separated from the water and GC-MS analysis has been performed for the characterization of the bio-oil produced in each test (a-Carbosorb MA 1.5, b-Carbosorb 360 C3, c-Carbosorb 53, d-Carbosorb 73). The main objective was both to study the composition, and to investigate the amount of sulfur in the bio-oil. The procedure has been already discussed in the method section. Bio-oil is mainly constituted by phenolic-like compounds which represent almost 93 wt.%, as reported also in literature [169,170].. In this fraction, the most relevant compounds are 2-methoxy-4-methyl phenol and 4-ethyl-2-methoxy phenol representing 25% and 12% of the total area of the GC spectra, respectively. However, several isomers are present including dimethyl, ethyl, and

propyl phenols in lower quantities. Other categories of compounds are also present in the bio-oil such as oxygenated compounds like aldehydes and ketones, and aromatic hydrocarbons such as alkyl and alkoxy benzenes. Branched non-aromatic hydrocarbons are also present. In Table 5 all the compounds with an area percentage greater than 0.5% have been reported. Sulfur-containing compounds have been also detected in small quantities in the forms of methyl and dimethyl thiophenes, polysulfides, and thiols in agreement with data presented by Auersvald et al. [171]. Authors investigated the composition of beech wood-derived fast pyrolysis oil using GCxGC-SCD and GC-MS and confirmed that sulfur in biomass pyrolysis is often release in liquids in the forms of alkyl thiols and sulfides, depending on the properties of the raw biomass.

Table 5: List of the most relevant compounds in the bio-oil deriving from GC-MS analysis of bio-oil produced in tests performed without the adsorption bed and tests performed with the four different activated carbons (a-Carbosorb MA 1.5, b-Carbosorb 360 C3, c-Carbosorb 53, d-Carbosorb 73)

| | | Area Percentage (%) | | | | |
|---|---|---|---|---|---|---|
| **Time** | **Compounds** | **-** | **a** | **b** | **c** | **d** |
| 6.59 | Phenol | 0.44 | 0.66 | 0.54 | 0.94 | 0.64 |
| 8.95 | Phenol, 3-methyl | 0.62 | 1.12 | 0.76 | 1.52 | 1.05 |
| 9.62 | Phenol, 2-methyl | 0.68 | 1.02 | 0.84 | 1.33 | 1.02 |
| 10.17 | Phenol, 2-methoxy | 8.66 | 14.12 | 14.21 | 16.32 | 14.19 |
| 11.94 | Phenol, 2,4-dimethyl | 1.02 | 1.76 | 0.9 | 2.48 | 1.52 |
| 12.91 | Phenol,4-methoxy-3-methyl | 0.94 | 1.16 | 1.12 | 1.25 | 1.25 |
| 13.39 | Phenol,2-methoxy,4-methyl | 16.57 | 25.14 | 24.94 | 27.16 | 24.22 |
| 13.52 | 1,2- Benzenediol | 2.65 | 3.24 | 2.73 | 2.7 | 2.58 |
| 14.70 | Phenol, -ethyl, -methyl | 0.52 | 0.8 | - | 1.03 | 0.69 |
| 15.36 | 1,2-benzenediol,4-methyl | 1.55 | 2.07 | 2.06 | 1.9 | 2.06 |
| 15.9 | Phenol, 4-ethyl, 2-methoxy | 8.84 | 12.02 | 12.28 | 11.6 | 11.86 |
| 16.2 | 1,2-Benzenediol, 4-methyl | 3.58 | 5.0 | 3.53 | 4.35 | 3.74 |
| 16.87 | 2-methoxy-4-vinylphenol | 2.51 | 1.03 | 1.12 | 0.82 | 1.24 |
| 17.99 | 1,2-benzenediol, 2,6-dimethyl | 0.59 | 0.64 | 0.52 | 0.52 | 0.57 |
| 18.16 | Phenol,2-methoxy-3-(2-propenyl) | 1.13 | 1.58 | 1.64 | 1.36 | 1.74 |
| 18.26 | Phenol,3-methoxy, trimethyl | 0.78 | 0.8 | 0.76 | 0.72 | 0.8 |
| 18.46 | Phenol,2-methoxy-4-propyl | 1.88 | 2.05 | 2.4 | 1.77 | 2.31 |
| 18.96 | 4-ethylcatechol | 1.66 | 1.64 | 1.2 | 1.54 | 1.3 |
| 19.42 | Vanillin | 1.40 | 1.55 | 1.9 | 1.52 | 1.72 |
| 19.69 | Phenol,2-methoxy-4-(1-propenyl)-,(E) | 1.45 | 1.86 | 1.62 | 1.6 | 1.95 |
| 20.89 | Phenol,2-methoxy-4-(1-propenyl)-,(Z) | 5.04 | 5.11 | 6.16 | 4.66 | 5.86 |
| 21.91 | Ethanone,1-(4-hydroxy-3-methoxyphenyl)- | 3.22 | 2.06 | 2.44 | 1.77 | 2.02 |
| 23.08 | 2-propanone, 1-(4-hydroxy-3 methoxy phenyl)- | 1.88 | 1.35 | 1.65 | 1.11 | 1.42 |

| | | | | | | |
|---|---|---|---|---|---|---|
| 24.4 | Ethanone,1-(3-hydroxy-4-methoxyphenyl)- | 1.27 | 0.82 | 0.98 | 0.7 | 0.9 |
| 25.97 | Benzeneacetic acid, hydroxy-methoxy | 3.65 | 1.52 | 2.48 | 1.0 | 1.86 |
| 39.28 | Phenol, 2-methoxy-4-propyl | 0.98 | 0.93 | 1.68 | 0.68 | 1.28 |

Table 6 reports a list of sulfur compounds detected in the bio-oils and their relative area percentages with and without the activated carbon treatment. The elemental sulfur percentage have been reported as well, considering the sulfur mass fraction of the different compounds. According to these calculations, the resulting elemental sulfur in bio-oils produced is 0.29 wt. % of the total oil. Also Eschenbacher at al., analyzed the sulfur percentage (wt.%) of the organic phase in bio-oil produced by gasification of wheat straw at 500°C showing a sulfur percentage in their oils ranging from 0.1 to 0.5 wt.%, Interestingly, the sulfur content decreases in a range between 0.1 and 0.19 wt.% in presence of the activated carbons. Thus, the adsorption of sulfur in the gas phase affects the overall mass balance and results in a redistribution of sulfur in the bio-oils, where the total content of sulfur decreases of 42% (a, d), and of 53% (b, c).

Table 6: List of most relevant sulfur compounds detected in bio-oils from GC-MS analysis. The total sulfur content is then calculated as the sum of the relative abundance of every singular sulfur compound. Then, the elemental sulfur has been calculated as a sum of the sulfur mass contained in each compound.

| **S-containing compounds** | **-** | **a** | **b** | **c** | **d** |
|---|---|---|---|---|---|
| Thiophene, methyl | - | - | 0.03 | 0.02 | - |
| dimethyl thiophene | 0.08 | 0.06 | 0.07 | 0.06 | 0.08 |
| Propanal, 3-(methylthio)- | 0.17 | 0.04 | 0.05 | 0.04 | 0.07 |
| 3-methylthiobutyraldehyde | 0.06 | 0.05 | 0.05 | 0.04 | 0.06 |
| Dimethyl trisulfide | - | 0.04 | - | 0.05 | - |
| Dimethyl sulfide | 0.24 | - | - | - | - |
| tetra sulfide dimethyl | 0.09 | - | - | - | - |
| hexanethiol | 0.09 | 0.06 | 0.05 | 0.05 | 0.08 |
| 2,3 dihydroxythiophene,1,1-dioxide | - | 0.06 | - | - | - |
| disulfide, methyl, (methylthio) methyl | 0.01 | 0.10 | 0.09 | 0.09 | 0.12 |
| Total (%) | 0.73 | 0.42 | 0.34 | 0.35 | 0.42 |
| Elemental sulfur (%) | 0.29 | 0.12 | 0.10 | 0.19 | 0.18 |

Knowing the sulfur content in chars and raw lignin from SEM-EDX, in bio-oil, and calculating the sulfur in gas by difference it is possible to obtain a distribution of elemental sulfur in products as reported in Table 7. This table reports the total amount of sulfur in the raw lignin, and how it is distributed in products as a percentage related to the weight of the products considered and the total amount of sulfur. Without the activated carbon, 58 wt.%

of sulfur in kraft lignin remains in the residue, 34% is released in the gas phase, the remaining 7.5 wt.% is trapped in the liquid matrix. Auersvald et al. (2021), reports for different sulfur-rich biomass the yields of sulfur converted into liquids. They report that for beech wood, Miscanthus,and straw, the percentage of the total sulfur that is converted in liquid phase is higher than 10%, and mostly concentrated in the organic phase. The adsorption activity of activated carbon influences the equilibrium of the products: thus, 42-44 wt.% .of sulfur goes in the gas phase, 3-5 wt.% stays in the liquid (carbon a and c, respectively), the rest (52-55%) remains in the biochar. The presence of activated carbon appears to enhance the release of sulfur-containing gas since the percentage (S (g) / $S_{tot}$(g)) increases from 34 to a maximum of 44 wt.%. However, this is reasonable due the adsorption of s-containing gas on the activated carbon that alters the equilibrium of products, and lead to a major release of the sulfur in the gas.

Table 7: Distribution of sulfur in terms of percentage ($A/A_{tot}$) in the different products and the corresponding mass (mg) for liquid and char. The calculation of the sulfur content in gas is made by difference, and include the sulfur adsorbed on the activated carbon. It is also reported the mass percentage over the total sulfur in the biomass. Tests with activated carbons (a,b,c,d) have been compared with experiments performed without activated carbon bed (-).

| **Total mass lignin (g)** | | 5 | | | |
|---|---|---|---|---|---|
| **Type AC** | | **-** | **S (%)** | **S (mg)** | **S (g)/ $S_{tot}$ (g) (%)** |
| **-** | | **Raw Biomass** | **1.10** | **55.00** | **0.055** |
| | Gas | 29.9 | 1.54 | 23.02 | 41.85 |
| a | Liquid | 26.7 | 0.12 | 1.60 | 2.92 |
| | Char | 43.4 | 1.40 | 30.38 | 55.24 |
| | Gas | 27.0 | 1.79 | 24.25 | 44.09 |
| b | Liquid | 27.8 | 0.10 | 1.39 | 2.53 |
| | Char | 45.2 | 1.30 | 29.36 | 53.38 |
| | Gas | 29.0 | 1.68 | 24.35 | 44.28 |
| c | Liquid | 27.9 | 0.19 | 2.65 | 4.82 |
| | Char | 43.1 | 1.30 | 27.99 | 50.90 |
| | Gas | 29.6 | 1.61 | 23.84 | 43.35 |
| d | Liquid | 26.1 | 0.18 | 2.35 | 4.26 |
| | Char | 44.3 | 1.30 | 28.81 | 52.38 |
| | Gas | 28.6 | 1.32 | 18.81 | 34.21 |
| - | Liquid | 28.7 | 0.29 | 4.16 | 7.57 |
| | Char | 42.7 | 1.50 | 32.03 | 58.23 |

## *5.3. Conclusions*

In this study, the influence of application an activated carbon adsorbing bed to gas evolved from kraft lignin pyrolysis, and the behavior of four different commercial activated carbons on pyrolysis products of kraft lignin have been investigated. The product yields are not affected by the addition of the adsorption unit.

The selectivity of the activated carbon towards sulfur compounds have been evaluated analyzing GC-MS results performed on gas samples after its permeation through the adsorption bed. Data showed that the sulfur compounds considered (i.e. $H_2S$, $CH_3SH$, COS) undergo a remarkable drop in their concentration in the evolved gases in the presence of the adsorbing bed. As an example, $H_2S$ concentration decreases by 88% in our unoptimized conditions. The efficiency of the carbon bed is important in all the test performed, with the only exception for the adsorption of COS for the Carbosorb 360 C3. This suggests that gas evolved from kraft lignin pyrolysis could be completely desulfurized in optimized conditions.

The characterization of biochar showed a slightly lower content of sulfur in the residue if compared to the tests performed without the adsorption unit. This can be attributed to the removal of sulfur in the gas phase since the adsorption act on the low of mass action.

Liquid composition agrees with the composition of the bio-oil obtained in previous pyrolysis tests. Phenol-2-methoxy-4-methyl and phenol-4-ethyl-2-methoxy represent the most relevant compound, with a percentage area of 27% and 12%, respectively. From GC-MS analysis of the bio-oil low amounts of sulfur compounds in the form of methyl and dimethyl thiophenes, thiols, and polysulfides have been detected. The sulfur content in oils without purification (i.e., 0.29 wt.%) is reduced of 42.5% for carbon a and d, and 53.4%, for carbon b and c. More than half of the total sulfur is retained in the solid residue matrix, and the great majority of the remaining sulfur is released in gas. Only 8 wt.% of the total sulfur is contained in the mixed oil, and its reduction is achievable using activated carbon. Therefore, their role in unoptimized gas-phase sulfur removal can have an impact in the reduction of the overall sulfur distribution, resulting in upgraded biochars and bio-oils with less sulfur content.

# *Chapter 6. Two-stage co-pyrolysis of Kraft lignin and palm oil mixture to biofuels: the role of lignin as a methylation agent for methyl ester formation*

Data reported in this chapter is under finalization for submission at the time of writing the present thesis:

**M. Borella**, A.A. Casazza, G. Garbarino, P. Riani, G. Busca, Two-stage co-pyrolysis of Kraft lignin and palm oil mixture to biofuels: the role of lignin as a methylation agent for methyl ester formation.

**Abstract:** In this work pyrolysis of palm oil and lignin has been investigated using a two-stage process at 550 °C, with a first step configuration of continuous condensation for vapors and separation of gases, and a second step with distillation of vapors. Experiments were realized as pyrolysis of pure palm oil, pure palmitic acid, and pure Kraft lignin, as well as co-pyrolysis of palm oil/lignin, palmitic acid/lignin and palmitic acid/guaiacol. It has been shown that the addition of lignin improves the quality of palm oil pyrolysis bio-oil, thanks to the conversion of fatty acids coproduct to their methyl esters. The production of methyl esters in the reaction environment in the presence of palm oil and lignin was studied by conducting experiments with palmitic acid and lignin, as well as palmitic acid and guaiacol (the main product obtained from lignin thermal treatment). The results highlighted that during pyrolysis, the production of fatty acids methyl esters (FAME) is a consequence of a direct esterification reaction on palmitic acid, rather than a transesterification process of triglycerides from palm oil. The formation of FAMEs during pyrolysis presents a promising avenue to optimize the utilization of palm oil by generating FAMEs as supplementary fuel products, Furthermore, it is possible to consider the application of the studied process for the conversion of free fatty acids into their respective methyl esters.

## *6.1. Materials and Methods*

### *6.1.1. Experimental Procedure and Equipment*

With the aim of preventing the rapid loss of compounds from the reaction environment and promoting a prolonged contact time at reaction temperatures, the overall pyrolysis experiments were performed in two separate stages of reaction. In the first stage (Figure 33a), a quartz tubular reactor is positioned inside a tubular furnace with a continuous

condenser connected on top. A latex balloon was used to collect pyrolytic gas to perform offline analyses. The system was heated up to 550°C with 5 min-long intermediate steps to 350°C and 450°C. Once the system reached the desired temperature, the vapors generated from the thermal degradation of lignin and palm oil enter a loop of condensation and vaporization for 1 h. Offline analyses were performed on the gas (G1) and the heavy residue (R1), which is a mixture of recondensed liquids and the solid residue of pyrolysis. The second stage (Figure 33b), performed in the same conditions used in stage 1, consisted in a reaction and distillation step to separate the condensable liquids or bio-oil, where the continuous condenser was substituted by a bio-oil collector as already discussed in our previous papers [145,165]. After the second stage, three reaction products can be collected and analyzed: a gas (G2), a biochar (R2), and a liquid bio-oil (L2). To maintain consistency with previous studies the total mass of the mixture was fixed at 10g. This mass was selected to maximize the production of liquid products, as indicated in earlier research [145,165].
Different ratios of lignin and palm oil were investigated such as 10, 30, and 50 wt. %. In general, pyrolysis products in the text will be reported using the letter corresponding to the type of product (L, G, R), the number of the stage considered, and the percentage of lignin relative to the text (e.g. G1_50% to indicate the pyrolytic gas from the first stage of the process, obtained from the pyrolysis of palm with 50% of lignin ).

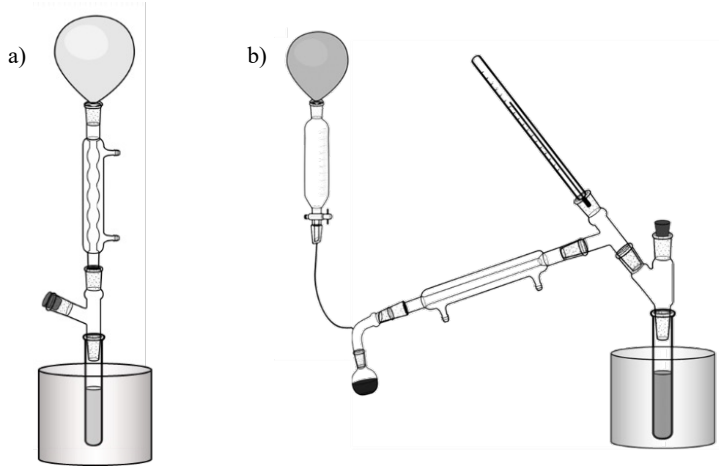


Figure 33: a graphic representation of the two stages pyrolysis setup

The overall yields have been calculated with the following equations, where M represents the total mass loaded into the reactor consisting in the sum of lignin and palm oil weights.

$$\text{Gas yield} = \frac{G1*M + G2*R1}{M} * 100 \quad \text{Eq. 1}$$

$$\text{Residue yield} = \frac{R1*R2}{100} \quad \text{Eq. 2}$$

$$\text{Liquid yield} = \frac{R1*L}{100} \quad \text{Eq. 3}$$

*6.1.2. Characterization of the products.*

Pyrolysis products have been characterized in all the different stages of the process. FT-IR analyses (Fourier Transform infrared spectroscopy, Nicolet 380 instrument, Thermo Scientific, Madison, WA, USA) have been performed on the gaseous streams using an inert glass cell equipped with KBr windows to store and analyze offline the gas (G1,G2) collected in a latex balloon. FT-IR has been also performed on the residues R1 and R2, and the liquid (L2) using a 1.000g KBr pressed disk placed in a specific support. Residues have been directly mixed with the KBr in a mass ratio of 1:100, while L2 measurements have been performed spreading a small drop of liquid samples on the disk surface. Semi-quantitative analysis of both gas (G1 and G2), and liquid (L2) have been conducted as well *via* gas chromatography-mass spectrometer (Focus-ISQ, Thermo Scientific, Milan, Italy).

## *6.2. Results*

*6.2.1. Characterization of the starting materials*

In Figure 34 the IR spectra of the reactants and reference materials, Kraft lignin and palm oil, palmitic acid, methyl palmitate and guaiacol, are reported. The spectrum of methyl palmitate is also reported as a reference. They agree with those reported and discussed in the literature for lignin [145,165,172], palm oil [172,173], palmitic acid [174], methyl palmitate [173], and guaiacol [175].

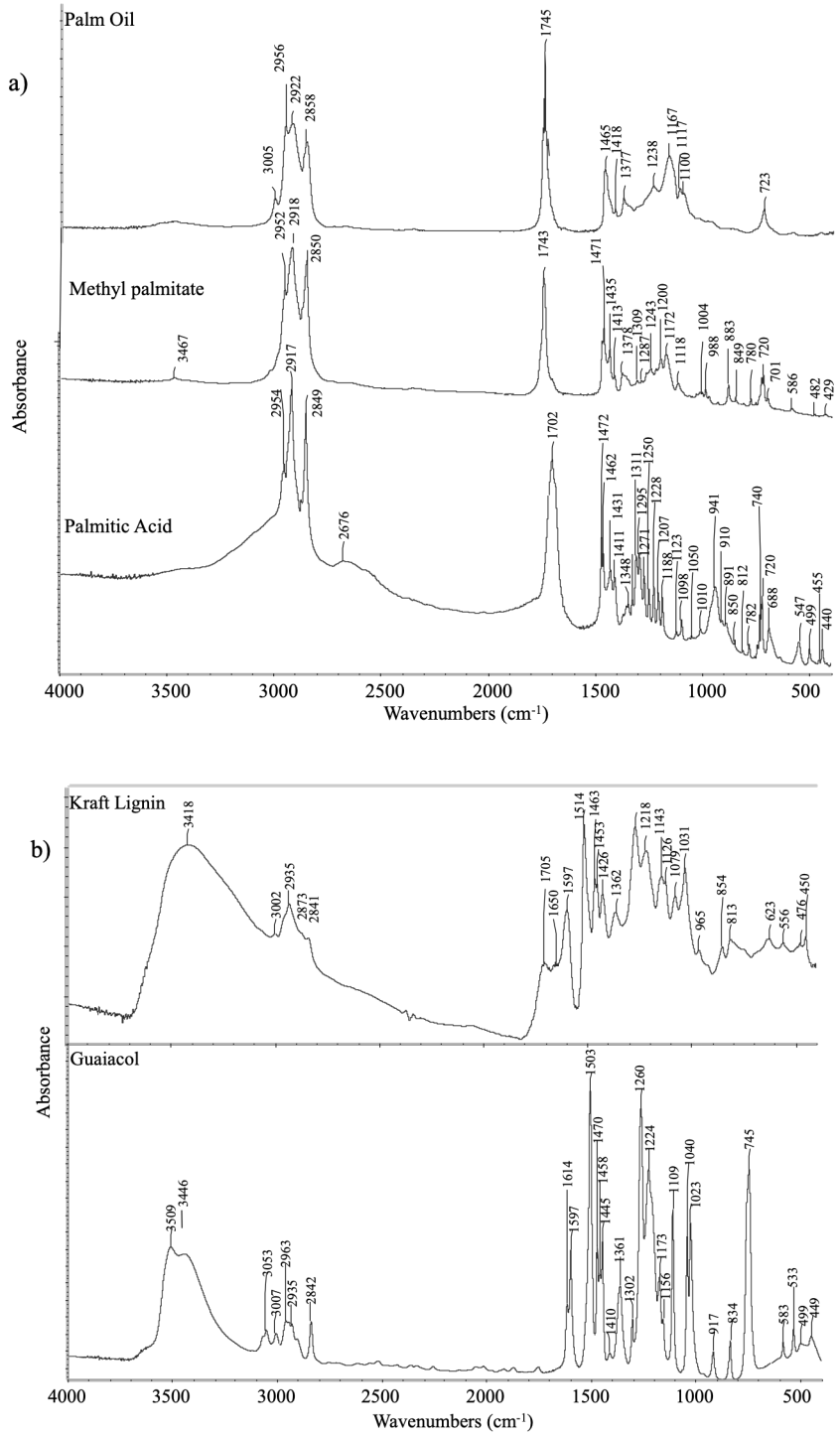


Figure 34: a) IR spectra of starting and reference materials: palm oil, methyl palmitate and palmitic acid. b) IR spectra of starting and reference materials: kraft lignin and guaiacol.

### *6.2.2. Process yields and products distributions in palm il and lignin pyrolysis experiments.*

In the following paragraphs, the reaction tests conducted with individual matrices will be described, as well as co-pyrolysis tests with palm oil and lignin, and with palmitic acid and lignin or guaiacol. IR analyses of the products and GC-MS analyses of liquid bio-oils at the

end of the two-stage process will be summarized. In Table 8, the distribution of product yields in the two stages of the pyrolysis reaction of palm oil and Kraft lignin is presented. As can be observed, the absence of lignin in the reaction environment results liquid-rich product, while increasing the percentage of lignin in the reactor contributes to an increase in gas and reaction residue at the expense of the liquid fraction. Sakulkit et al., in a study of co-pyrolysis of rubber wood and palm oil trunk obtained similar yields in terms of pyrolysis products. They achieved yields of 38-46 wt.% in bio-oil, 22-28 wt.% in biochar and around 30-36 wt.% of pyrolytic gas using a mixing ratio of 50:50 (wt.) [176]. These yields would agree with the results obtained in the second stage of the process as reported in the Table 1. However, taking in consideration the different nature of the matrix used, we obtained, for the same mass ratio, slightly lower oil yield, and higher yields of biochar and pyrolysis gas. In addition, data reported by Abnisa et al., shows pyrolysis yield of palm shell, EFB, and Mesocarp fiber, whose content in lignin represented almost the 44, 21, and 27 wt.%, respectively. In this case they obtained higher oil yields around 45%, despite the different content in lignin which is in contrast with our results, where lignin content appears to limit the oil production [177].

Table 8: Yields percentages of pyrolysis products in the two stages of the process, as a function of lignin percentage (% Lig, in wt.%). G1 and R1 are the products of the condensation stage, while G2, R2, and L2 are the final products of the distillation step , all reported as wt.% of the total mass loaded.

| | 0% Lig. | 10% Lig. | 30% Lig. | 50% Lig. | 100% Lig. |
|---|---|---|---|---|---|
| G1 [wt.%] | 9.1 | 14.3 | 18.9 | 26.9 | 18.0 |
| R1 [wt.%] | 90.9 | 85.7 | 81.1 | 73.1 | 82.0 |
| G2 [wt.%] | 11.5 | 21.5 | 18.7 | 17.9 | 19.8 |
| L2 [wt.%] | 76.0 | 63.4 | 52.8 | 40.2 | 23.4 |
| R2 [wt.%] | 12.5 | 15.1 | 28.5 | 41.9 | 56.8 |
| Gas [wt.%] | 19.5 | 32.7 | 34.1 | 40.0. | 34.3 |
| Liquid [wt.%] | 69.2 | 54.3 | 42.8 | 29.4 | 19.2 |
| Residue [wt.%] | 11.3 | 13.0 | 23.1 | 30.6 | 46.5 |

### *6.2.3. Pyrolysis of pure palm oil (0% Lig.)*

Figure 35 shows the FT-IR spectra of gaseous products after the first (a) and the second reaction steps (b). The results for pure palm oil are similar to those reported previously [172]. The spectrum of G1_0% shows the rotovibrational features [178] of $CO_2$ (3715, 3612, 2340

and 669 $cm^{-1}$), CO (2143 $cm^{-1}$), acrolein (2800, 2692, 1724, 1158 and 957 cm-1), ethylene (949 $cm^{-1}$) and propene (988, 912 $cm^{-1}$), as well as of other hydrocarbons (CH stretchings and deformations in the regions 3000-2800 $cm^{-1}$ and 1500-1400 $cm^{-1}$ respectively). These data suggest that palm oil cracking at the esters bonds occurs with different paths, giving rise to acrolein (when the C3 chain of glycerol is retained), $CO_2$ and CO, while ethylene and propene can arise both from fatty acid chain cracking and from glycerol chain cracking. In the spectrum of G2_0% the same molecules are observed except that the features of acrolein are almost completely absent. . Yang et al. (2006) reported the composition of pyrolytic gas from palm oil wastes. Micro-GC analysis showed the presence of mainly $H_2$, $CO_2$, CO, $CH_4$, and traces of $C_2H_4$ and $C_2H_6$, in a different temperature range from 500 to 900°C.

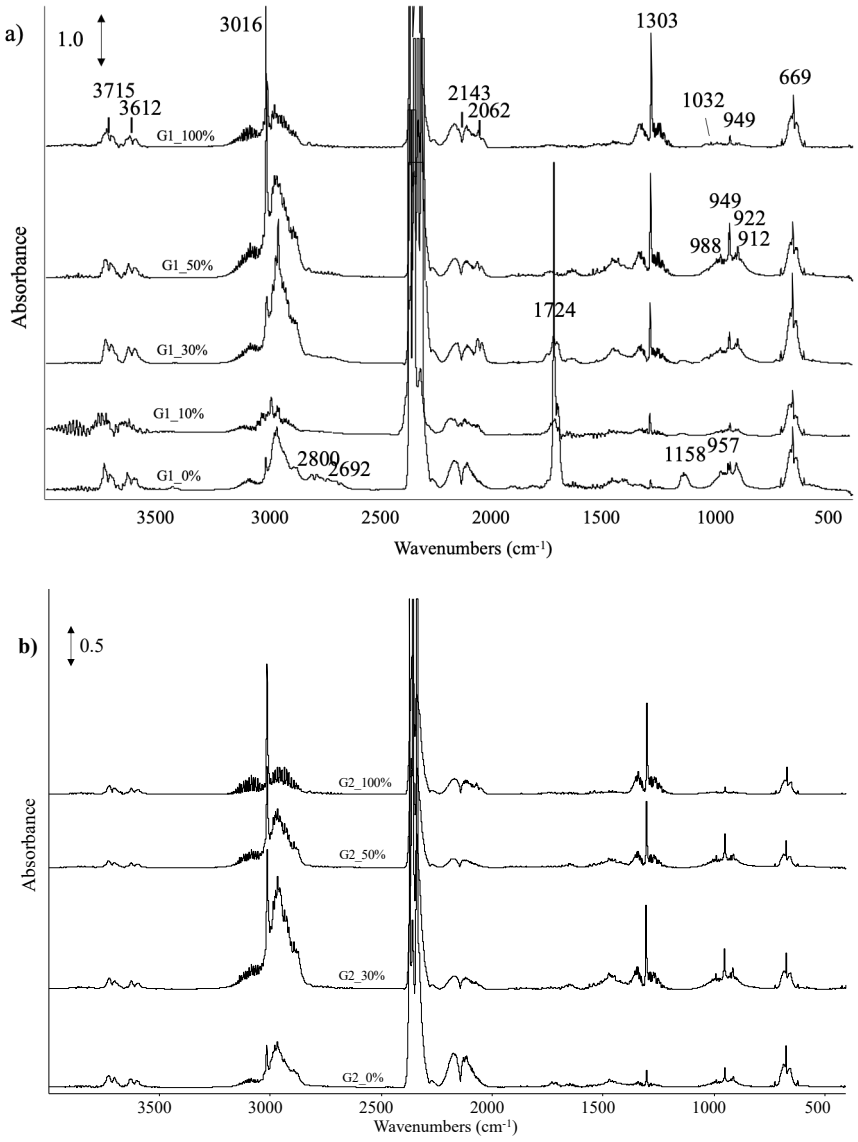


Figure 35: a) FT-IR spectra of G1 gases produced during the first stage. b) FT-IR spectra of G2 produced at the end of the process

The spectra of the condensed products starting from pure palm oil, are compared in Figure 36. In the spectrum of the residue obtained after the first pyrolysis step, R1, the features of palm oil are still present, showing that its conversion is far uncomplete. Additionally, the formation of molecules containing the carbonyl and the carboxyl groups is evident from the formation of the C=O stretching band centered at 1713 $cm^{-1}$, with a lower frequency component near 1700 $cm^{-1}$. In particular, the presence of fatty acids is made evident by the broad absorption in the 3500-2500 $cm^{-1}$ range, due to OH stretching of H-bonded dimers, the C=O stretching component at 1700 $cm^{-1}$, the C-O stretching at 1115 $cm^{-1}$ and the band at 943 $cm^{-1}$, also due to H-bonded dimers [174]. The presence of carbonyl and carboxyl compounds is still evident in the spectrum of the liquid L2, that is however dominated by intrinsically very intense CH stretching and bending modes of aliphatic hydrocarbon chains but contains the above cited features of fatty acids and the C=O stretching band of carbonyls at 1713 $cm^{-1}$. The band near 3420 $cm^{-1}$ is likely due to OH stretchings of alcohols. The spectrum of the residue R2 is essentially that of pure hydrocarbons, showing also a weak C=C band stretching of olefinic compounds at 1608 $cm^{-1}$, and only traces of carbonyl and alcoholic compounds. Other studies report the FT-IR characterization of the bio-oil derived from fast pyrolysis of palm oil biomass. These spectra present different features, mainly due to the lignin content of the palm oil biomass which consist in almost 29 wt. %. In fact, the spectrum reported for the bio-oil produced at 550°C showed a wide band between 3200-3400 $cm^{-1}$ assigned to the OH stretching vibrations of phenolic compounds.

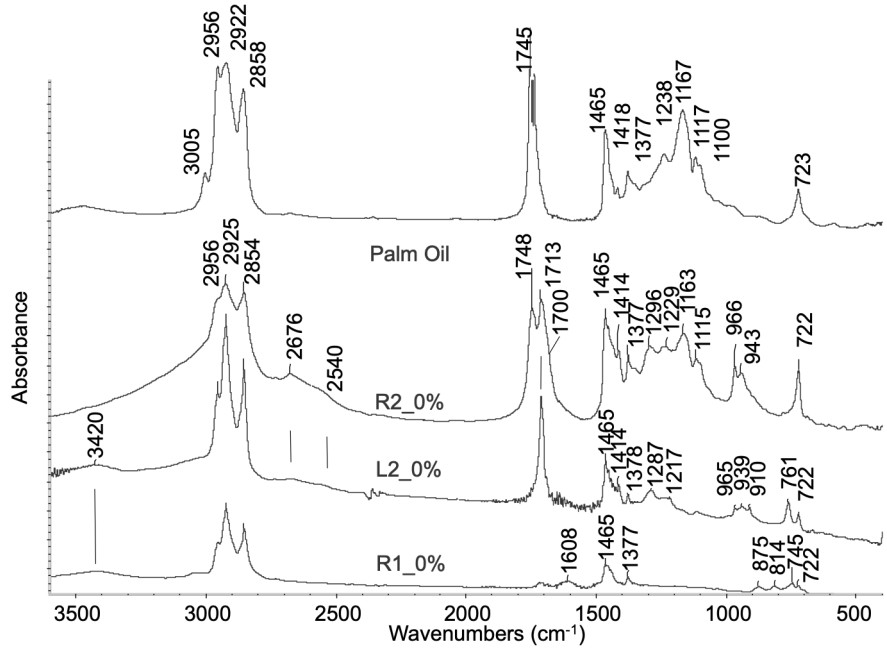


Figure 36: FT-IR spectra of palm oil conversion condensates

In the following figures (Figure 37 and Figure 38), GC-MS analysis of bio-oils have been reported. In Figure 37, the term “aromatics” includes aromatic compounds without the phenolic hydroxy group, mostly in the form of alkylated benzenes, where the alkyl radicals are mostly long chain hydrocarbon in the C6+ range. The most relevant are decyl-, heptyl-, and hexyl-benzenes. Polyaromatic are also formed but in lower amounts. Oxygenated compounds mostly include long chain ketones from palm oil degradation such as heptadecanone, octadecanone, and dodecanone. The GC-MS analysis of the L2_0% bio-oil (Table 9 and Figure 37), produced in the two stage process with 69% yield, allows a quantitive determination of the main compounds. Indeed almost 60% of this oil is constituted by linear paraffins and olefins, but the most abundant individual compound is palmitic (hexadecanoic) acid. Also medium chain linear fatty alcohols are present in moderate amounts (11 %) while other oxygenated compounds such as long chain linear ketones represent roughly 5 % of the biooil mass. It seems interesting also to remark that 75 % of the hydrocarbon products (Figure 38) fall in the Diesel fuel range (C13-C20) while also alcoholic compounds mostly fall in the Diesel gasoil boiling point range (180–360 °C). Anyway, the presence of high percentages of free fatty acids (20 %) represents an issue for this product. Interestingly, different results were obtained by Kim et al.(2010) performing the pyrolysis on fluidized palm kernel shells. Even if the content of lignin in palm kernel shell is about 45 wt.% , bio-oil content of phenolic compounds achieved is around 55 wt.% at 533°C, far from the results obtained in this paper with the lignin-palm oil mixture with similar lignin content. Abdullah er al. (2019) report palm oil catalytic pyrolysis results, where almost 85 % of bio-oil consists in hydrocarbons, with lower amount of acids (0.86%) and higher content of esters if compared to our bio-oil [179], while Supriyanto et al. (2018) produced a bio-oil from the pyrolysis of sludge palm oil with 76% of hydrocarbons, 8 % of esters, and 13% of alcohols [180].

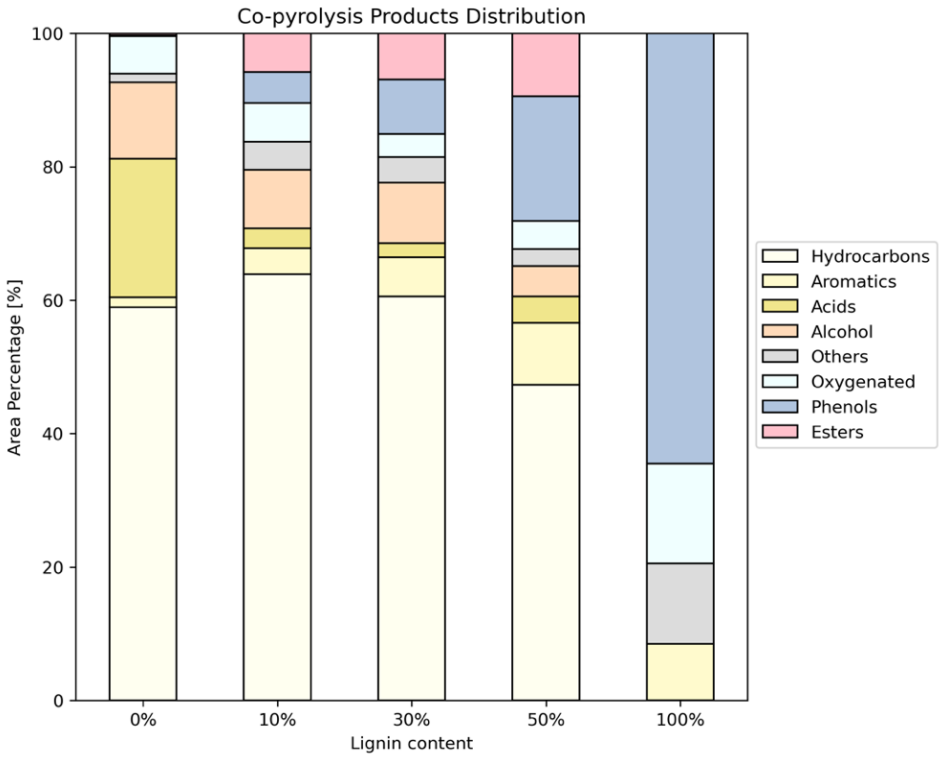


Figure 37: GC-MS products Distribution of palm oil and lignin pyrolysis and co-pyrolysis experiments

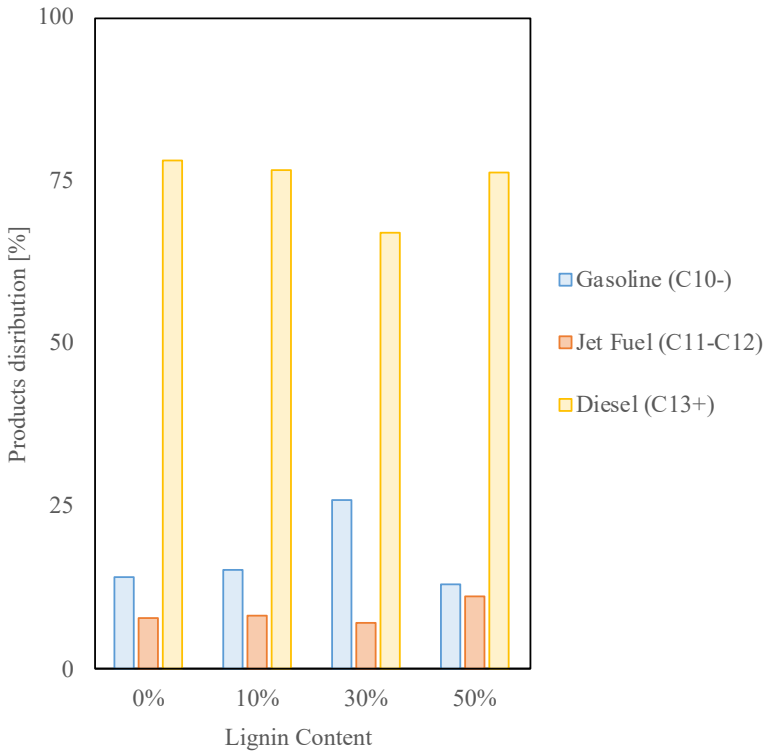


Figure 38: Distribution of hydrocarbon products in fuel ranges in experiments of palm oil and palm oil + lignin pyrolysis.

Table 9: List of the most abundant compounds present in the different bio-oil produced from palm oil – lignin mixtures. The reported percentage is calculated as the ratio between the area of the peak related to the compound considered and the total area.

| 0% | | 10% | | 30% | | 50% | |
|---|---|---|---|---|---|---|---|
| Name | % | Name | % | Name | % | Name | % |
| N-Hexadecanoic Acid | 15,7 | Pentadecane | 10,8 | Pentadecane | 11,5 | Pentadecane | 8,4 |
| Pentadecane | 9,5 | Tetradecane | 5,3 | 2-Nonene | 10,6 | Phenol,2-Methoxy-4-Methyl- | 4,7 |
| Heptadecane | 3,0 | 3-Octadecene | 4,1 | Tetradecane | 4,5 | Tetradecane | 3,8 |
| Tetradecane | 2,6 | Tetradecane | 3,9 | Heptadecane | 4,3 | Hexadecanoic Acid, Methyl Ester | 3,7 |
| 3-Hexadecene,(Z)- | 2,5 | Heptadecane | 3,7 | Hexadecanoic Acid, Methyl Ester | 4,1 | Phenol,4-Ethyl-2-Methoxy- | 3,2 |
| Tetradecane | 2,3 | 1-Tridecanol | 3,3 | Tetradecane | 3,2 | 3-Hexadecene | 2,9 |
| 3-Octadecene | 2,2 | 3-Hexadecene | 3,1 | 3-Octadecene | 3,1 | Heptadecane | 2,8 |
| 9-Hexacosene | 2,2 | Dodecane | 2,5 | 8-Heptadecene | 2,5 | Heptadecene | 2,8 |
| 8-Heptadecene | 1,9 | Hexadecanoic Acid, Methyl Ester | 2,5 | 1-Tridecanol | 2,4 | 4-methoxyphenol | 2,7 |
| Dodecane | 1,7 | Hexadecane | 2,4 | 3-Hexadecene | 2,3 | Tetradecane | 2,6 |
| Nonane | 1,7 | N-Hexadecanoic Acid | 2,2 | Hexadecane | 2,3 | N-Hexadecanoic Acid | 2,5 |
| 1-Tridecanol | 1,7 | 4-methoxyphenol | 2,0 | Dodecane | 2,1 | 1-Tridecene | 2,2 |
| 1-Undecanol | 1,5 | Nonane | 1,9 | 4-methoxyphenol | 2,0 | Hexadecane | 1,9 |
| Octane | 1,4 | Undecane | 1,9 | N-Hexadecanoic Acid | 1,8 | Cyclopropane, Nonyl- | 1,7 |

### *6.2.4. Pyrolysis of pure kraft lignin (100% Lig.)*

At the end of the two stage pyrolysis process kraft lignin primarily generates non-condensable gases and a solid residue. The pure lignin pyrolysis results are apparently different from those reported previously [145], where, however, experiments were performed with setup b (reaction and distillation) only, for 3 h. In the previous case, in fact, after 3 h pyrolysis time at 550 °C, 28.7% liquid yield, rich in methyl, methoxy, and methyl-methoxy- phenols was obtained, while gas yield was less than 30%. Here, the liquid L2 obtained is a 23.4 % suggesting that during the first condensation stage, some condensable gases may crack into gaseous products, or polymerize into solids reducing the pyrolysis oil yield. Despite the difference in yields, the composition of bio-oil results is similar to the one obtained without stage a. The spectrum of G1_100% (Figure 35a) shows the features of $CH_4$, $CO_2$, CO, and ethylene together with those of carbonyl sulphide, COS, (rotovibrational asymmetric stretching band at 2062 $cm^{-1}$ [181]) and of methanol (rotovibrational CO stretching band at 1032 $cm^{-1}$) and small amounts of other hydrocarbons. The formation of COS reflects the presence of sulfur in kraft lignin, while that of methanol is the result of cracking of lignin's methoxy groups. It is also interesting to remark that the amount of $CH_4$ produced from lignin is definitely higher than from palm oil while the reverse is true for olefins and higher hydrocarbons, while the ratio $CO_2$/CO is similar in the two cases. A similar spectrum is also observed for G2_100% (Figure 35b), where COS is still detected, suggesting that sulfur compounds are released during both stages of the reaction. The spectra

of residue R1_100% (Figure 39) shows very weak bands confirming that, even after 1 h treatment at 550 °C, biochar is essentially produced from lignin with a modest residual content of oxygenated functional groups.

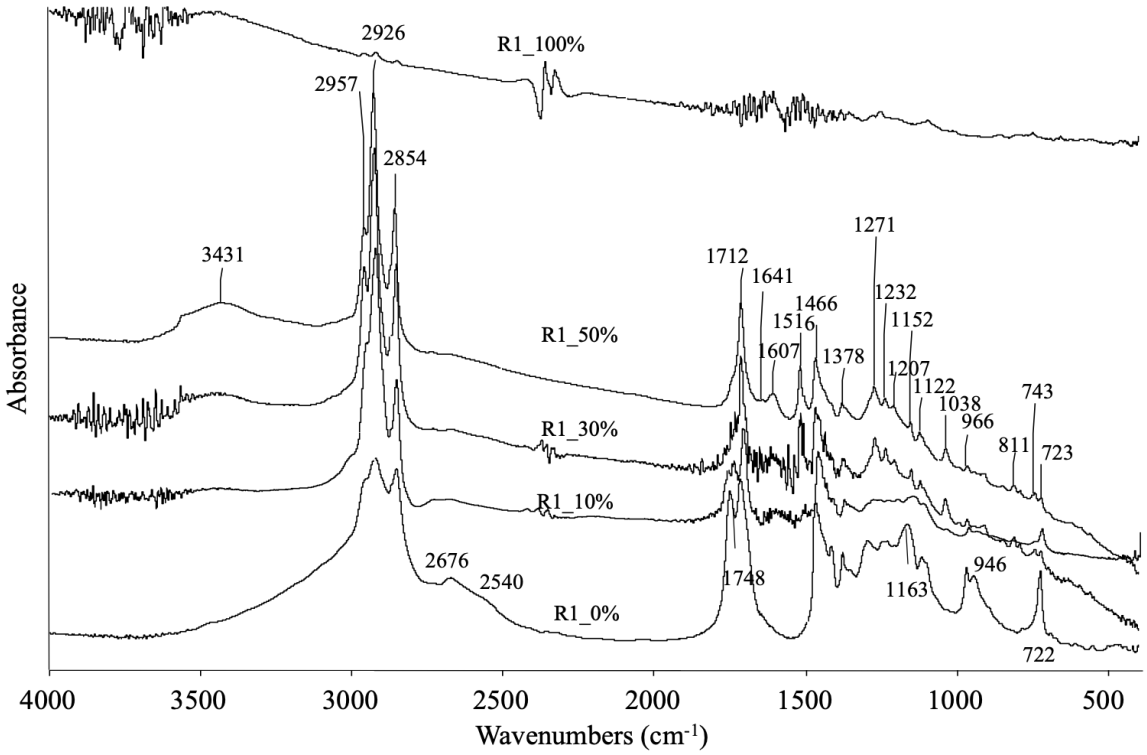


Figure 39: IR spectra of residues from palm oil + lignin co-pyrolysis experiments

*6.2.5. Pyrolysis of palm oil - kraft lignin mixtures.*

The quantitative data reported in Table 9 show that the addition of lignin to palm oil gives rise to a progressive increase in the production of gases in the first pyrolysis reaction step, whose amount roughly depends on the lignin content. The IR spectra of the produced gases G1 (Figure 35a) show that the presence of lignin results in the almost disappearing evolution of acrolein, suggesting that acrolein coming from palm oil cracking can react with solid lignin. On the other hand, it seems that the evolution of higher hydrocarbons and COS, with respect to the evolution of methane and CO, increases and has its relative maximum at 30 and 50 % lignin. These data suggest that lignin or the resulting biochar may have a catalytic effect in the evolution of hydrocarbons, while palm oil somehow favors the realease of sulfur from kraft lignin as COS. The IR analysis of G2 gases (Figure 35b) shows that the amount of methane evolved increases with lignin content while COS evolution is almost disappeared, suggesting that most sulfur is released in the first reaction step. The spectra of

the condensate residues obtained after the first reaction stage are reported in Figure 39. The spectra show that the addition of lignin seems to increase the conversion of palm oil and in particular, of palmitic acid (the corresponding bands at 2676, 2540, 1748, 1163, 946 $cm^{-1}$ are strongly decreased in intensity already with 10 % lignin), with the increased formation of aliphatic hydrocarbons (main CH stretching bands). A number of additional bands are formed: in particular two evident bands at 3430, 1607 and 1516 $cm^{-1}$ can be due to OH stretchings and aromatic ring stretchings of alkyl/alkoxy phenols coming from lignin decomposition as also reported from FT-IR characterization of palm kernel oil produced by Suikran et al. and in our previous studies [145]. The spectra of the liquids distilled in the second reaction step (L2) are reported in Figure 40. They also show the formation of the bands near 3430, 1607 and 1516 $cm^{-1}$, likely due due to alkyl/alkoxy phenols. Additionally, the spectra of liquids obtained in contact of palm oil with lignin have less evident bands of palm oil and more evident a component of C=O stretching at 1743 $cm^{-1}$. This peak can be due to esters and coincides with that of methyl palmitate (Figure 34). Methyl ester formation is observed also in the study reporting the pyrolysis of palm kernel shell performed by Kim et al. (2014). They report the presence of dodecanoic acid methyl esters in the oil produced by non-catalytic test performed at 485°C, whose formation is attributed the cracking of fatty acids and tryglicerides . Also in this case, the content of methyl esters is limited while the content in carboxylyic acid is far higher. Adding a catalyst like ZSM-5, they report a decrease of dodecanoic acid and its relative esters due to the favored decarbonylation and decarboxylation.

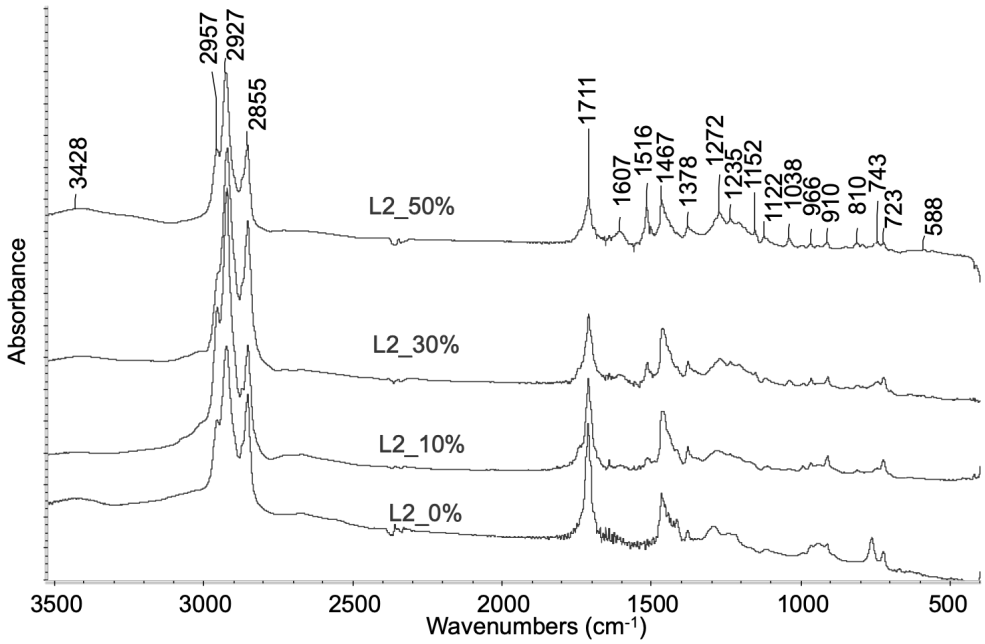

Figure 40: IR spectra of L2 liquids after palm oil + lignin co-pyrolysis experiments

The GC analysis of L2 liquids (Table 9 and Figure 37) in fact reveals the predominant formation of linear paraffins and olefins, the strong decrease of palmitic acid among the products, and the appearance of alkyl/alkoxy phenols as well as of methyl esters (up to 10%), in particular methyl pamitate, likely due to the reaction of palmitic acid or triglicicerides with the methoxy groups of lignin. A similar result was observed by Babinszky et al. (2022). Authors observed an *in situ* FAME formation during pyrolysis of oil palm empty fruit bunch (EFB) biomass, and this was explained by the reaction of the lipid and lignin contents of the biomass; i.e., the fatty acid moieties of triglycerides were methylated by the methoxy side groups of lignin during the thermal treatment.

### *6.2.6. Pyrolysis of palmitic acid acid and co-pyrolysis of palmitic acid and lignin or guaiacol.*

To investigate the reaction mechanism leading to the formation of fatty acid methyl esters (FAMEs), additional pyrolysis experiments of pure palmitic acid and co-pyrolysis experiments of palmitic acid with 10% lignin or guaiacol were conducted to investigate the reaction mechanism leading to the formation of fatty acid methyl esters (FAMEs). In Figure 41, the IR spectra of the gas and liquid products obtained from the pyrolysis of pure palmitic acid are reported. In the spectrum of G1 big amounts of $CO_2$ are present, together with methane, ethylene, propylene, higher hydrocarbons, and CO. This suggests that decarboxylation of the acid occurred in the first reaction step, together with some chain cracking. Hydrocarbons from $C_1$-$C_7$ have been observed by Asomaning et al., during the pyrolysis of pure oleic acid 450°C, where they noticed that C1-C4 range hydrocarbons increase with the increasing of the temperature [182]. In parallel, in the spectrum of the liquid residue R1 the features of unconverted palmitic acid are almost absent, but only those belonging to paraffinic hydrocarbons and small amounts of ketones, appear evident. These compounds have been observed also in the liquid fraction derived from the pyrolysis of oleic acid, where linear saturated alkanes represent the main compounds [182]. In the spectrum of G2 $CO_2$ is almost absent, confirming that full decarboxylation of palmitic acid essentially occurred in the first reaction step. Only some CO, methane and other hydrocarbons are observed, indicating that chain cracking and some ketone decarbonylation occurred.

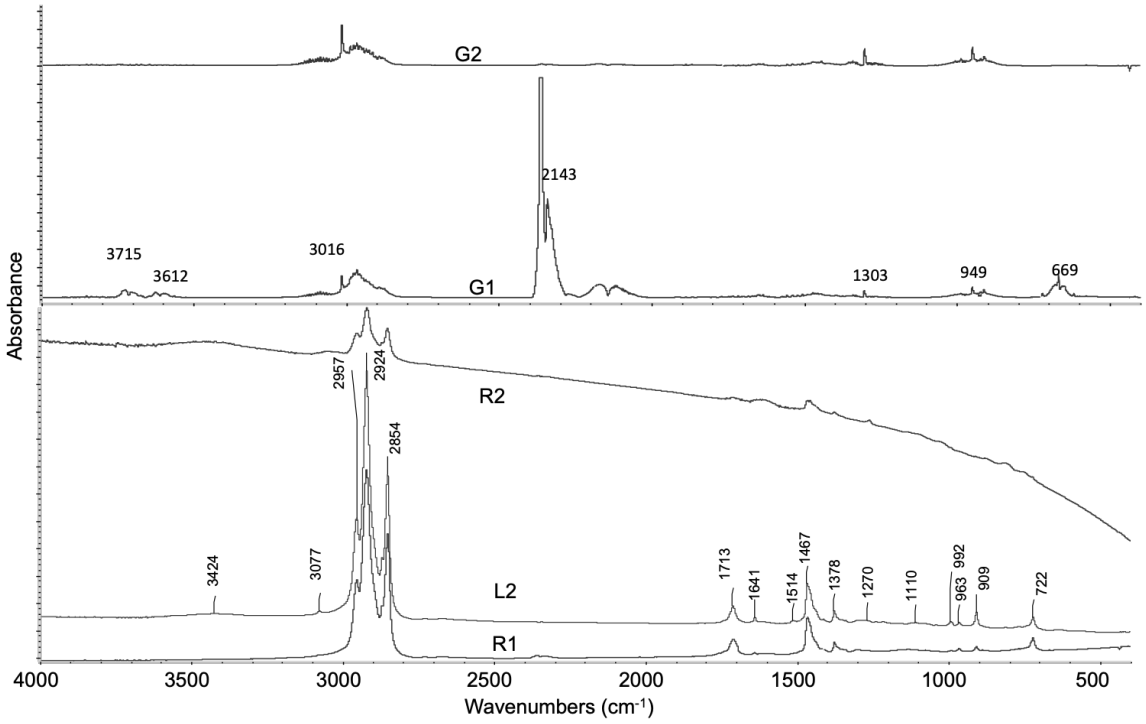


Figure 41: IR spectra of palmitic acid pyrolysis products

The spectra of L2 and R2 are dominated by the features of paraffinic and olefinic hydrocarbons, with moderate amounts of ketones (CO stretching at 1713 $cm^{-1}$) and alcohols (OH stretching near 3430 $cm^{-1}$). GC analysis (Table 10 and Figure 42) indeed shows that the product of simple palmitic acid decarboxylation, i.e. pentadecane, is the most abundant product in L2 together with linear paraffins and olefins, but that the amount of alcohols is higher than from pyrolysis of palm oil. The overall mixture produced falls almost entirely in the boiling range of Diesel gasoil. Deoxygenation and pyrolysis of oleic acid gives rise also to cycloalkanes formation which are partially observed also in the bio-oil from pure palmitic acid, and palmitic acid/guaiacol mixture. Moreover, the mass balances (Table 11) show that the gases produced are only slightly more than those expected by simple palmitic acid decarboxylation.

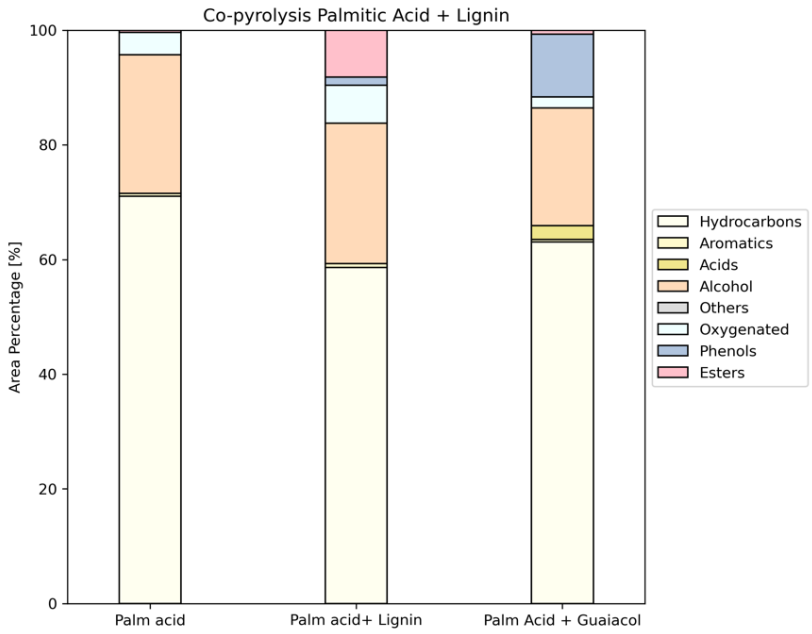


Figure 42: composition of palmitic acid pyrolysis oil compared to co-pyrolysis results with lignin and guaiacol

The full conversion of palmitic acid when pyrolyzed alone, somehow contrasts with its detection as a significant product of palmitic oil pyrolysis. This could be explained supposing that interaction of palmitic acid with palmitic oil or other chemical compounds coming from it may stabilize palmitic acid and hinder its conversion. On the other hand, palmitic acid and palm oil give essentially the same pyrolysis products, supporting that palmitic acid is one of the intermediates in palm oil pyrolysis, as also reported in literature [183,184].

Mixtures of palmitic acid with lignin have also been co-pyrolyzed. As a model of the co-pyrolysis experiments, also the reaction of palmitic acid-guaiacol mixtures have been investigated. The IR spectra of the condensate residues are quite similar to each other, and to those coming from palmitic acid (due to paraffinic and olefinic hydrocarbons and ketones) with the addition of bands arising from aromatic compounds (ca 1600 and 1503 $cm^{-1}$) similar to those present in the spectrum of guaiacol itself and other alkyl/alkoxyphenols. The analysis of the C=O stretching shows that three bands are present in the residue of the first step (R1), at around 1765, 1743 and 1715-1705 $cm^{-1}$. The last band is due to CO stretchings of ketones coming from palmitic acid pyrolysis and to unconverted palmitic acid, while the first band found near 1765 $cm^{-1}$ can be confidently assigned to CO stretching of phenyl esters (substituted phenyl palmitates) formed by esterification of palmitic acid with phenols coming from lignin decomposition and from guaiacol itself [185]. The intermediate band, which is far more evident in presence of lignin than in presence of guaiacol, coincides with

that of methyl palmitate (Figure 34) and of other fatty acid methyl esters. The band near 1765 $cm^{-1}$ is essentially not present in the spectra of the distilled liquids L2 in both cases, likely due to the much lower volatility of phenyl palmitates, or to their cracking during the second reaction steps. Also, in the liquids L2 produced by two-step pyrolysis of palm oil – lignin mixtures this band is not observed.

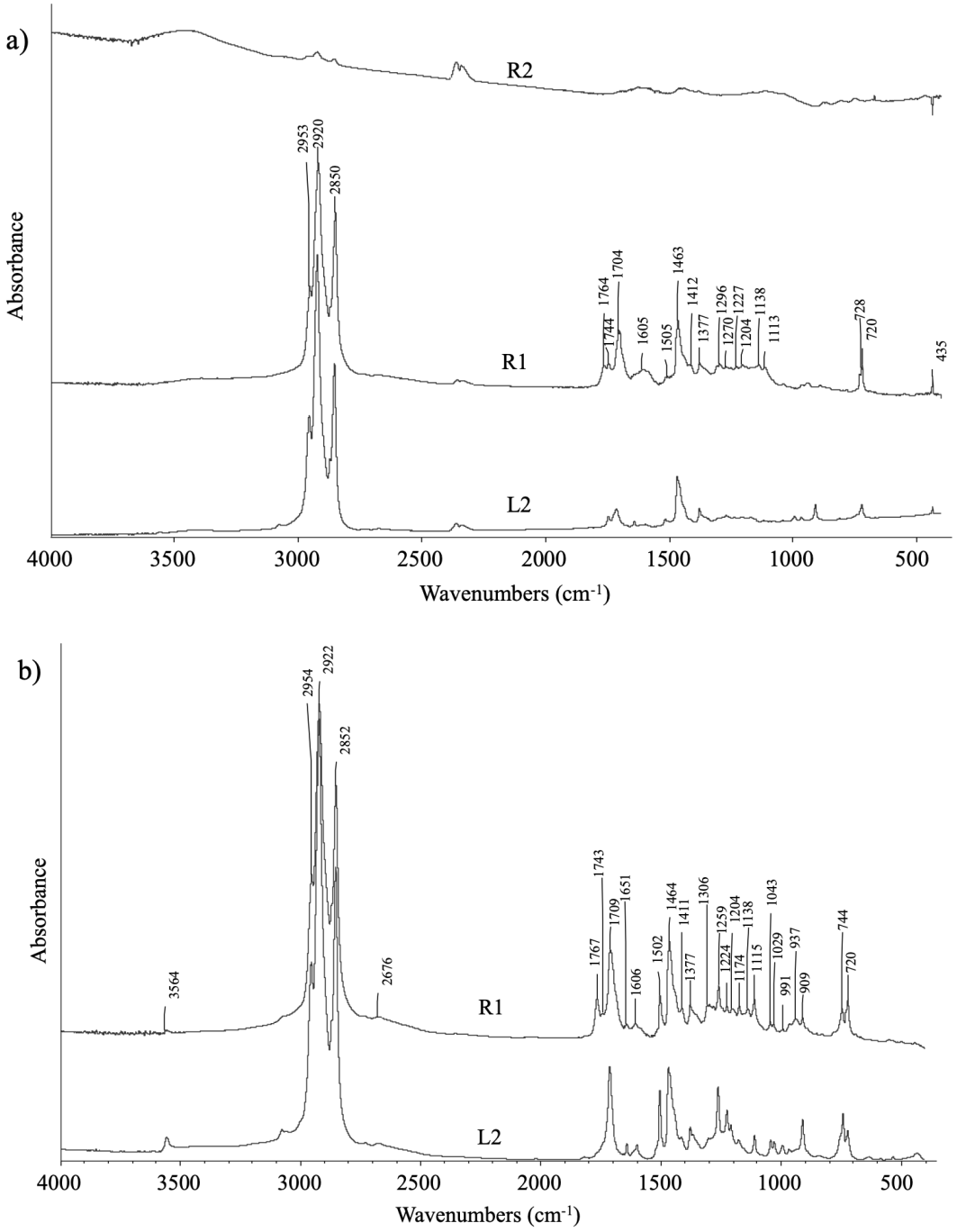


Figure 43: Condensed products of two stage pyrolsys of palmitic acid +lignin mixtures (a), and palmitic acid+guaiacol mixture (b)

The GC analyses confirm that L2 liquid from palmitic acid + lignin co-pyrolysis contains significant amounts of methyl esters, together with hydrocarbons and alcohols, while only a very limited amount of methyl esters are formed from palmitic acid + guaiacol mixtures. This suggests that methoxy groups linked to the solid polymer constituent of lignin are more reactive than those of guaiacol, considering that guaiacol is a volatile compound in reaction conditions and that it also reacts at the phenolic group producing substituted phenyl esters. According to Asomaning et al. (2014), for saturated acids the deoxygenation is more favoured than C-C bond breaking, due to the lower dissociation energy [183]. Moreover, they report the formation of n-heptadecane due to the deoxygenation of stearic acid during pyrolysis, like in this work deoxygenation of palmitic acid occurs, leading to the formation of pentadecane.

Table 10: List of the most abundant compounds present in the different bio-oil produced from palmitic acid (AP) – lignin and -guaiacol mixtures. The reported percentage is calculated as the ratio between the area of the peak related to the compound considered and the total area.

| AP | | AP+LIG | | AP+G | |
|---|---|---|---|---|---|
| Name | % | Name | % | Name | % |
| Pentadecane | 31,83 | Pentadecane | 22,26 | Pentadecane | 37,13 |
| 1-Hexadecanol | 7,58 | Tetradecane | 7,84 | Mequinol | 10,05 |
| 1-Tridecanol | 5,21 | 1-Hexadecanol | 7,34 | 1-Tridecanol | 8,35 |
| Pentadecane | 4,73 | Hexacanoic acid, methyl ester | 6,93 | 1-Hexadecanol | 7,86 |
| Tetradecane | 4,23 | 1-Hexadecanol | 6,12 | Tridecane | 4,07 |
| Dodecane | 3,53 | Tetradecane | 5,24 | Tetradecane | 4,03 |
| 1-Tridecanol | 3,38 | 2-Heptadecanone | 4,73 | 1-Tridecanol | 3,60 |
| 3-Dodecene | 3,29 | 1-Tridecanol | 4,06 | 3-Dodecene, (E)- | 2,49 |
| 1-Undecanol | 3,29 | Dodecane | 3,34 | Dodecane | 2,41 |
| Cyclooctane,1,2-dimethyl- | 2,95 | Undecane | 2,08 | n-Hexadecanoic acid | 2,40 |
| Undecane | 2,65 | Hexadecane | 2,01 | Cyclopropane, 1-heptyl-2-methyl- | 2,29 |
| 1-Nonene | 2,56 | 1-Dodecene | 1,92 | cis-2-Nonene | 2,05 |
| 1-Octene | 2,36 | 1-Undecanol | 1,77 | Undecane | 1,71 |
| Decane | 2,27 | Decane | 1,65 | Octane | 1,50 |

Table 11: Yields percentages of products in the two stages pyrolysis of palmitic acid as such and mixed with lignin and guaiacol reported as wt.% of the total mass loaded.

| | Palmitic acid + Lignin | Palmitic acid as such | Palmitic acid + guaiacol |
|---|---|---|---|
| G1 [wt.%] | 40.9 | 57.1 | 24.2 |
| R1 [wt.%] | 59.1 | 42.9 | 75.8 |
| G2 [wt.%] | 27.1 | 31.5 | 35.6 |
| L2 [wt.%] | 53.3 | 56.0 | 57.8 |
| R2 [wt.%] | 19.6 | 12.5 | 6.6 |
| Gas [wt.%] | 56.9 | 70.6 | 51.2 |
| Liquid [wt.%] | 31.5 | 24.0 | 43.8 |
| Residue [wt.%] | 11.6 | 5.4 | 5.0 |

## *6.3. Conclusions.*

The study reported here confirms that the pyrolysis of palm oil can produce a liquid bio-oil mostly constituted by linear paraffins and olefins with smaller amounts oxygenated compounds, a large part of it falling in the distillation range of Diesel fuels. The quality of the bio-oil is somehow reduced by the presence of significant amounts of carboxylic acids, primarily palmitic acid. It is also confirmed that, in contrast, the pyrolysis of fatty acids such as palmitic acid produces an even better gasoil liquids than those coming from triglycerides, because full conversion of pure fatty acids acid can be achieved. This is interpreted assuming that fatty acid stability is increased during pyrolysis of vegetable oils by interaction with the triglycerides or reaction intermediates. On the other hand, availability of palmitic and other fatty acids is limited, thus being not a good source of biofuels. It is reported here that the quality of the biooils produced from a vegetable oil such as palm oil can be improved if pyrolysis is realized in the presence of lignin, a low-cost waste of paper and bioethanol productions. This is because in the presence of lignin, fatty acids coming from triglyceride pyrolysis are in large part converted to fatty acid methyl esters, in this case mainly methyl palmitate.

# *Chapter 7. Catalytic upgrading of bio-oil produced by Kraft lignin pyrolysis: effect of process parameters and sulfur content*

Data reported in this chapter is under finalization for submission at the time of writing the present thesis:

**M. Borella**, M.A. Palazzolo, H.H. van de Bovenkamp, P.J. Deuss, A.A. Casazza, G. Garbarino, G. Busca, Catalytic upgrading of bio-oil produced by Kraft lignin pyrolysis: effect of process parameters and sulfur content.

In this work, a new pyrolysis setup was built trying to optimize the production and the recovery of the lignin oil. Since most of the time pyrolysis oil quality need to be improved due to the presence of wide spectrum of compounds, a characterization step is necessary to understand chemical composition and address the further catalytic upgrade. GC-MS, GPC, NMR, and elemental analysis have been performed on pyrolysis products. $Cu/TiO_2$-P25 catalyst active in the selective demethoxylation of guaiacols (abundant in the bio-oil) was tested to obtain valuable chemical intermediates such as phenols. A catalytic hydrotreatment in continuous configuration was used to monitor the activity of $Cu/TiO_2$ in the conversion of 4 methyl guaiacol in presence of thiophene in different concentration to reproduce the sulfur content of the bio-oil. Direct catalytic HDO of the oil in batch configuration has been performed with high $H_2$ pressure (100 bar) at 350°C.

## *7.1. Materials and methods*

### *7.1.1. Catalyst preparation*

The $Cu/TiO_2$ catalyst was prepared by wetness impregnation dissolving copper nitrate trihydrate in an amount of Milli-Q water equal to the measured pore volume for water of the support. The solution was added dropwise to the $TiO_2$-P25 support at room temperature. The mixture was then dried at 100 °C for 12 h, and calcinated at 400 °C using a temperature ramp of 2 °C/min for 2 h.

### *7.1.2. Oil production and characterization*

In this work, the valorization of Kraft lignin is obtained by pyrolysis at 550˚C with a continuous $N_2$ flow of 2 L/min as shown in Figure 44. Each run has been performed for a time of 20 minutes, after 10 minutes of $N_2$ purge. The heating system allow to reach 550 ˚C

in three minutes, with a maximum peak of temperature around 600 ˚C. For each test, 30g of biomass is loaded in the heating zone of the reactor after a drying step in the oven at 110 ˚C to limit the production of water during the pyrolysis. The biomass consists in a thin powder of diameter of 70 µm, which is kept together and supported by a metal sponge. This allows to fix the lignin in the heating zone of the reactor and let the products to permeate (gas and oil). A first light fraction (CB1) of the oil is separated in an ice trap, where also water is inevitably produced and collected. A second oil fraction (CB2) is collected in a trap with liquid $N_2$. The condensed oils in the cold traps have been then recovered with acetone, together with the oil remained in the lines (LINES). The total oil has been then collected after the evaporation of the acetone through rotary evaporation (50°C, 0.2 psi), and analyzed using GPC, GC-MS, 2D-GC, and NMR analysis. A scheme of the oil processing after pyrolysis is reported in Figure 44b. The water content of the oil has been then evaluated by titration, while C, H, and S content have been performed with CHNS elemental analysis. Non-condensable gasses flowing together with $N_2$, due to the sulfur content present in the Kraft lignin will contain sulfur compounds such as $H_2S$ and $SO_2$ (Borella et al. manuscript in preparation). A solution of NaOH have been used to neutralize part of the sulfur gases produced. However, gas products were not collected and analyzed in this process.

a)

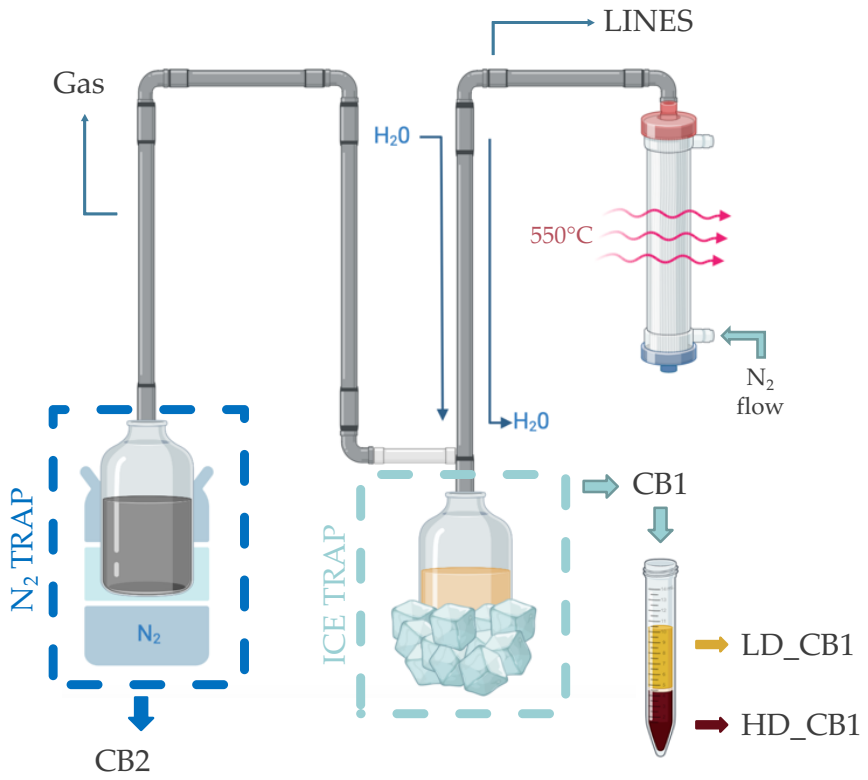

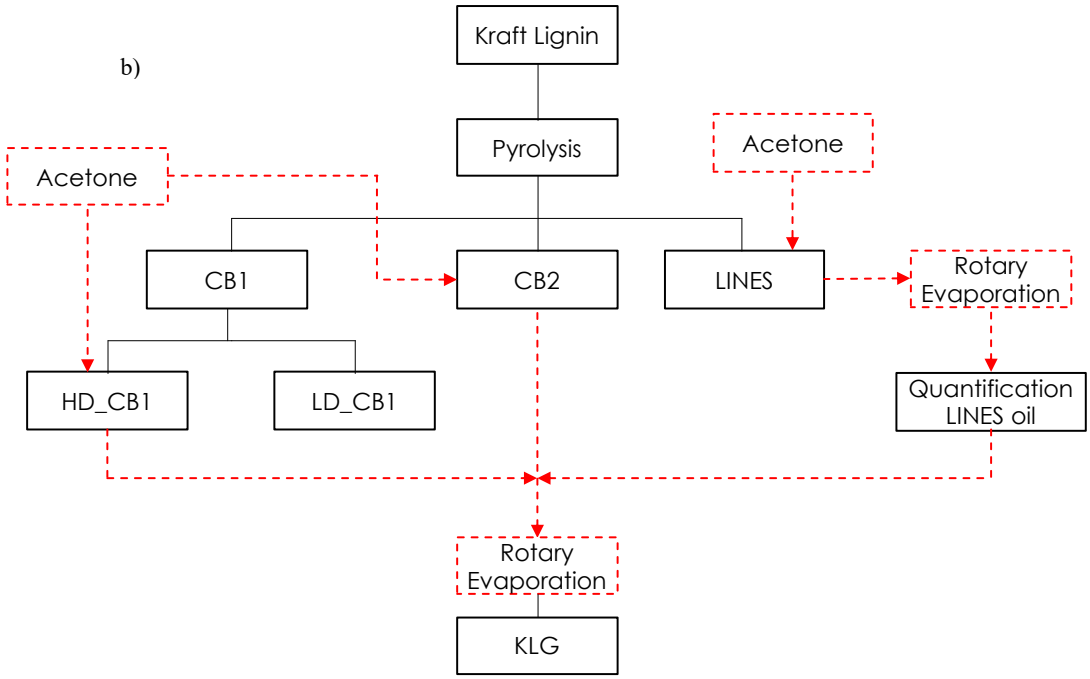


Figure 44: scheme of the pyrolysis setup proposed for the process (a), and the post-process collection procedure of the oil to separate the different fractions (b).

### *7.1.3. Sulfur tolerance of $Cu/TiO_2$ catalyst for the selective demethoxylation of bio-oil*

The sulfur in the bio-oil, even in small quantities, can deposit on the catalyst surface and affect the catalytic activity. Therefore, a deeper study of the poisoning mechanism is needed to understand the deactivation of the catalyst with different sulfur concentrations. A catalytic hydrotreatment experiment was performed using a model bio-oil feed of 4-methyl guaiacol (5 wt.% in toluene), being alkylated guaiacols the most relevant compounds in the obtained pyrolytic oil. Then, thiophene was add to the feed an external sulfur source to reproduce the sulfur content of the oil that have been calculated from CHNS analysis. The reaction was carried out in a fixed-bed stainless steel reactor with an outer diameter of 6.35 mm and an inner diameter of 4.55 mm. Each experiment was performed with 0.100g of $Cu/TiO_2$ catalyst mixed with 0.200g of SiC, and reduced *in-situ* for 2h at 360 °C and 6 bar, under a constant $H_2$ flow of 20 mL/min.

After the reduction, the feed was pumped through the reactor with an HPLC pump at a Weighted Hourly Space Velocity (WHSV) of 23 $h^{-1}$, according to previous experiments performed with bio-oil enriched with guaiacols [65]. The flow rate (F) was calculated based on the set WHSV and the catalyst loading. Samples were collected at intervals of 1h, for a total time of stream (TOS) of 8 hours, and then analyzed by GC-MS. Dodecane was added to the solution as an internal standard (IS). First, a solution made with 50 mg of each sample

was mixed with 1ml of THF. Then, 270 μL of this solution was mixed with 30 μL of THF containing 5000ppm decane as an external standard.

### *7.1.4. Catalytic hydrotreatment of bio-oil*

Parr reactor was used to perform the catalytic hydrotreatment of the pyrolysis oil using the 5 wt.% $Cu/TiO_2$ catalyst used in previous steps. The experiment was carried out using 15g of pyrolytic oil and 0.5g of $Cu/TiO_2$. The reactor was pressurized with $H_2$ up to 100 bar, and then purged three times to atmospheric pressure to ensure the removal of air. A stirrer at 800 rpm ensured a good mixing inside the reactor. Once the reactor is pressurized up to 100 bar, a temperature ramp was set to reach 300 °C for 1h, and then increase again up to 350°C for other 2h. Together with temperature also the pressure is increasing up to more than 200 bar. The resulting oil was then analyzed through GPC, GC-MS, and NMR.

### *7.1.5. Nomenclature*

The setup, as mentioned above, include two different condensation steps, first with an ice trap and, then with a liquid $N_2$ trap, allowing the separation of two oil fraction referred to as ''CB1'' and ''CB2'', respectively. These fractions have been first characterized separately, as well as the oil remained in the process line referred to as ''LINES''. Moreover, CB1 consist of two phases: a low-density phase (LD_CB1) made of water and water-soluble aromatics, and a high-density oil phase (HD_CB1), and both have been analyzed with GPC and GC-MS. CB1 nomenclature is referred to the total oil collected in the ice trap and include both LD_CB1 and HD_CB1. CB1, CB2 and LINES were collected in acetone and the overall oil will be referred to as KLG. The oil after the hydrotreatment will be referred to as hydrotreated oil (HTO).

## *7.2. Results and discussion*

### *7.2.1. Pyrolysis yield*

The target of the process is to produce oil for the further upgrade. For this reason, biochar and gas products have not been characterized. The yield of the pyrolytic oil obtained is around 30%, the char around 35% as well as the gas yield calculated by difference, as shown in Figure 45, where products distribution obtained in the same process conditions for several tests is reported. The LD_CB1 fraction consist of 7% of the total products and almost 30% of the final oil. In Table 12 data for all the test performed are reported. From KLG1 to KLG5

oil collected include the water layer LD_CB1, while from KLG6 to KLG11 the water rich fraction has been removed and separately characterized. Water content analysis of the oil fractions have been performed by Karl-Fisher titration and reported in Table 12. The known $H_2O$ content in the oils allows the calculation of the water-soluble aromatic part of the LD_CB1. In CB1, water represents the 16.2 wt.%, which is completely collected in the LD_CB1 fraction. Water in LD_CB1 ($H_2O$_LD) represents the 22-28 wt.%, hence the water-soluble aromatic part could be estimated around 70 wt.%, and its characterization has been performed with GC-MS. Results showed that LD_CB1 composition is rich in benzenediols, alkylated benzenediols, phenols, guaiacols and other valuable compounds like vanillin (Arom_LD). Therefore, it would be worthy to design an optimized separation process to extract these high value compounds.

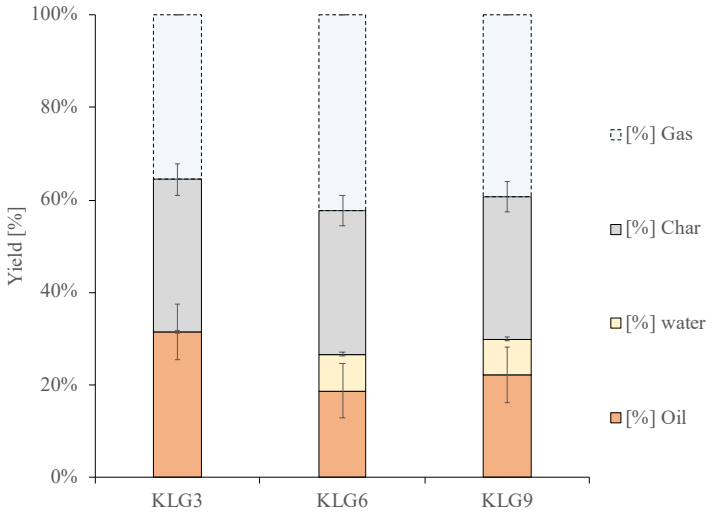


Figure 45: Distribution of pyrolysis products

Table 12:Summary table for the oil fractionation and yields

| Pyrolysis test | Lignin [g] | CB1 [g] | HD_CB1 [g] | LD_CB1 [g] | Arom_LD [g] | $H_2O$_LD [g] | CB2 Oil [g] | Lines Oil [g] | Char [g] |
|---|---|---|---|---|---|---|---|---|---|
| KLG1 | 30.13 | 4.03 | - | - | - | - | 3.61 | 1.76 | 7.17 |
| KLG2 | 28.66 | 3.68 | - | - | - | - | 3.01 | 1.67 | 9.58 |
| KLG3 | 28.73 | 3.39 | - | - | - | - | 4.60 | 1.05 | 9.47 |
| KLG4 | 29.84 | 4.00 | - | - | - | - | 2.99 | 1.72 | 9.77 |
| KLG5 | 29.65 | 3.66 | - | - | - | - | 3.04 | 1.70 | 10.38 |
| KLG6 | 29.87 | 3.40 | 1.05 | 2.35 | 1.80 | 0.55 | 2.87 | 1.68 | 9.27 |
| KLG8 | 29.63 | 3.41 | 0.95 | 2.46 | 1.90 | 0.55 | 3.42 | 1.63 | 8.07 |
| KLG9 | 29.31 | 4.00 | 1.73 | 2.27 | 1.62 | 0.65 | 3.03 | 1.74 | 9.04 |
| KLG10 | 29.17 | 3.35 | 1.17 | 2.18 | 1.64 | 0.54 | 3.22 | 1.48 | 9.57 |
| KLG11 | 29.04 | 3.02 | 0.89 | 2.13 | 1.64 | 0.49 | 2.35 | 1.06 | 8.60 |
| $H_2O$ content [%] | - | 16.19 | - | - | - | - | 0.87 | 1.52 | - |

### *7.2.2. Oil characterization-Gel Permeation Chromatography*

To understand the efficiency of the depolymerization during the process, GPC analyses of the THF-soluble part of Kraft lignin have been performed. The normalized molecular weight distributions (MWD) of different replicas of the pyrolytic oil (KLG1, KLG2 and KLG10) have been compared to the Kraft lignin profile in Figure 46a, where we can see a good grade of depolymerization and, good data reproducibility of the oil produced.

The oils presented in Figure 46a differ because KLG1 and KLG2 include the low-density fraction of CB1 (LD_CB1) which is not included in KLG10. This difference is highlighted by the presence of the shoulder around 170 g/mol for the KLG1 and KLG2, which is corresponding to the main peak of the LD_CB1 fraction. In Figure 46b, CB1 is the only curve exhibiting a shoulder in that molar mass range since it is the fraction with the highest content of the water-soluble phase.

From the setup design we could expect differences in terms of composition in the oil fractions of the two traps. In fact, HD_CB1 oil shows a higher peak at lower molar masses, while in CB2 and LINES fractions the highest peak is shifted to slightly higher molar weight. Despite these differences, CB1 and CB2 cannot be considered two different fractions of the oil since from the composition point of view they showed more similarities than differences. Parameters such as flow velocity and retention time can strongly influence the condensation rate in each stage and therefore the composition of the fractionated oil. In this work, we used a high and constant nitrogen flow which on one hand, can push the pyrolysis vapors through the lines, but on the other side it lowers the residence time in the traps and, consequently, the condensation efficiency. In Table 13, Number average molecular weight (Mn), and weighted average molecular weight (Mw) have been reported providing evidence of the depolymerization grade of the Kraft lignin and the molar mass range distribution for all the different fractions of oil collected.

Table 13:GPC values for all the oil fractions

| Molecular Weight Distribution | Mw | Mn | Dispersity value |
|---|---|---|---|
| Kraft Lignin | 975.80 | 568.80 | 0.58 |
| LD_CB1 | 169.20 | 159.50 | 0.94 |
| CB1 | 231.60 | 182.10 | 0.79 |
| CB2 | 234.20 | 185.90 | 0.79 |
| Lines | 236.50 | 191.70 | 0.81 |
| KLG10 | 228.40 | 186.80 | 0.82 |

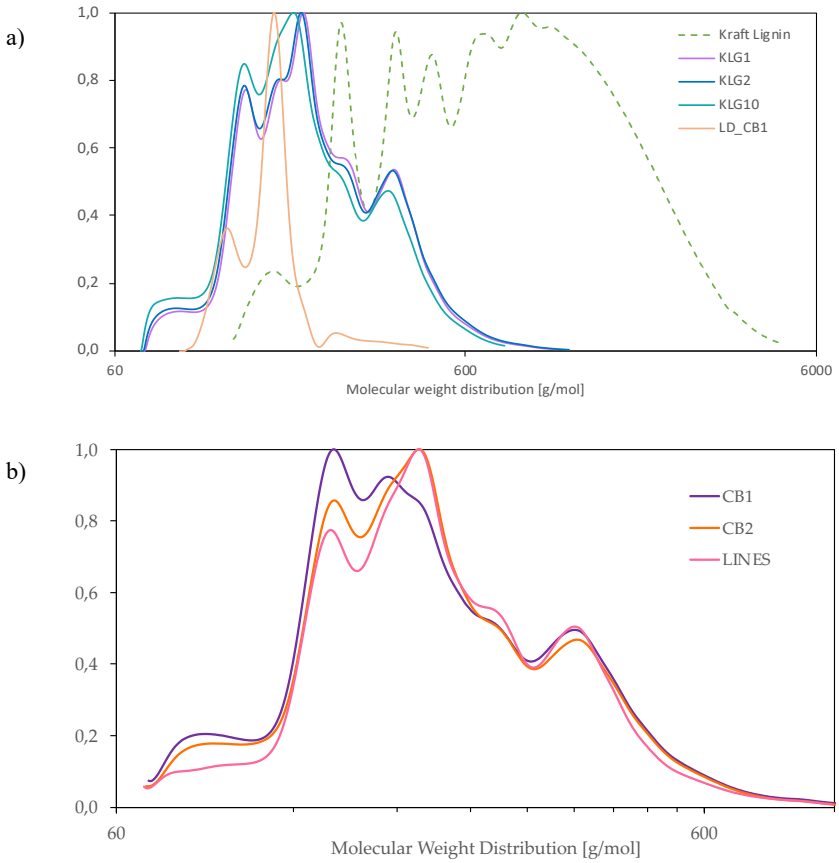


Figure 46: a) Kraft lignin THF-soluble and lignin-derived oils GPC profile. b) comparison between the three different oil fractions derived from ice trap (CB1), $N_2$ trap (CB2), and the lines.

### *7.2.3. Oil characterization-GC-MS*

Further analyses have been performed using GC-MS. The collection of the oil must pass through the use of solvents like acetone to ensure the complete recovery of the oil produced. However, during the solvent removal, some volatiles compound can evaporate with the acetone due to low pressures and temperature. Therefore, characterizing the single fractions separately become crucial to have a complete picture of the oil composition. Despite HD_CB1 and CB2 showed many similarities, some differences can be noted especially in the first 7 minutes of the analysis, where it is possible to identify many sulfur-containing compounds in the CB2 oil profile which are not able to condense in the HD_CB1 oil fraction. Dimethyl disulfide, thiols, thiophene and methyl thiophene have been detected even if in small quantities. Other compounds such as benzene, ethylbenzene, dimethyl benzene, and toluene are also present, however, their quantification is difficult due to the low peak area as shown in Figure 47.

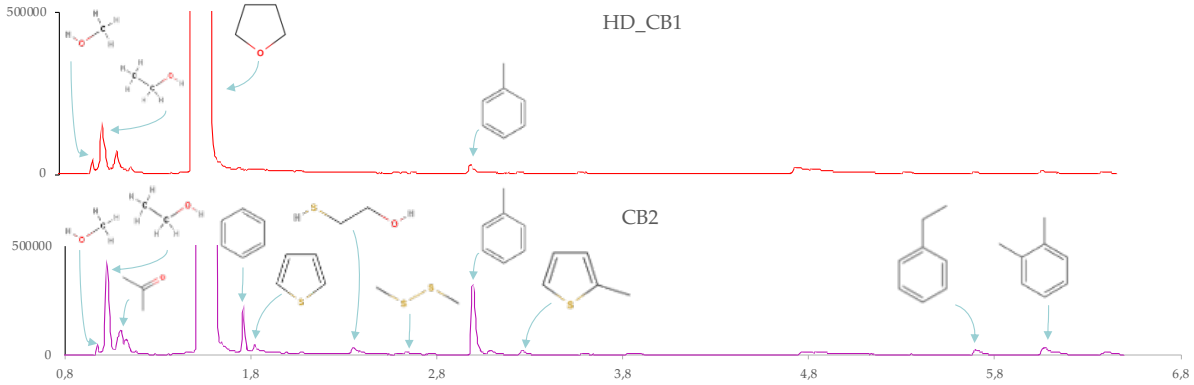


Figure 47: GC-MS chromatograms of the two different oil fraction HD_CB1 and CB2

A more quantitative result is obtained from the GC-MS analysis performed on the total bio-oil (KLG). After the collection, the solvent has been removed, and the oil sample have been diluted 10 times in THF. In Figure 48a, the entire chromatogram is reported together with a list of the most relevant compounds. The quantification has been performed considering the ratio between the peak area of a compound and the total area obtained as the sum of all the areas considered. In this case, as already observed in other papers [145,165], guaiacols, catechols, and their alkylated forms represent the most abundant compounds. To have a better representation of the products distribution, the compounds have been classified in different categories and reported in Figure 48b.

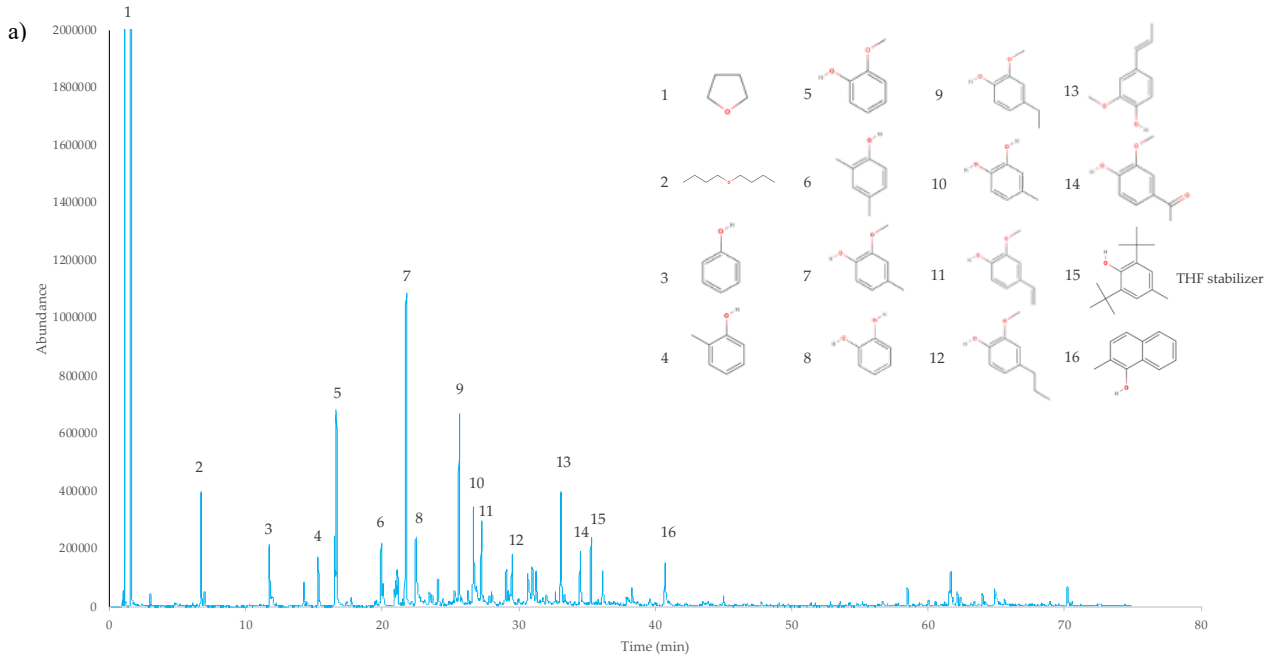

b)

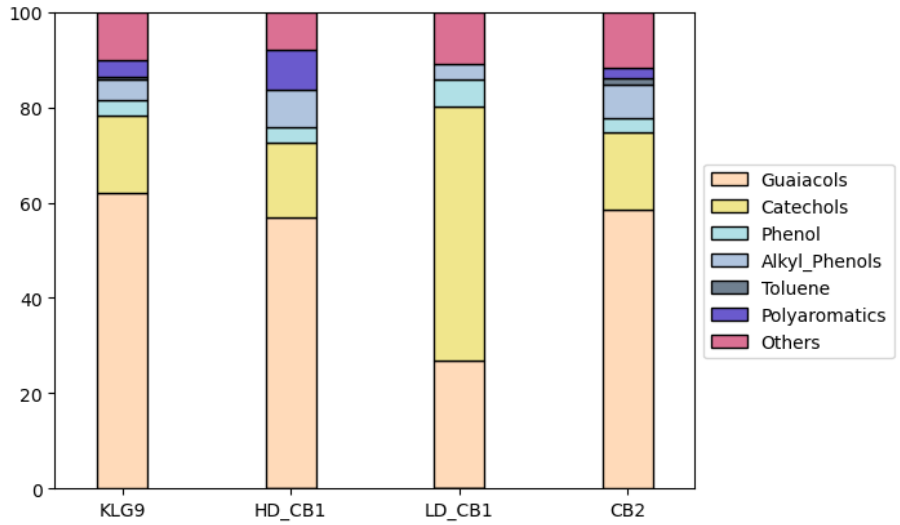


Figure 48: a) GC-MS chromatogram of bio-oil (KLG9) with the presentation of the most relevant compounds. b) Comparison between the composition of the different fraction LD_CB1, HD_CB1, CB2, and KLG9

The overall composition of the oil also confirms the molecular weight distribution presented in the previous part in Figure 46a, in which a first shoulder between 60 and 100 g/mol can be related to both phenol and simple aromatics, but also to the presence of some acetone remained in the oil after its removal. The sharp peak in the range between 120-160 g/mol can be related to guaiacols, and alkylated guaiacols, together with alkylated catechols, while the following peak is assigned to higher-molecular weight compounds such as polyaromatics that are formed during pyrolysis.

Other analyses have been performed to confirm the GC-MS results, and in Table 14 the results from GCxGC-MS have been reported in Figure 50, and, also in this case, the methoxyphenols category represent the most relevant one together with phenols and polyaromatics. Also, $C^{13}$-NMR analysis in Figure 49 showed a clear peak at 57 ppm for the methoxy groups linked to the aromatic ring, different peaks in the aliphatic area due to the alkylated guaiacols and catechols, and a wide pool of phenols and aromatic compounds in the aromatic region.

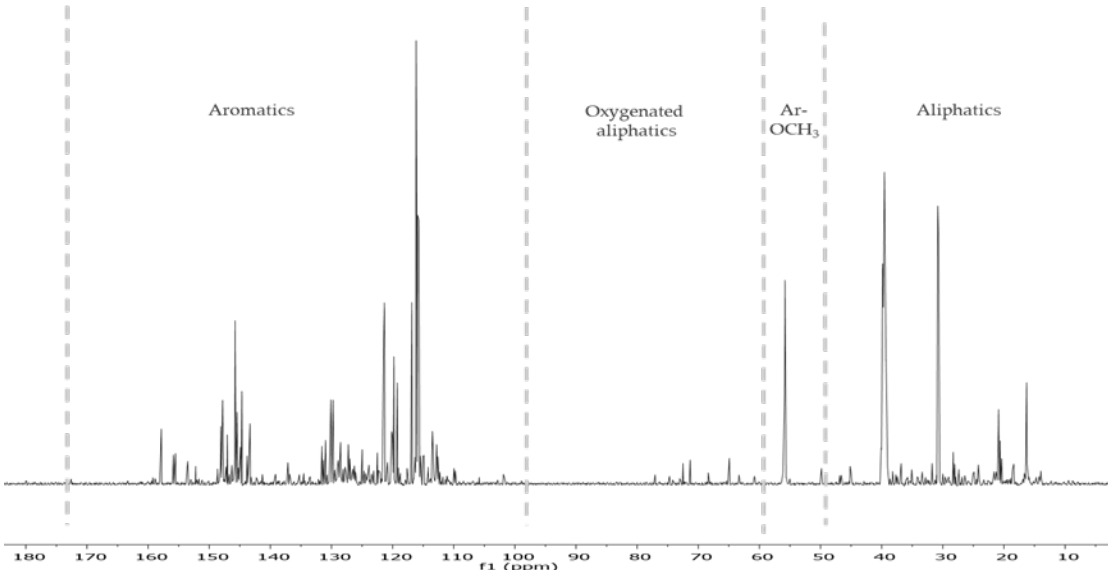


Figure 49: $C^{13}$-NMR spectrum of the pyrolysis oil

Table 14: GCxGC-MS results

| Chemical Group | KLG2 | KLG6 |
|---|---|---|
| Aromatics | 0.38 | 0.69 |
| Dihydroxybenzenes | 0.06 | 1.60 |
| Hydrocarbons | 0.00 | 0.01 |
| Ketones | 0.35 | 0.88 |
| Methoxyphenols | 8.58 | 13.14 |
| Naphthalenes | 0.64 | 2.43 |
| Phenols | 3.88 | 9.38 |
| VFA | 0.04 | 0.09 |
| Total [wt%] | 13.93 | 28.22 |

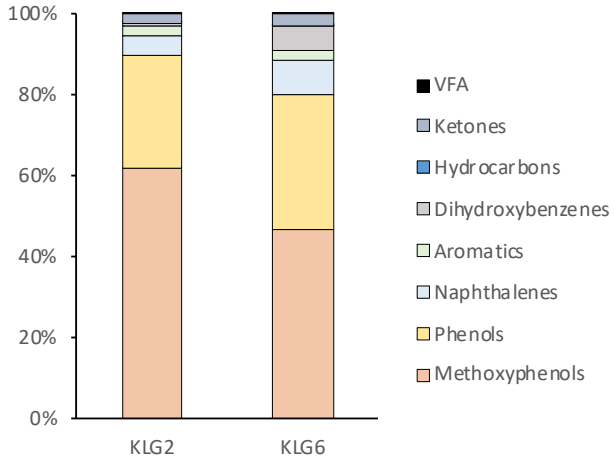


Figure 50:GCxGC results for the oils obtained from pyrolysis.

The main objective of this project was to upgrade the bio-oil produced by pyrolysis addressing its wide chemical composition to more valuable intermediates such as phenols.

For this reason, a deep characterization was necessary to know the starting point of the upgrading step. The presence of sulfur compounds, highlighted by GC-MS analysis, was confirmed also by the CHNS elemental analysis performed on the different oil fractions. Table 15 shows the different sulfur content of the different fractions and of the bio-oil, and this quantification is important for the following upgrade since it can influence the activity of the catalyst. From Table 15 it is possible to evaluate the total amount of sulfur in the biomass, knowing the dried biomass loaded in the reactor. Moreover, according to pyrolysis yield shown above around 20-30 wt.% of biomass is converted to oil whose sulfur content is reported in Table 15A. In a previous study from our group is reported that S content in biochar from Kraft Lignin pyrolysis is around 1.3-1.5% (Borella et al., manuscript in preparation), while the yield of biochar, according to Figure 45, is around 30%.

From mass balances it is then possible to evaluate how sulfur is distributed in pyrolysis products. During pyrolysis, half of the total sulfur of the biomass was transferred to liquid and char, while the other half has been released in the gas phase. In the final oil (KLG6) the amount of sulfur is 0.67 wt.%, as shown in Table 15B. In KLG1 reported in Table 15A the value of sulfur and hydrogen is slightly higher than in KLG6 due to the LD_CB1 phase, poor in sulfur and richer in hydrogen.

Table 15: Table A reports the elemental analysis of different oil fraction in terms of wt.% of elemental C, H, and S. Table B reports the expected sulfur weight calculations based on CHNS values.

| A | C [%] | H [%] | S [%] |
|---|---|---|---|
| Kraft Lignin | 61.22 | 5.89 | 1.23 |
| KLG1 | 68.34 | 7.09 | 0.69 |
| LD_CB1 | 4.04 | 10.68 | 0.07 |
| KLG6 | 69.61 | 6.85 | 0.67 |

| B | Weight [g] | S [%] | Sulfur [g] |
|---|---|---|---|
| Kraft Lignin | 29.87 | 1.23 | 0.37 |
| KLG6 - Oil | 5.59 | 0.67 | 0.04 |
| KLG6 - Gas | 15.01 | - | 0.21 |
| KLG6 - Biochar | 9.27 | 1.3 | 0.12 |

### *7.2.4. Selective demethoxylation of model bio-oil in continuous*

To understand how the percentage of sulfur in the oil could affect the catalytic activity in the selective demethoxylation of the pyrolytic oil, a catalytic study on a model bio-oil in presence of an external sulfur source have been carried out using as a catalyst $Cu/TiO_2$-P25

in a continuous flow setup. We studied the behavior of *4-methyl guaiacol* as a model compound, since, according to GC-MS analysis abovementioned, guaiacols and alkyl guaiacol represent almost the 60% of the bio-oil composition.

To study the influence of sulfur on the selected Cu-based catalyst, thiophene was added to the model compound because it was one of the less volatile detectable sulfur compounds present in the oil. The mixture of 4 methyl guaiacol and thiophene will be referred to as ‘‘model bio-oil’’ and different experiments have been carried out tuning the mass percentage of S in the mixture, knowing the mass of sulfur in thiophene. Calculation have been made to have a model bio-oil with no sulfur and with 0.1, 1, 2 and 10 wt.% of sulfur content. GC-MS analysis has been performed on sample collected every hour. The products distribution has been monitored considering a relative area percentage of different categories of compounds. The area percentage of 4-methyl guaiacol was monitored to understand the activity in the selective demethoxylation of the $Cu/TiO_2$-P25 catalyst.

The main products of the reaction consisted in alkylated phenols, mainly methyl, dimethyl and trimethyl phenols with a limited production of phenols. Other compounds were also produced during the process; however, low quality identification did not allow a proper classification. Previous papers proved the stability of toluene at 300°C[65]. To verify toluene does not react at 360 °C its GC-MS area was monitored for the whole reaction time, confirming its stability also at higher temperature. However, further investigation must be considered regarding the changes of the catalytic activity and the reactivity of toluene related to sulfur content. The presence of alkylated phenols demonstrates the demethoxylation activity of the catalysts as showed in Figure 51, reporting the results of the experiments carried out with no sulfur in the model bio-oil. In this case, the test has been performed for a TOS of 8 h, and the reaction reaches an equilibrium point after 2 h where alkylated phenols compounds represent around the 90% of the product mixture.

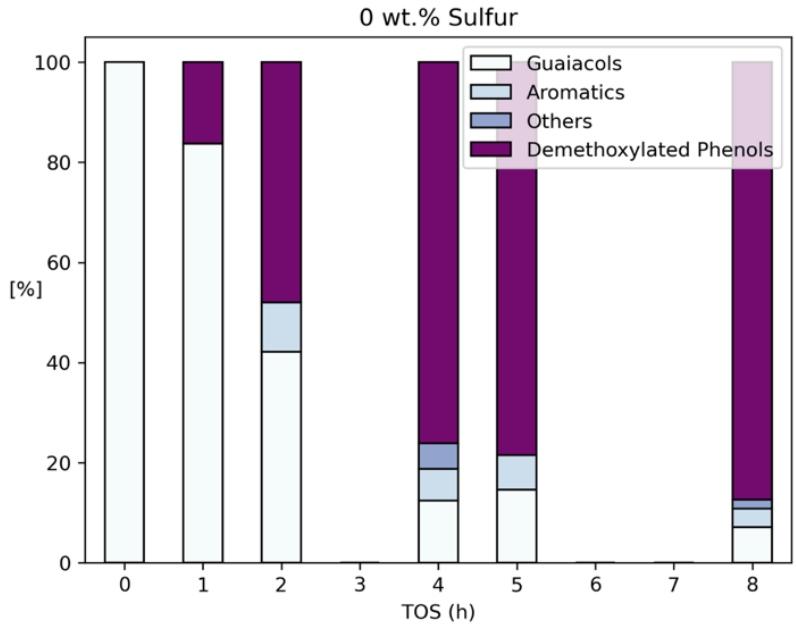


Figure 51: Representation of area percentage of main categories of compounds for no-sulfur model bio-oil tests over time (TOS). Light blue bars represent the 4 methyl guaiacol while purple bars demethoxylated compounds. The blue bar includes others compound such as aromatics, such as methoxy benzenes and other alkylated forms of benzene.

A similar behavior can be noted on the test performed with 0,1 and 1% of S, reported in Figure 52a and b, run for a TOS of 8 h. Also in this case, we can observe a consumption of the model bio-oil which is stabilized after 3 and 4 h, respectively, but alkylated products reach lower conversions, confirming the influence of sulfur in the conversion mechanism. The effect of sulfur in the 4-methyl guaiacol conversion , however, seems to be limited lowering the overall conversion of 10% while the selective demethoxylation occurs anyway despite the presence of higher sulfur content. In the first hours of reaction, mono methyl-phenols and dimethyl-phenols are produced with selectivity of 64% and 35%, respectively. Then, trimethyl and tetramethyl phenols are also produced at higher reaction times. After 6 h, once the reaction is stable, the selectivity towards mono methyl phenols is around 40%, while to dimethyl is around 30%. The selectivity towards trimethyl and tetramethyl is stable around 20 and 10%, respectively.

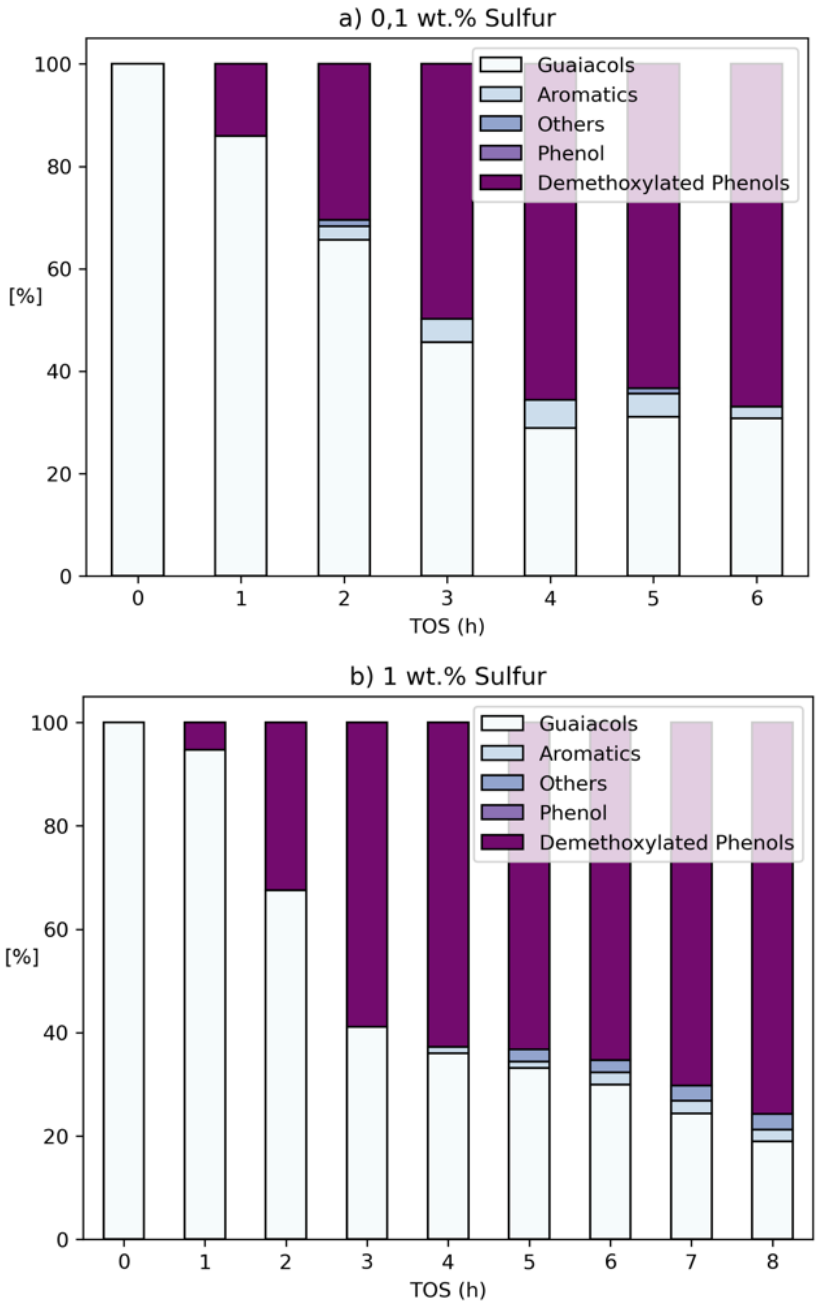


Figure 52: representation of area percentage of main categories of compounds for low-sulfur bio-oil tests over time: 0,1 wt. S % (a), and 1 wt. S % (b), respectively. Light blue bars represent the 4 methyl guaiacol while purple bars demethoxylated compounds. The blue bar includes others compound such as aromatics, such as methoxy benzenes and other alkylated forms of benzene.

Additional experiments have been performed to see the effect of higher sulfur content in the catalytic activity. The increased percentages also allow a detection of thiophene that was not detected before because of the high dilution of the sample in toluene. In Figure 53a, together with the reaction products is reported also the thiophene content amount during the entire process. In this case, increasing up to 2% the content of sulfur shows as the most remarkable effect the shift of process stabilization time even if the production of desired demethoxylated

guaiacols appear to be unchanged. The same behavior can be noticed in Figure 53b reporting data from the demethoxylation of model bio-oil with 10% of S. While in the first two experiments with lower sulfur content the stabilization was reached after 4h, in both tests with higher S content this stabilization is obtained after 6h, suggesting that sulfur may have a role in the conversion rate of guaiacols. Some assumptions can be made speculating about the role of sulfur in the process but further analysis on exhaust catalysts can clarify the effect of sulfur species on the catalytic surface.

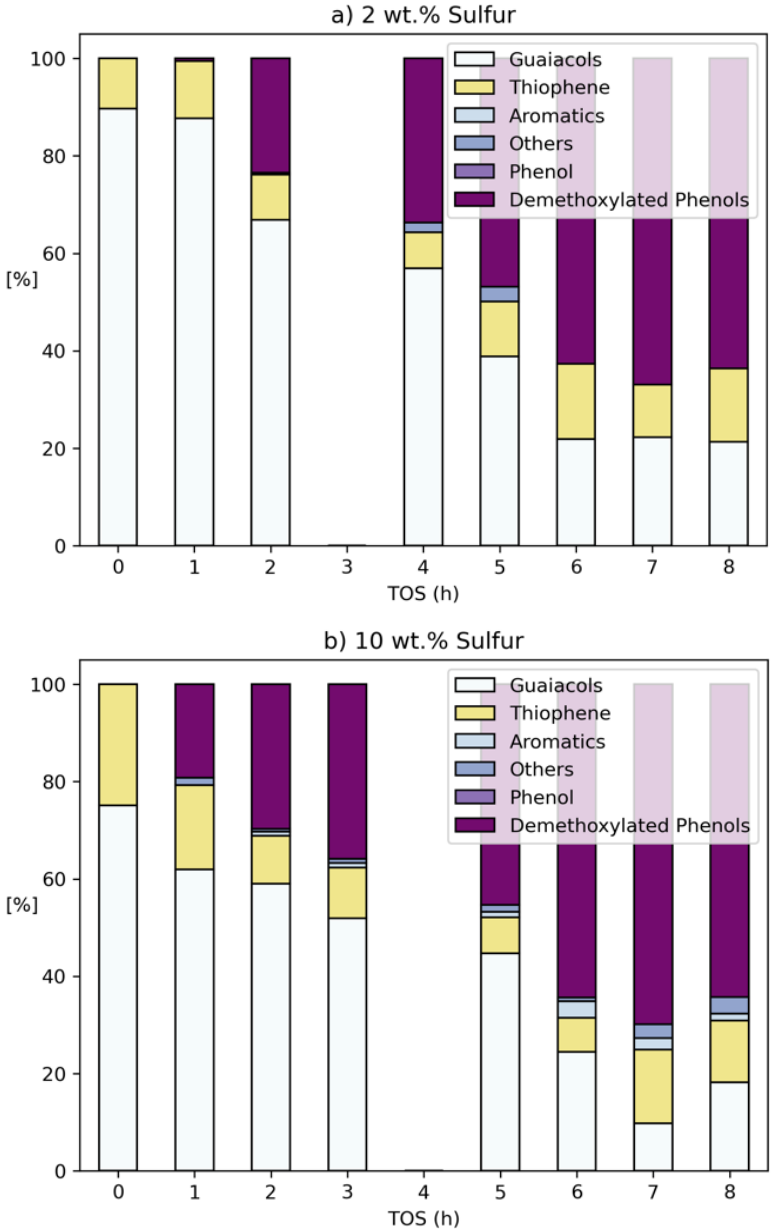


Figure 53: representation of area percentage of main categories of compounds for high-sulfur model bio-oil tests over time: 2 wt. S % (a), and 10 wt. S % (b), respectively. The color scheme is the same as Figure 52. The yellow bars represent the thiophene area percentage.

From CHNS analysis we know that the content of sulfur of bio-oil is 0.69 wt.%, which is in the same range of the sulfur content of the experiments in Figure 52 (a,b). For this reason, we can expect a similar behavior of the pyrolytic oil in terms of conversion to demethoxylated products. In Figure 54, the results for the selective demethoxylation of pyrolytic oil are presented where in the guaiacol category (light blue) are considered all the methoxy-phenols in the bio-oil. In this case, since the bio-oil is composed of a wide pool of alkylated guaiacols, the main products of their demethoxylation consist of alkylated phenols. Moreover, the catalyst promotes further alkylation. The difference between the composition of the pyrolytic oil characterized in the previous section and the bio-oil at 0h presented here is mainly due to the high dilution with toluene that was not considered in the plot but represents the 95 wt.% of the total solution. For this reason, many compounds detected from GC-MS of the bio-oil after pyrolysis were not detected in the 0h sample.

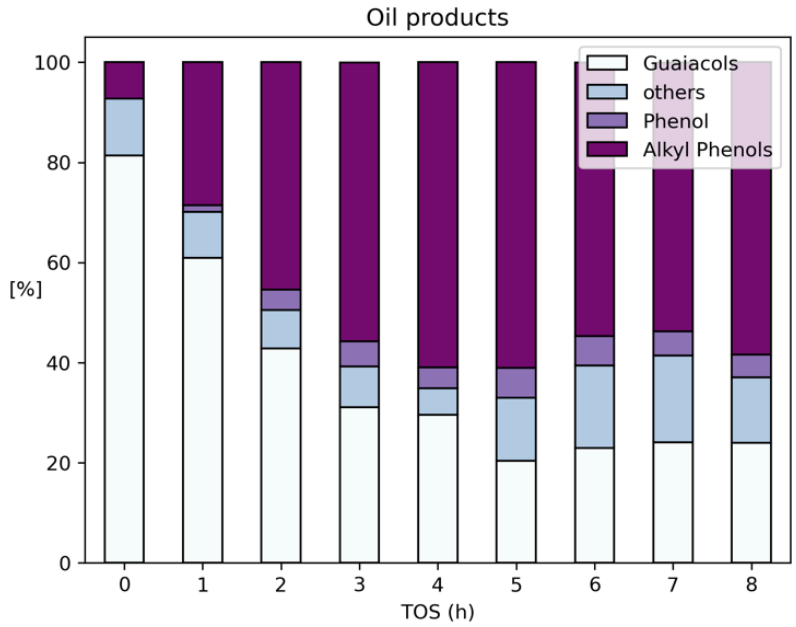


Figure 54: Products distribution and evolution of the pyrolysis oil over time in presence of Cu/$TiO_2$-P25 catalyst.

The conversion of the 4-methyl guaiacol enriched with thiophene has been reported in Figure 55, where values for conversion have been calculated considering the area percentages instead of molar fractions, according to the following equation:

$$X_g = \frac{\mathrm{A}_{g,i} - \mathrm{A}_{g,0}}{A_{g,0}} * 100$$

Here, $A_{g,i}$ is the area percentage of 4-methyl guaiacol at reaction time *i* and $A_{g,0}$ is the area percentage at the initial time. Data after 6 h of reaction appear to not be influenced by the increasing presence of sulfur; the catalyst ensure a conversion around 70% in all the experiments. However, it would be misleading to neglect the role of sulfur in the deactivation of the catalyst according to only the final value of conversion, since conversion rate is significantly influenced by sulfur content in the bio-oil. Conversion of 40% can be obtained after slightly more than 1 hour for the test with no sulfur, 2 h for the test with low sulfur content (i.e., 0.1, and 1%), around 4 h for the test with 2%, and around 5 h for the test with 10%. The catalytic test performed on the oil provided the best results and stability, probably due to the wider range of methoxylated compounds available to the demethoxylation and the low sulfur content. Alkylated groups such as ethyl-, propyl-, and propylen- methoxyphenols were present and this may influence the methoxy group removal. It is also evident that, in test with higher sulfur content, due to the different rate in the conversion of methoxy phenols, longer tests may be required to determine with more accuracy the stabilization time.

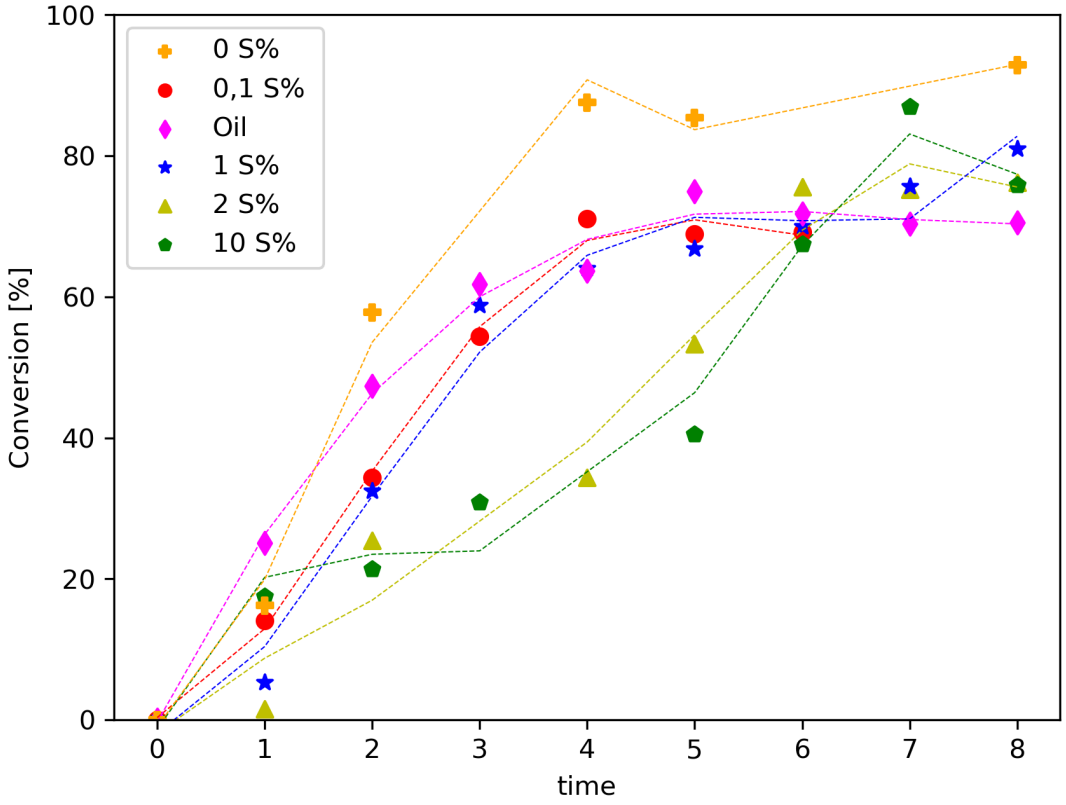


Figure 55: Conversion values for all the experiments performed with Cu/$TiO_2$-P25 compared to the conversion of alkyl guaiacol compounds in the oil (pink).

### *7.2.5. Selective demethoxylation- Batch*

Once the sulfur characterization was performed, the catalyst has been tested in batch conditions (Parr reactor) with high hydrogen pressure (100 bar). While in the continuous reactor dilution was needed to reduce the viscosity of the reagent solution, in batch experiment the raw pyrolysis oil was used directly. GPC, GC-MS, and NMR analyses have been performed on the hydrotreated bio-oil (HTO). In Figure 56, molar mass distribution has been reported and compared with the pyrolysis oil . The HTO showed a sharp peak in the region between 100 and 200 g/mol, as a main result from hydrotreatment. This range includes the molar masses of most of demethoxylated compounds produced such as alkylated phenols, and deoxygenated guaiacols such as methoxy and methyl-methoxy benzenes, together with other dealkylated aromatics. The other relevant peak is related to polyaromatics formed during the hydrogenation.

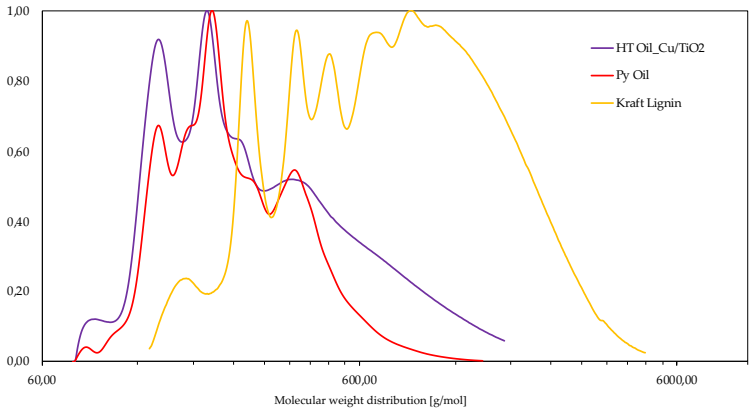


Figure 56: GPC profiles of initial kraft lignin (yellow) , pyrolysis oil (red) l, and hydrotreated oil (purple).

GC-MS shows remarkable changes in the HTO composition, as reported in Figure 57. More than 50% of guaiacols in the pyrolysis oil (KLG9) are converted. Phenols and alkyl-phenols can be obtained as a direct demethoxylation of guaiacols, or from dehydroxygenation of catechols. Side demethylation of guaiacols may occur, but demethoxylation is more relevant resulting in an increase from 7% to almost 40% of overall phenol content. Other aromatics like methoxy benzenes can be formed as well from direct dihydroxylation of guaiacols. Polyaromatic content increase up to 11% and a possible mechanism is given by Reizer et al. [186], explaining naphthalene and anthracene formation. These conversion values agree with the data obtained from the catalytic study on the model bio-oil. Continuous experiments showed that after 3h, the conversion of guaiacols is about 60%, with a high selectivity towards alkylated phenols. Working with oil directly from pyrolysis without dilution allows a better characterization of HTO composition. However, conversion of guaiacols is in the

same range of the continuous flow, around 56%. The selectivity of the catalyst towards alkylated phenols was around 80% in continuous configuration, which can be related to the increase of demethoxylated compound in the HTO.

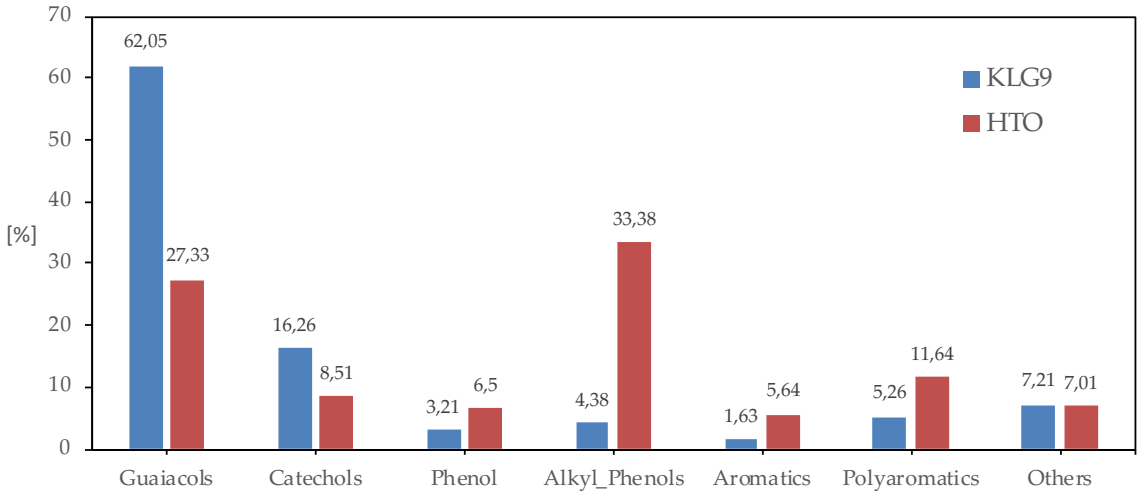


Figure 57: GC-MS analysis of the hydrotreated pyrolysis oil. The most relevant categories of compounds have been compared to the initial composition of pyrolysis oil to show the results of hydrotreatment.

## *7.3. Conclusions*

The pyrolysis of Kraft lignin performed with a double stage condensation step allowed to produce oil percentage in agreement with values reported in literature, around 30 wt.%. The lighter fraction of the oil has around 30% of water content and the remaining 70 wt.% is a lipophilic fraction, made of water-soluble aromatics. Catechols , guaiacols, and other valuable compounds such as vanillin can be recovered from this stream with solvent extractions to valorize side-products and reduce wastes according to zero-waste biorefinery concept.

Continuous reactor configurations exhibited a sulfur-related poisoning of the catalyst within the reaction time considered in the experiments, which influences the conversion rate of guaiacols. However, sulfur affects mainly the stabilization time, but it seems to have limited effect on the final conversion and the selectivity towards demethoxylated products. Stabilization is reached after 4h in low-sulfur experiments (i.e., 0.1%, 1%), and after 6h for high-sulfur ones (i.e., 2%, 10%). Of course, from and engineering point of view, time is a key factor in the economy of a process as well as in continuous flow setup aimed to look at the transitory phase of a reaction. Conversion values of 4-methyl guaiacol reach 70% in the experiments with model bio-oil, with high selectivity towards demethoxylated products.

Bio-oil hydrotreatment in continuous configuration results in similar conversions and similar stabilization times to the low-sulfur content experiments. Batch configuration was performed to hydrotreat the oil without dilution, to work with higher concentrations. Almost 50% of guaiacols and catechols can be converted, resulting in an increase of demethoxylated products (i.e., phenols and alkyl phenols) from 7.5 to 33%, and higher content of dehydroxylated aromatics and polyaromatics. Longer stabilization (12h and 24h) experiments and catalysts characterization must be done to optimize the process for the scale-up. Nevertheless, these results are encouraging for the design of HDO unit for the upgrade of kraft-lignin derived bio-oil using $Cu/TiO_2$ as catalyst.

# *Chapter 8. General conclusions*

A complete study on Kraft lignin as raw material for pyrolysis process has been performed in this thesis work. The approach of this work, started with a proper Kraft lignin characterization from a structural point of view, studying the chemical bonds that may incur in cleavage during thermal degradation. Pyrolysis, as one of the most powerful methods for biomass degradation, has been studied. Due the possible reaction pathways that can occur, several temperatures have been evaluated to understand how operative conditions can influence products distribution and composition. Data presented in chapter 1 confirmed that the reactions above 450°C are consistently different than those for lower temperature. The energy provided by temperature higher than 450°C can set a threshold above which a larger number of chemical linkages are broken, and higher number of condensable gases are release and then condensed in the bio-oil. The amount of bio-oil increase with the increasing temperature up to 550°C despite the chemical composition is not influenced by reaction temperature. For these reasons, 550°C was set as a reference temperature in order to enhance bio-oil production. Chemical composition of the pyrolysis products revealed that many phenolic and aromatic oxygenated compounds can be obtain from the thermal degradation of lignin, together with pyrolytic gas containing mainly methane, carbon dioxide and carbon monoxide. The high sulfur content is the major challenge in the valorization of Kraft lignin. In fact, sulfur distribution is widely spread in all the pyrolysis products limiting their applicability and lowering their quality. In general, the bio-oil is the most valuable product to be used as a platform for chemical intermediates production. The extraction of phenolic compounds was then considered as an alternative to increase the value of pyrolytic bio-oil. NaOH/water solution did not allow a complete extraction of phenolic compounds but, interestingly, the extracted solution was sulfur-free. Most of the sulfur was released in the gas phase reducing its value and possible utilization as a heat and energy source through its combustion.

However, the sustainability of a process is strongly related to its optimization and to the value of secondary products. Therefore, further studies have been performed to understand the evolution of sulfur related to pyrolysis temperature and biomass loading. In general, hydrogen sulfide represents the most abundant compound released. Its evolution mainly occurs in the early stage of the reaction, probably because its formation is easier compared to other compounds such as methanethiol whose release occurs after a partial cracking of lignin polymer. The removal of gaseous sulfur compounds can be obtained through a

purification step with activated carbon adsorbents which remove selectively sulfur compounds. The distribution of sulfur in the pyrolysis product changes due to its capture from the gas phase. In fact, sulfur is redistributed in the pyrolysis products resulting in a decrease of the sulfur in the oil higher than 50%. This achievement is relevant considering the unoptimized working conditions adopted. Moreover, most of the sulfur remain in the char.

The need to valorize biomass pyrolysis products to obtain valuable compounds can be addressed also to the production of biofuels, improving the quality of lignin oil with the help of a co-reagent in co-pyrolysis studies. High content of hydrogen may lead to a better stabilization of the radicals and less formation of repolymerized products. On the other hand, the pyrolysis of vegetable oil such palm oil is already known as biodiesel precursor source. Therefore, beside the valorization of lignin as such, it is also possible to use lignin wastes as a secondary feedstock, to improve biodiesel properties. The study of the interaction between palm oil and lignin allowed to produce oils with more than 75% of hydrocarbon composition in the diesel range. Pyrolysis of palm oil as such, produced a liquid containing almost 20% of carboxylic acid that limit the oil utilization as biofuels due to its low solidification temperature. The synergic interaction between palm oil and lignin was achieved with a pre-condensation step to increase the retention time of reagents in the reactor. Interestingly, co-pyrolysis at the tested condition allowed the formation of methylated esters of the carboxylic acids. Methylated esters are valuable product for biofuels applications, and their formation is related to the reaction between the methoxy groups formed from the cracking of lignin-guaiacols and long chain carboxylic acids formed by the cleavage of triglycerides of palm oil. Therefore, esters formation has a double positive effect due to the production of biodiesel-suitable compounds and the simultaneous consumption of carboxylic acid content. Thus, the presence of a waste such as lignin stabilizes the palm oil pyrolysis bio-oil producing esters (up to 10%) and allowing its utilization as biomass-derived fuel.

Despite the high content of aromatics, bio-oils need further upgrading for their utilization as a high value product. To do so, it is important to find catalytic pathways that allows a sulfur resistant activity in the upgrading process. Among the different catalysts studied in recent years, $Cu/TiO_2$ was selected as cheap alternative to noble metal and because of its activity in selective demethoxylation of guaiacols. The study performed in the last chapter investigates the effect of sulfur content on the selective demethoxylation of sulfur-containing model bio-oils. Conversion of 90% are achieve with no-sulfur model oils, while 80 % is obtained adding thiophene as external sulfur source. The understanding of the possible reaction pathways for

the guaiacol demethoxylation and mechanism of catalyst deactivation due to sulfur was a fundamental step to proper upgrade to the produced oil. Nevertheless, the high activity of the catalysts, in sulfur rich environment, is a remarkable result. The catalyst showed a high resistance to sulfur and ensured good performances in terms of oxygen removal. Moreover, the presence of sulfur content in continuous process configuration showed an effect on reaction stabilization time, which is the time needed to reach a constant conversion. Activation time of the catalyst is proportional to the content of sulfur, going from 2h for low-sulfur test to more than 5h for higher sulfur content. Further investigation on sulfur deposition in the catalyst active sites might provide evidence for a more complete overall picture. However, the resistance of the catalyst in sulfur-rich condition ensures its activity in harsh conditions. Direct hydrotreatment of the oil allowed a high conversion of guaiacols and alkylated guaiacols (more than 50% ) in the oil with high selectivity to demethoxylated products as alkylated phenols, and methoxy benzenes, showing a possible valuable path for the lignin-derived oil upgrading. Side production of by-products such as polyaromatics is also obtained, however, an excellent grade of overall deoxygenation was obtained.

In conclusion, this study demonstrated the versatility of a molecule like lignin and some of the many possibilities for its valorization as row material through pyrolysis process. This valorization process should comprehend all the pyrolysis products obtained by lignin depolymerization. For this reason, the purification of gas from sulfur compounds was then an important step to make the overall process more sustainable and environmentally friendly. However, the deoxygenation of pyrolysis-derived lignin monomers represented the main object of investigation of this thesis, to improve the quality of the oils and their possible applications. Interestingly, in the studies in which lignin was used as such, good quality of oils has been obtained via catalytic hydrogenation, reducing the oxygen content of guaiacols, and increasing the alkylated phenol compounds. However, the use of wastes as lignin as co-reactant with vegetable oils can be also used to reduce the oxygen content in biofuels and increase the value of pyrolysis products.

# Bibliography


[1] H. Wang, G. Di Pietro, X. Wu, R. Lahdelma, V. Verda, I. Haavisto, Renewable and Sustainable Energy Transitions for Countries with Different Climates and Renewable Energy Sources Potentials, (2018). https://doi.org/10.3390/en11123523.

[2] B.D. Solomon, K. Krishna, The coming sustainable energy transition: History, strategies, and outlook, Energy Policy 39 (2011) 7422–7431. https://doi.org/10.1016/J.ENPOL.2011.09.009.

[3] F. Cherubini, G. Jungmeier, T. Willke, Toward a common classifi cation approach for biorefi nery systems, (2009). https://doi.org/10.1002/bbb.172.

[4] M. Kumar, A. Kushwaha, L. Goswami, A.K. Singh, M. Sikandar, A review on advances and mechanism for the phycoremediation of cadmium contaminated wastewater, Clean Eng Technol 5 (2021) 100288. https://doi.org/10.1016/J.CLET.2021.100288.

[5] C. Mustansar Hussain, S. Singh, L. Goswami, Emerging trends to Approaching Zero Waste: Environmental and Social Perspectives, 2022.

[6] L. Goswami, R. Kayalvizhi, P.K. Dikshit, K.C. Sherpa, S. Roy, A. Kushwaha, B.S. Kim, R. Banerjee, S. Jacob, R.C. Rajak, A critical review on prospects of bio-refinery products from second and third generation biomasses, Chemical Engineering Journal 448 (2022) 137677. https://doi.org/10.1016/J.CEJ.2022.137677.

[7] A. Singh, A. Kushwaha, S. Sen, S. Goswami, S. Katiyar, A. Kumar, S.N. Borah, L. Goswami, C.M. Hussain, Recent advancement in microwave-assisted pyrolysis for biooil production, Waste-to-Energy Approaches Towards Zero Waste: Interdisciplinary Methods of Controlling Waste (2022) 197–219. https://doi.org/10.1016/B978-0-323-85387-3.00014-8.

[8] Y. Li, M. Horsman, N. Wu, C.Q. Lan, N. Dubois-Calero, ARTICLES: BIOCATALYSTS AND BIOREACTOR DESIGN Biofuels from Microalgae, (2008). https://doi.org/10.1021/bp.070371k.

[9] C. Conteratto, F.D. Artuzo, O.I. Benedetti Santos, E. Talamini, Biorefinery: A comprehensive concept for the sociotechnical transition toward bioeconomy, Renewable and Sustainable Energy Reviews 151 (2021). https://doi.org/10.1016/j.rser.2021.111527.

[10] A.T. Ubando, C.B. Felix, W.H. Chen, Biorefineries in circular bioeconomy: A comprehensive review, Bioresour Technol 299 (2020) 122585. https://doi.org/10.1016/J.BIORTECH.2019.122585.

[11] S. Wang, G. Dai, H. Yang, Z. Luo, Lignocellulosic biomass pyrolysis mechanism: A state-of-the-art review, Prog Energy Combust Sci 62 (2017) 33–86. https://doi.org/10.1016/J.PECS.2017.05.004.

[12] O.J. Rojas Editor, Cellulose Chemistry and Properties: Fibers, Nanocelluloses and Advanced Materials, n.d. http://www.springer.com/series/12.

[13] D. Klemm, B. Heublein, H.P. Fink, A. Bohn, Cellulose: Fascinating biopolymer and sustainable raw material, Angewandte Chemie - International Edition 44 (2005) 3358–3393. https://doi.org/10.1002/anie.200460587.

[14] F. Carolin C, T. Kamalesh, P.S. Kumar, R. V. Hemavathy, G. Rangasamy, A critical review on sustainable cellulose materials and its multifaceted applications, Ind Crops Prod 203 (2023) 117221. https://doi.org/10.1016/J.INDCROP.2023.117221.

[15] F. Carvalheiro, L.C. Duarte, F.M. Gírio, F.M. Gírio, Hemicellulose biorefineries: A review on biomass pretreatments, 2008. https://www.researchgate.net/publication/236878322.

[16] F.M. Gírio, C. Fonseca, F. Carvalheiro, L.C. Duarte, S. Marques, R. Bogel-Łukasik, Hemicelluloses for fuel ethanol: A review, Bioresour Technol 101 (2010) 4775–4800. https://doi.org/10.1016/J.BIORTECH.2010.01.088.

[17] L. Jiang, A. Zheng, Z. Zhao, F. He, H. Li, W. Liu, Obtaining fermentable sugars by dilute acid hydrolysis of hemicellulose and fast pyrolysis of cellulose, Bioresour Technol 182 (2015) 364–367. https://doi.org/10.1016/J.BIORTECH.2015.01.032.

[18] Y. Luo, Z. Li, X. Li, X. Liu, J. Fan, J.H. Clark, C. Hu, The production of furfural directly from hemicellulose in lignocellulosic biomass: A review, Catal Today 319 (2019) 14–24. https://doi.org/10.1016/J.CATTOD.2018.06.042.

[19] R. Patel, P. Dhar, A. Babaei-Ghazvini, M. Nikkhah Dafchahi, B. Acharya, Transforming lignin into renewable fuels, chemicals, and materials: A review, Bioresour Technol Rep 22 (2023) 101463. https://doi.org/10.1016/J.BITEB.2023.101463.

[20] Z. Wang, P.J. Deuss, The isolation of lignin with native-like structure, Biotechnol Adv 68 (2023) 108230. https://doi.org/10.1016/J.BIOTECHADV.2023.108230.

[21] H. Yang, R. Yan, H. Chen, D.H. Lee, C. Zheng, Characteristics of hemicellulose, cellulose and lignin pyrolysis, Fuel 86 (2007) 1781–1788. https://doi.org/10.1016/J.FUEL.2006.12.013.

[22] F. Cotana, G. Cavalaglio, A. Nicolini, M. Gelosia, V. Coccia, A. Petrozzi, L. Brinchi, Lignin as co-product of second generation bioethanol production from ligno-cellulosic biomass, in: Energy Procedia, Elsevier Ltd, 2014: pp. 52–60. https://doi.org/10.1016/j.egypro.2014.01.007.

[23] J. Ralph, C. Lapierre, W. Boerjan, Lignin structure and its engineering, Curr Opin Biotechnol 56 (2019) 240–249. https://doi.org/10.1016/J.COPBIO.2019.02.019.

[24] H. Wang, M. Tucker, Y. Ji, Recent Development in Chemical Depolymerization of Lignin: A Review, Journal of Applied Chemistry 2013 (2013) 1–9. https://doi.org/10.1155/2013/838645.

[25] A. Eraghi Kazzaz, P. Fatehi, Technical lignin and its potential modification routes: A mini-review, Ind Crops Prod 154 (2020) 112732. https://doi.org/10.1016/J.INDCROP.2020.112732.

[26] G. Wang, H. Chen, Enhanced lignin extraction process from steam exploded corn stalk, Sep Purif Technol 157 (2016) 93–101. https://doi.org/10.1016/j.seppur.2015.11.036.

[27] J.A. Hemmingson, Steam-explosion lignins: Fractionation, composition, structure and extractives, Journal of Wood Chemistry and Technology 7 (1987) 527–553. https://doi.org/10.1080/02773818708085284.

[28] J. Li, G. Gellerstedt, K. Toven, Steam explosion lignins; their extraction, structure and potential as feedstock for biodiesel and chemicals, Bioresour Technol 100 (2009) 2556–2561. https://doi.org/10.1016/J.BIORTECH.2008.12.004.
[29] J. Li, G. Henriksson, G. Gellerstedt, Lignin depolymerization/repolymerization and its critical role for delignification of aspen wood by steam explosion, Bioresour Technol 98 (2007) 3061–3068. https://doi.org/10.1016/J.BIORTECH.2006.10.018.
[30] A. Guerra, I. Filpponen, L.A. Lucia, D.S. Argyropoulos, Comparative evaluation of three lignin isolation protocols for various wood species, J Agric Food Chem 54 (2006) 9696–9705. https://doi.org/10.1021/jf062433c.
[31] Wu S., Argyropoulos D.S., An improved method for isolating lignin with high yield and purity, Journal of Pulp and Paper Science 29 (2003).
[32] X. Su, Y. Fu, Z. Shao, M. Qin, X. Li, F. Zhang, Light-colored lignin isolated from poplar by ultrasound-assisted ethanol extraction: Structural features and anti-ultraviolet and anti-oxidation activities, Ind Crops Prod 176 (2022) 114359. https://doi.org/10.1016/J.INDCROP.2021.114359.
[33] H. Yang, J.R.J. Strien, R.K. Chowdari, Z. Wang, H.J. Heeres, P.J. Deuss, Enhanced Catalytic Depolymerization of a Kraft Lignin by a Mechanochemical Approach, (2022). https://doi.org/10.1021/acs.energyfuels.2c01109.
[34] T. Ikeda, K. Holtman, J.F. Kadla, H.M. Chang, H. Jameel, Studies on the effect of ball milling on lignin structure using a modified DFRC method, J Agric Food Chem 50 (2002) 129–135. https://doi.org/10.1021/jf010870f.
[35] D.S. Zijlstra, C.W. Lahive, C.A. Analbers, M.B. Figueirê, Z. Wang, C.S. Lancefield, P.J. Deuss, Mild Organosolv Lignin Extraction with Alcohols: The Importance of Benzylic Alkoxylation, (2020). https://doi.org/10.1021/acssuschemeng.9b07222.
[36] M. Pals, M. Lauberts, D.S. Zijlstra, J. Ponomarenko, A. Arshanitsa, P.J. Deuss, Mild Organosolv Delignification of Residual Aspen Bark after Extractives Isolation as a Step in Biorefinery Processing Schemes, Molecules 27 (2022). https://doi.org/10.3390/molecules27103185.
[37] D. Morais De Carvalho, J.L. Colodette, Lignin vs. sugar hydrolysis, 2017.
[38] P. Laopaiboon, A. Thani, V. Leelavatcharamas, L. Laopaiboon, Acid hydrolysis of sugarcane bagasse for lactic acid production, Bioresour Technol 101 (2010) 1036–1043. https://doi.org/10.1016/J.BIORTECH.2009.08.091.
[39] D. Morais De Carvalho, J.L. Colodette, Lignin vs. sugar hydrolysis, 2017.
[40] D.R. Lobato-Peralta, E. Duque-Brito, H.I. Villafán-Vidales, A. Longoria, P.J. Sebastian, A.K. Cuentas-Gallegos, C.A. Arancibia-Bulnes, P.U. Okoye, A review on trends in lignin extraction and valorization of lignocellulosic biomass for energy applications, J Clean Prod 293 (2021) 126123. https://doi.org/10.1016/J.JCLEPRO.2021.126123.
[41] P. Bajpai, Pulping Fundamentals, in: Biermann's Handbook of Pulp and Paper, Elsevier, 2018: pp. 295–351. https://doi.org/10.1016/b978-0-12-814240-0.00012-4.
[42] F. José Borges Gomes, R.E. de Souza, E.O. Brito, R.C. Costa Lelis, A review on lignin sources and uses, Journal of Applied Biotechnology & Bioengineering (2020) 100–105. https://doi.org/10.15406/jabb.2020.07.00222.
[43] M. Kienberger, S. Maitz, T. Pichler, P. Demmelmayer, processes Systematic Review on Isolation Processes for Technical Lignin, (2021). https://doi.org/10.3390/pr9050804.
[44] P. Tomani, P. Axegård, N. Berglin, A. Lovell, D. Nordgren, INTEGRATION OF LIGNIN REMOVAL INTO A KRAFT PULP MILL AND USE OF LIGNIN AS A BIOFUEL, 2011.
[45] D. Dondi, A. Zeffiro, A. Speltini, C. Tomasi, D. Vadivel, A. Buttafava, The role of inorganic sulfur compounds in the pyrolysis of Kraft lignin, J Anal Appl Pyrolysis 107 (2014) 53–58. https://doi.org/10.1016/J.JAAP.2014.02.002.
[46] D. Daniel, L. Khachatryan, C. Astete, R. Asatryan, C. Marculescu, D. Boldor, Sulfur contaminations inhibit depolymerization of Kraft lignin, Bioresour Technol Rep 8 (2019) 100341. https://doi.org/10.1016/J.BITEB.2019.100341.
[47] C.G. Overberger, The subject matter of the entire series represents much work on the part of, n.d.
[48] Evdokimov Andrey N., Kurzin Alexander V., Fedorova Olesya V., Lukanin Pavel V., Kazakov Vladimir G, Trifonova Alena D., desulphurization of kraft lignin, Wood Sci Technol 52 (2018) 1165–1174.
[49] R. Roy, M.S. Rahman, T.A. Amit, B. Jadhav, Recent Advances in Lignin Depolymerization Techniques: A Comparative Overview of Traditional and Greener Approaches, Biomass 2 (2022) 130–154. https://doi.org/10.3390/biomass2030009.
[50] W.B. Hewson, H. Hibbert, Studies on Lignin and Related Compounds. LXV. Re-ethanolysis of Isolated Lignins [1], J Am Chem Soc 65 (1943) 1173–1176. https://doi.org/10.1021/ja01246a044.
[51] N. Mahmood, Z. Yuan, J. Schmidt, C.C. Xu, Hydrolytic depolymerization of hydrolysis lignin: Effects of catalysts and solvents, Bioresour Technol 190 (2015) 416–419. https://doi.org/10.1016/j.biortech.2015.04.074.
[52] Y. Ye, Y. Zhang, J. Fan, J. Chang, Novel Method for Production of Phenolics by Combining Lignin Extraction with Lignin Depolymerization in Aqueous Ethanol, Ind. Eng. Chem. Res 51 (2012) 103–110. https://doi.org/10.1021/ie202118d.
[53] M. Peng, M. Nakabayashi, K. Kim, K. Kamiya, E.W. Qian, Lignin depolymerization with alkaline ionic liquids and ethylene glycol in a continuous flow reactor, Fuel 335 (2023) 126960. https://doi.org/10.1016/J.FUEL.2022.126960.
[54] V.Z. Ong, K.J. Yong, T.Y. Wu, Production of aromatic monomers at one atmospheric pressure through depolymerization of lignin using combined alkaline solution and aqueous ChCl:urea, Ind Crops Prod 192 (2023) 115911. https://doi.org/10.1016/J.INDCROP.2022.115911.
[55] Z. Yuan, S. Cheng, M. Leitch, C.C. Xu, Hydrolytic degradation of alkaline lignin in hot-compressed water and ethanol, Bioresour Technol 101 (2010) 9308–9313. https://doi.org/10.1016/J.BIORTECH.2010.06.140.
[56] C. Chio, M. Sain, W. Qin, Lignin utilization: A review of lignin depolymerization from various aspects, Renewable and Sustainable Energy Reviews 107 (2019) 232–249. https://doi.org/10.1016/J.RSER.2019.03.008.

[57] S. Karagöz, T. Bhaskar, A. Muto, Y. Sakata, Hydrothermal upgrading of biomass: Effect of K2CO3 concentration and biomass/water ratio on products distribution, Bioresour Technol 97 (2006) 90–98. https://doi.org/10.1016/J.BIORTECH.2005.02.051.
[58] J. Chang, T. Danuthai, S. Dewiyanti, C. Wang, A. Borgna, Hydrodeoxygenation of guaiacol over carbon-supported metal catalysts, ChemCatChem 5 (2013) 3041–3049. https://doi.org/10.1002/cctc.201300096.
[59] Y. Li, Nishu, D. Yellezuome, C. Li, R. Liu, Deactivation mechanism and regeneration effect of bi-metallic Fe-Ni/ZSM-5 catalyst during biomass catalytic pyrolysis, Fuel 312 (2022). https://doi.org/10.1016/j.fuel.2021.122924.
[60] M. Abdus Salam, Y. Wayne Cheah, P. Hoang Ho, D. Bernin, A. Achour, E. Nejadmoghadam, O. Öhrman, P. Arora, L. Olsson, D. Creaser, Elucidating the role of NiMoS-USY during the hydrotreatment of Kraft lignin, Chemical Engineering Journal 442 (2022) 136216. https://doi.org/10.1016/J.CEJ.2022.136216.
[61] A. Achour, D. Bernin, D. Creaser, L. Olsson, Evaluation of kraft and hydrolysis lignin hydroconversion over unsupported NiMoS catalyst, Chemical Engineering Journal 453 (2023) 139829. https://doi.org/10.1016/J.CEJ.2022.139829.
[62] J. Osorio Velasco, I. Van Der Linden, P.J. Deuss, H.J. Heeres, Efficient depolymerization of lignins to alkylphenols using phosphided NiMo catalysts, Catal Sci Technol 11 (2021) 5158–5170. https://doi.org/10.1039/d1cy00588j.
[63] C.R. Kumar, N. Anand, A. Kloekhorst, C. Cannilla, G. Bonura, F. Frusteri, K. Barta, H.J. Heeres, Solvent free depolymerization of Kraft lignin to alkyl-phenolics using supported NiMo and CoMo catalysts, Green Chemistry 17 (2015) 4921–4930. https://doi.org/10.1039/c5gc01641j.
[64] B.-S. Li, B.-X. , feng, K.-Y. , wu, T.-H. , yang, Hydrodeoxygenation of lignin derived bio-oil into aromatic hydrocarbons over Ni-Cu-Ru/HZSM-5 catalyst, (2023). https://doi.org/10.1016/S1872-5813(22)60061-6.
[65] H. Yang, X. Zhu, H.W. Amini, B. Fachri, M. Ahmadi, G.H. ten Brink, P.J. Deuss, H.J. Heeres, Efficient Cu-based catalysts for the selective demethoxylation of guaiacols, Appl Catal A Gen 654 (2023) 119062. https://doi.org/10.1016/J.APCATA.2023.119062.
[66] V.N. Bui, D. Laurenti, P. Afanasiev, C. Geantet, Hydrodeoxygenation of guaiacol with CoMo catalysts. Part I: Promoting effect of cobalt on HDO selectivity and activity, Appl Catal B 101 (2011) 239–245. https://doi.org/10.1016/j.apcatb.2010.10.025.
[67] B. Güvenatam, O. Kurşun, E.H.J. Heeres, E.A. Pidko, E.J.M. Hensen, Hydrodeoxygenation of mono- and dimeric lignin model compounds on noble metal catalysts, Catal Today 233 (2014) 83–91. https://doi.org/10.1016/j.cattod.2013.12.011.
[68] Q. Lu, W. Li, X. Zhang, Z. Liu, Q. Cao, X. Xie, S. Yuan, Experimental study on catalytic pyrolysis of biomass over a Ni/Ca-promoted Fe catalyst, Fuel 263 (2020) 116690. https://doi.org/10.1016/J.FUEL.2019.116690.
[69] X. Dou, W. Li, C. Zhu, X. Jiang, Catalytic waste Kraft lignin hydrodeoxygenation to liquid fuels over a hollow Ni-Fe catalyst, Appl Catal B 287 (2021). https://doi.org/10.1016/j.apcatb.2021.119975.
[70] M.M. Campos Fraga, B. Lacerda de Oliveira Campos, H. Hendrawidjaja, C. Carriel Schmitt, K. Raffelt, N. Dahmen, Fast Pyrolysis Oil Upgrading via HDO with Fe-Promoted Nb2 O5-Supported Pd-Based Catalysts, Energies (Basel) 15 (2022). https://doi.org/10.3390/en15134762.
[71] T.D.H. Bugg, J.J. Williamson, G.M.M. Rashid, Bacterial enzymes for lignin depolymerisation: new biocatalysts for generation of renewable chemicals from biomass, Curr Opin Chem Biol 55 (2020) 26–33. https://doi.org/10.1016/J.CBPA.2019.11.007.
[72] T.D.H. Bugg, R. Rahmanpour, Enzymatic conversion of lignin into renewable chemicals, Curr Opin Chem Biol 29 (2015) 10–17. https://doi.org/10.1016/J.CBPA.2015.06.009.
[73] T.D.H. Bugg, M. Ahmad, E.M. Hardiman, R. Singh, The emerging role for bacteria in lignin degradation and bio-product formation, Curr Opin Biotechnol 22 (2011) 394–400. https://doi.org/10.1016/J.COPBIO.2010.10.009.
[74] D. Rodríguez-Escribano, F. De Salas, R. Pliego, G. Marques, T. Levée, A. Suonpää, A. Gutiérrez, Á.T. Martínez, P. Ihalainen, J. Rencoret, S. Camarero, Depolymerisation of Kraft Lignin by Tailor-Made Alkaliphilic Fungal Laccases, (2023). https://doi.org/10.3390/polym15224433.
[75] R.R. Singhania, A.K. Patel, T. Raj, C.W. Chen, V.K. Ponnusamy, N. Tahir, S.H. Kim, C. Di Dong, Lignin valorisation via enzymes: A sustainable approach, Fuel 311 (2022) 122608. https://doi.org/10.1016/J.FUEL.2021.122608.
[76] W. Wang, C. Zhang, X. Sun, S. Su, Q. Li, R.J. Linhardt, Efficient, environmentally-friendly and specific valorization of lignin: promising role of non-radical lignolytic enzymes, World J Microbiol Biotechnol 33 (2017) 125. https://doi.org/10.1007/s11274-017-2286-6.
[77] K. Dashora, M. Gattupalli, G. Datta Tripathi, Z. Javed, S. Singh, M. Tuohy, P.K. Sarangi, D. Diwan, H.B. Singh, V. Kumar Gupta, Fungal Assisted Valorisation of Polymeric Lignin: Mechanism, Enzymes and Perspectives, (2023). https://doi.org/10.3390/catal13010149.
[78] A. Kumar, R. Chandra, Ligninolytic enzymes and its mechanisms for degradation of lignocellulosic waste in environment, Heliyon 6 (2020) e03170. https://doi.org/10.1016/J.HELIYON.2020.E03170.
[79] M.P. Pandey, C.S. Kim, Lignin Depolymerization and Conversion: A Review of Thermochemical Methods, Chem Eng Technol 34 (2011) 29–41. https://doi.org/10.1002/ceat.201000270.
[80] Y. Yu, J. Wu, X. Ren, A. Lau, H. Rezaei, M. Takada, X. Bi, S. Sokhansanj, Steam explosion of lignocellulosic biomass for multiple advanced bioenergy processes: A review, Renewable and Sustainable Energy Reviews 154 (2022). https://doi.org/10.1016/j.rser.2021.111871.
[81] C. Chio, M. Sain, W. Qin, Lignin utilization: A review of lignin depolymerization from various aspects, Renewable and Sustainable Energy Reviews 107 (2019) 232–249. https://doi.org/10.1016/j.rser.2019.03.008.
[82] T. Maqsood, J. Dai, Y. Zhang, M. Guang, B. Li, Pyrolysis of plastic species: a review of resources and products, J Anal Appl Pyrolysis 159 (2021) 105295. https://doi.org/10.1016/j.jaap.2021.105295.

[83] D.S. Bajwa, G. Pourhashem, A.H. Ullah, S.G. Bajwa, A concise review of current lignin production, applications, products and their environment impact, Ind Crops Prod 139 (2019). https://doi.org/10.1016/j.indcrop.2019.111526.
[84] B. Joffres, D. Laurenti, N. Charon, A. Daudin, A. Quignard, C. Geantet, Conversion thermochimique de la lignine en carburants et produits chimiques: Une revue, Oil and Gas Science and Technology 68 (2013) 753–763. https://doi.org/10.2516/ogst/2013132.
[85] P. Azadi, O.R. Inderwildi, R. Farnood, D.A. King, Liquid fuels, hydrogen and chemicals from lignin: A critical review, Renewable and Sustainable Energy Reviews 21 (2013) 506–523. https://doi.org/10.1016/j.rser.2012.12.022.
[86] S. Kumar, P.N. Sheth, F. Akgun, Z. McCaffrey, C. B-s, P. Thy, M. Long, M. Oliveira, L. Wang, L. Torres, T. Aktas, B.-S. Chiou, W. Orts, B.M. Jenkins, Air and Steam Gasification of Almond Biomass, Frontiers in Energy Research | Www.Frontiersin.Org 1 (2019) 84. https://doi.org/10.3389/fenrg.2019.00084.
[87] X. Meng, W. de Jong, N. Fu, A.H.M. Verkooijen, Biomass gasification in a 100 kWth steam-oxygen blown circulating fluidized bed gasifier: Effects of operational conditions on product gas distribution and tar formation, Biomass Bioenergy 35 (2011) 2910–2924. https://doi.org/10.1016/J.BIOMBIOE.2011.03.028.
[88] S. Mishra, R.K. Upadhyay, Review on biomass gasification: Gasifiers, gasifying mediums, and operational parameters, Mater Sci Energy Technol 4 (2021) 329–340. https://doi.org/10.1016/J.MSET.2021.08.009.
[89] Bhavanam A., Sastry R.C., Biomass Gasification Processes in Downdraft Fixed Bed Reactors: A Review, International Journal of Chemical Engineering and Applications 2 (2011) 425–433.
[90] A. Molino, V. Larocca, S. Chianese, D. Musmarra, Biofuels Production by Biomass Gasification: A Review, (n.d.). https://doi.org/10.3390/en11040811.
[91] S.K. Sansaniwal, M.A. Rosen, S.K. Tyagi, Global challenges in the sustainable development of biomass gasification: An overview, Renewable and Sustainable Energy Reviews 80 (2017) 23–43. https://doi.org/10.1016/J.RSER.2017.05.215.
[92] A. V Bridgwater, Opportunities for Biomass Pyrolysis Liquids Production and Upgrading, n.d. https://pubs.acs.org/sharingguidelines.
[93] A. V. Bridgwater, G.V.C. Peacocke, Fast pyrolysis processes for biomass, Renewable and Sustainable Energy Reviews 4 (2000) 1–73. https://doi.org/10.1016/S1364-0321(99)00007-6.
[94] Z. Ma, J.A. Van Bokhoven, Deactivation and Regeneration of H-USY Zeolite during Lignin Catalytic Fast Pyrolysis, (n.d.). https://doi.org/10.1002/cctc.201200401.
[95] Q. Lu, W.Z. Li, X.F. Zhu, Overview of fuel properties of biomass fast pyrolysis oils, Energy Convers Manag 50 (2009) 1376–1383. https://doi.org/10.1016/J.ENCONMAN.2009.01.001.
[96] M. Bartoli, L. Rosi, P. Frediani, M. Frediani, Bio-oils from microwave assisted pyrolysis of kraft lignin operating at reduced residual pressure, Fuel 278 (2020) 118175. https://doi.org/10.1016/j.fuel.2020.118175.
[97] Z. Xiong, J. Guo, W. Chaiwat, W. Deng, X. Hu, H. Han, Y. Chen, K. Xu, S. Su, S. Hu, Y. Wang, J. Xiang, Assessing the chemical composition of heavy components in bio-oils from the pyrolysis of cellulose, hemicellulose and lignin at slow and fast heating rates, Fuel Processing Technology 199 (2020) 106299. https://doi.org/10.1016/j.fuproc.2019.106299.
[98] M. Zhang, Y. Hu, H. Wang, H. Li, X. Han, Y. Zeng, C.C. Xu, A review of bio-oil upgrading by catalytic hydrotreatment: Advances, challenges, and prospects, Molecular Catalysis 504 (2021). https://doi.org/10.1016/j.mcat.2021.111438.
[99] Catalytic Steam Reforming of Fast Pyrolysis Bio-Oil in Fixed Bed and Fluidized Bed Reactors, (2010). https://doi.org/10.1002/ceat.201000169.
[100] R. Trane, S. Dahl, M.S. Skjøth-Rasmussen, A.D. Jensen, Catalytic steam reforming of bio-oil, Int J Hydrogen Energy 37 (2012) 6447–6472. https://doi.org/10.1016/J.IJHYDENE.2012.01.023.
[101] P. Lahijani, M. Mohammadi, A.R. Mohamed, F. Ismail, K.T. Lee, G. Amini, Upgrading biomass-derived pyrolysis bio-oil to bio-jet fuel through catalytic cracking and hydrodeoxygenation: A review of recent progress, Energy Convers Manag 268 (2022) 115956. https://doi.org/10.1016/J.ENCONMAN.2022.115956.
[102] Q. Dang, Z. Luo, J. Zhang, J. Wang, W. Chen, Y. Yang, Experimental study on bio-oil upgrading over Pt/SO42-/ZrO2/SBA-15 catalyst in supercritical ethanol, Fuel 103 (2013) 683–692. https://doi.org/10.1016/J.FUEL.2012.06.082.
[103] M.W. Nolte, J. Zhang, B.H. Shanks, Ex situ hydrodeoxygenation in biomass pyrolysis using molybdenum oxide and low pressure hydrogen, Green Chemistry 18 (2015) 134–138. https://doi.org/10.1039/c5gc01614b.
[104] A. Eschenbacher, A. Saraeian, B.H. Shanks, P.A. Jensen, C. Li, J.Ø. Duus, A.B. Hansen, U.V. Mentzel, U.B. Henriksen, J. Ahrenfeldt, A.D. Jensen, Enhancing bio-oil quality and energy recovery by atmospheric hydrodeoxygenation of wheat straw pyrolysis vapors using Pt and Mo-based catalysts, Sustain Energy Fuels 4 (2020) 1991–2008. https://doi.org/10.1039/c9se01254k.
[105] H. Yang, W. Yin, X. Zhu, P.J. Deuss, H.J. Heeres, Selective Demethoxylation of Guaiacols to Phenols using Supported MoO3 Catalysts, ChemCatChem 14 (2022). https://doi.org/10.1002/cctc.202200297.
[106] A. Gutierrez, R.K. Kaila, M.L. Honkela, R. Slioor, A.O.I. Krause, Hydrodeoxygenation of guaiacol on noble metal catalysts, Catal Today 147 (2009) 239–246. https://doi.org/10.1016/j.cattod.2008.10.037.
[107] G.G. Zeelani, S.L. Pal, A Review on Desulfurization Techniques of Liquid Fuels, International Journal of Science and Research (IJSR) 5 (2016) 2413–2419. https://doi.org/10.21275/v5i5.nov164036.
[108] S. Cheah, D.L. Carpenter, K.A. Magrini-Bair, Review of mid- to high-temperature sulfur sorbents for desulfurization of biomass- and coal-derived syngas, Energy and Fuels 23 (2009) 5291–5307. https://doi.org/10.1021/ef900714q.
[109] E.H. Lee, R. su Park, H. Kim, S.H. Park, S.C. Jung, J.K. Jeon, S.C. Kim, Y.K. Park, Hydrodeoxygenation of guaiacol over Pt loaded zeolitic materials, Journal of Industrial and Engineering Chemistry 37 (2016) 18–21. https://doi.org/10.1016/j.jiec.2016.03.019.

[110] M. Ishikawa, M. Tamura, Y. Nakagawa, K. Tomishige, Demethoxylation of guaiacol and methoxybenzenes over carbon-supported Ru-Mn catalyst, Appl Catal B 182 (2016) 193–203. https://doi.org/10.1016/j.apcatb.2015.09.021.
[111] G. Bellussi, V. Calemma, P. Pollesel, G. Rispoli, The Hydrogenation of Vegetable Oil to Jet and Diesel Fuels in a Complex Refining Scenario, 2016.
[112] S. Wang, X. Zhang, C. Zhang, T. Li, J. Wu, L. Zhu, Selective demethoxylation of lignin-derived methoxyphenols to phenols over lignin-derived-biochar-supported Mo2C catalysts, Energy and Fuels 35 (2021) 17138–17148. https://doi.org/10.1021/acs.energyfuels.1c01894.
[113] X. Zhang, C. Zhang, T. Li, J. Wu, L. Zhu, S. Wang, Selective Demethoxylation of Lignin-Derived Methoxyphenols to Phenols over Lignin-Derived-Biochar-Supported Mo 2 C Catalysts, (2021). https://doi.org/10.1021/acs.energyfuels.1c01894.
[114] D.S. Bajwa, G. Pourhashem, A.H. Ullah, S.G. Bajwa, A concise review of current lignin production, applications, products and their environmental impact, Ind Crops Prod 139 (2019) 111526. https://doi.org/10.1016/J.INDCROP.2019.111526.
[115] S. Mishra, R.K. Upadhyay, Review on biomass gasification: Gasifiers, gasifying mediums, and operational parameters, Mater Sci Energy Technol 4 (2021) 329–340. https://doi.org/10.1016/J.MSET.2021.08.009.
[116] L. Schmalz, United States Patent (19) Dilling et al. (54) LIGNIN AMINE SALTAS BINDER FOR AQUEOUS PRINTING INK COMPOSITION, 1990.
[117] T. Aso, K. Koda, S. Kubo, T. Yamada, I. Nakajima, Y. Uraki, Preparation of novel lignin-based cement dispersants from isolated lignins, Journal of Wood Chemistry and Technology 33 (2013) 286–298. https://doi.org/10.1080/02773813.2013.794841.
[118] Z.-Z. Chang, B.-J. Yu, C.-Y. Wang, Lignin-derived hierarchical porous carbon for high-performance supercapacitors, (n.d.). https://doi.org/10.1007/s10008-016-3146-2.
[119] J.L. Espinoza-Acosta, P.I. Torres-Chávez, J.L. Olmedo-Martínez, A. Vega-Rios, S. Flores-Gallardo, E.A. Zaragoza-Contreras, Lignin in storage and renewable energy applications: A review, Journal of Energy Chemistry 27 (2018) 1422–1438. https://doi.org/10.1016/J.JECHEM.2018.02.015.
[120] D. Stewart, Lignin as a base material for materials applications: Chemistry, application and economics, Ind Crops Prod 27 (2008) 202–207. https://doi.org/10.1016/J.INDCROP.2007.07.008.
[121] C.A. Esteves Costa, C.A. Vega-Aguilar, A.E. Rodrigues, R. Frias, molecules Added-Value Chemicals from Lignin Oxidation, (2021). https://doi.org/10.3390/molecules26154602.
[122] E. Kocaturk, T. Salan, O. Ozcelik, M.H. Alma, Z. Candan, Recent Advances in Lignin-Based Biofuel Production, Energies (Basel) 16 (2023). https://doi.org/10.3390/en16083382.
[123] B.R. Albuquerque, S.A. Heleno, M. Beatriz, P.P. Oliveira, L. Barros, I.C.F.R. Ferreira, Cite this: Food Funct, 12 (2021) 14. https://doi.org/10.1039/d0fo02324h.
[124] G. Busca, Production of Gasolines and Monocyclic Aromatic Hydrocarbons: From Fossil Raw Materials to Green Processes, (2021). https://doi.org/10.3390/en14134061.
[125] G. Busca, Production of gasolines and monocyclic aromatic hydrocarbons: From fossil raw materials to green processes, Energies (Basel) 14 (2021). https://doi.org/10.3390/en14134061.
[126] M.S. Ganewatta, H.N. Lokupitiya, C. Tang, polymers Lignin Biopolymers in the Age of Controlled Polymerization, (n.d.). https://doi.org/10.3390/polym11071176.
[127] K. Akhtar, S.A. Khan, S.B. Khan, A.M. Asiri, Scanning electron microscopy: Principle and applications in nanomaterials characterization, in: Handbook of Materials Characterization, Springer International Publishing, 2018: pp. 113–145. https://doi.org/10.1007/978-3-319-92955-2_4.
[128] CHNS Elemental Analysers, (2008). www.rsc.org/amc.
[129] L. Krotz, G. Giazzi, Elemental Analysis: CHNS/O determination of marine samples, MIlan, n.d.
[130] B.H. Stuart, Infrared Spectroscopy: Fundamentals and Applications, 2004.
[131] Basic principles of gas chromatography, in: n.d.
[132] T.M. Lovestead, K.N. Urness, Gas Chromatography-Mass Spectrometry (GC−MS) *, n.d.
[133] Hites Ronald A., Gas Chromatography Mass Spectrometry, (n.d.).
[134] Gas Chromatography-Mass Spectroscopy, n.d.
[135] G. Kaur, S. Sharma, M.S. Student, Gas Chromatography-A Brief Review, 2018. http://ijics.com/.
[136] GC-Basics-and-Fundamentals, (n.d.).
[137] J. V Seeley, S.K. Seeley, Multidimensional Gas Chromatography: Fundamental Advances and New Applications, (2012). https://doi.org/10.1021/ac303195u.
[138] K. Sutherland, Gas chromatography/mass spectrometry techniques for the characterisation of organic materials in works of art, Physical Sciences Reviews 4 (2019). https://doi.org/10.1515/psr-2018-0010.
[139] R.G. Leonard, K. Quigley, Adhesive and sealants, 2005.
[140] J.C. Moore, Gel Permeation Chromatography. I. A New Method for Molecular Weight Distribution of High Polymers, n.d.
[141] Agilent Technologies, An Introduction to Gel Permeation Chromatography and Size Exclusion Chromatography, 2015.
[142] T.L. James, Chapter 1 Fundamentals of NMR, n.d.
[143] E. Cheung, D. Cash, Fundamentals of Nuclear Magnetic Resonance spectroscopy (NMR) and its applications, in: Characterization of Biological Membranes: Structure and Dynamics, De Gruyter, 2019: pp. 195–229. https://doi.org/10.1515/9783110544657-006.
[144] K. Zia, T. Siddiqui, S. Ali, I. Farooq, M.S. Zafar, Z. Khurshid, Nuclear Magnetic Resonance Spectroscopy for Medical and Dental Applications: A Comprehensive Review, Eur J Dent 13 (2019) 124–128. https://doi.org/10.1055/s-0039-1688654.

[145] M. Borella, A.A. Casazza, G. Garbarino, P. Riani, G. Busca, A Study of the Pyrolysis Products of Kraft Lignin, Energies (Basel) 15 (2022). https://doi.org/10.3390/en15030991.
[146] P. Joshi, R. Mishra, R.J. Narayan, Biosensing applications of carbon-based materials, Curr Opin Biomed Eng 18 (2021) 100274. https://doi.org/10.1016/j.cobme.2021.100274.
[147] A. Ház, M. Jablonský, I. Šurina, F. Kačík, T. Bubeníková, J. Ďurkovič, Chemical composition and thermal behavior of kraft lignins, Forests 10 (2019). https://doi.org/10.3390/f10060483.
[148] K.G. Latham, L. Matsakas, J. Figueira, U. Rova, P. Christakopoulos, S. Jansson, Examination of how variations in lignin properties from Kraft and organosolv extraction influence the physicochemical characteristics of hydrothermal carbon, J Anal Appl Pyrolysis 155 (2021). https://doi.org/10.1016/j.jaap.2021.105095.
[149] T. Rashid, C.F. Kait, T. Murugesan, A "fourier Transformed Infrared" Compound Study of Lignin Recovered from a Formic Acid Process, in: Procedia Eng, Elsevier Ltd, 2016: pp. 1312–1319. https://doi.org/10.1016/j.proeng.2016.06.547.
[150] C.G. Boeriu, D. Bravo, R.J.A. Gosselink, J.E.G. Van Dam, Characterisation of structure-dependent functional properties of lignin with infrared spectroscopy, in: Ind Crops Prod, 2004: pp. 205–218. https://doi.org/10.1016/j.indcrop.2004.04.022.
[151] C. Setter, K.L. Sanchez Costa, T.J. Pires de Oliveira, R. Farinassi Mendes, The effects of kraft lignin on the physicomechanical quality of briquettes produced with sugarcane bagasse and on the characteristics of the bio-oil obtained via slow pyrolysis, Fuel Processing Technology 210 (2020). https://doi.org/10.1016/j.fuproc.2020.106561.
[152] D.V. Cuong, B.M. Matsagar, M. Lee, M.S.A. Hossain, Y. Yamauchi, M. Vithanage, B. Sarkar, Y.S. Ok, K.C.W. Wu, C.H. Hou, A critical review on biochar-based engineered hierarchical porous carbon for capacitive charge storage, Renewable and Sustainable Energy Reviews 145 (2021) 111029. https://doi.org/10.1016/j.rser.2021.111029.
[153] L. Chen, J. Yuan, T. Li, X. Jiang, S. Ma, W. Cen, W. Jiang, A regenerable N-rich hierarchical porous carbon synthesized from waste biomass for H2S removal at room temperature, Science of the Total Environment 768 (2021) 144452. https://doi.org/10.1016/j.scitotenv.2020.144452.
[154] A.A. Casazza, B. Aliakbarian, A. Lagazzo, G. Garbarino, M.M. Carnasciali, P. Perego, G. Busca, Pyrolysis of grape marc before and after the recovery of polyphenol fraction, Fuel Processing Technology 153 (2016) 121–128. https://doi.org/10.1016/j.fuproc.2016.07.014.
[155] Q. Yan, R. Arango, J. Li, Z. Cai, Fabrication and characterization of carbon foams using 100% Kraft lignin, Mater Des 201 (2021). https://doi.org/10.1016/j.matdes.2021.109460.
[156] F.Â. de Â, R. Cadet, C. Robert, B. Offmann, Simultaneous Determination of Sugars by Multivariate Analysis Applied to Mid-Infrared Spectra of Biological Samples, 1997.
[157] T.K. Phung, A.A. Casazza, P. Perego, P. Capranica, G. Busca, Catalytic pyrolysis of vegetable oils to biofuels: Catalyst functionalities and the role of ketonization on the oxygenate paths, Fuel Processing Technology 140 (2015) 119–124. https://doi.org/10.1016/j.fuproc.2015.08.042.
[158] A.A. Casazza, E. Spennati, A. Converti, G. Busca, Study on the thermal decomposition of plastic residues, Chem Eng Trans 74 (2019) 1141–1146. https://doi.org/10.3303/CET1974191.
[159] C. Liu, R. Zhang, S. Wei, J. Wang, Y. Liu, M. Li, R. Liu, Selective removal of H2S from biogas using a regenerable hybrid TiO2/zeolite composite, Fuel 157 (2015) 183–190. https://doi.org/10.1016/j.fuel.2015.05.003.
[160] H. Ma, L. Zhou, S. Lv, J.W. Chew, Z. Wang, Review on Reaction Mechanisms of Sulfur Species during Coal Combustion, Journal of Energy Resources Technology, Transactions of the ASME 141 (2019) 1–7. https://doi.org/10.1115/1.4043554.
[161] T.A. Sokolova, S.A. Alekseeva, Adsorption of sulfate ions by soils (a review), Eurasian Soil Science 41 (2008) 140–148. https://doi.org/10.1134/s106422930802004x.
[162] E. Spennati, A.A. Casazza, A. Converti, G. Busca, Thermocatalytic pyrolysis of exhausted arthrospira platensis biomass after protein or lipid recovery, Energies (Basel) 13 (2020). https://doi.org/10.3390/en13205246.
[163] T.A. Amit, R. Roy, D.E. Raynie, Thermal and structural characterization of two commercially available technical lignins for potential depolymerization via hydrothermal liquefaction, Current Research in Green and Sustainable Chemistry 4 (2021). https://doi.org/10.1016/j.crgsc.2021.100106.
[164] R.M. Filho, E. Ranzi, L. Tognotti, M. Borella, A.A. Casazza, G. Garbarino, P. Riani, G. Busca, Conversion of Lignin to Chemical Intermediates: a Study of Pyrolysis of Kraft Lignin, in: Chemical Engineering Transactions, 2022. https://doi.org/10.3303/CET2292106.
[165] M. Borella, A.A. Casazza, G. Garbarino, P. Riani, G. Busca, Conversion of Lignin to Chemical Intermediates: a Study of Pyrolysis of Kraft Lignin, Chem Eng Trans 92 (2022) 631–636. https://doi.org/10.3303/CET2292106.
[166] P. Azadi, O.R. Inderwildi, R. Farnood, D.A. King, Liquid fuels, hydrogen and chemicals from lignin: A critical review, Renewable and Sustainable Energy Reviews 21 (2013) 506–523. https://doi.org/10.1016/j.rser.2012.12.022.
[167] T. Han, N. Sophonrat, P. Evangelopoulos, H. Persson, W. Yang, P. Jönsson, Evolution of sulfur during fast pyrolysis of sulfonated Kraft lignin, J Anal Appl Pyrolysis 133 (2018) 162–168. https://doi.org/10.1016/j.jaap.2018.04.006.
[168] R. Yan, D.T. Liang, L. Tsen, J.H. Tay, Kinetics and mechanisms of H2S adsorption by alkaline activated carbon, Environ Sci Technol 36 (2002) 4460–4466. https://doi.org/10.1021/es0205840.
[169] H. Kawamoto, Lignin pyrolysis reactions, Journal of Wood Science 63 (2017) 117–132. https://doi.org/10.1007/s10086-016-1606-z.
[170] P.J. de Wild, W.J.J. Huijgen, A. Kloekhorst, R.K. Chowdari, H.J. Heeres, Biobased alkylphenols from lignins via a two-step pyrolysis – Hydrodeoxygenation approach, Bioresour Technol 229 (2017) 160–168. https://doi.org/10.1016/j.biortech.2017.01.014.

[171] M. Auersvald, L. Kejla, A. Eschenbacher, H.D. Thi, K.M. Van Geem, P. Šimáček, Detailed characterization of sulfur compounds in fast pyrolysis bio-oils using GC × GC-SCD and GC–MS, J Anal Appl Pyrolysis 159 (2021). https://doi.org/10.1016/j.jaap.2021.105288.
[172] T.K. Phung, A.A. Casazza, P. Perego, P. Capranica, G. Busca, Catalytic pyrolysis of vegetable oils to biofuels: Catalyst functionalities and the role of ketonization on the oxygenate paths, Fuel Processing Technology 140 (2015) 119–124. https://doi.org/10.1016/J.FUPROC.2015.08.042.
[173] A. Rohman, Infrared spectroscopy for quantitative analysis and oil parameters of olive oil and virgin coconut oil: A review, Int J Food Prop 20 (2017) 1447–1456. https://doi.org/10.1080/10942912.2016.1213742.
[174] A. Filopoulou, S. Vlachou, S.C. Boyatzis, L. Astolfi, M.P. Sammartino, E. Dell'aglio, molecules Fatty Acids and Their Metal Salts: A Review of Their Infrared Spectra in Light of Their Presence in Cultural Heritage, (2021). https://doi.org/10.3390/molecules26196005.
[175] Y. Gao, F. Jiang, • Lei Zhang, Y. Cui, Enzymatic synthesis of polyguaiacol and its thermal antioxidant behavior in polypropylene, Polym. Bull 73 (2016) 1343–1359. https://doi.org/10.1007/s00289-015-1551-9.
[176] P. Sakulkit, A. Palamanit, R. Dejchanchaiwong, P. Reubroycharoen, Characteristics of pyrolysis products from pyrolysis and co-pyrolysis of rubber wood and oil palm trunk biomass for biofuel and value-added applications, J Environ Chem Eng 8 (2020) 104561. https://doi.org/10.1016/J.JECE.2020.104561.
[177] F. Abnisa, A. Arami-Niya, W.M.A.W. Daud, J.N. Sahu, Characterization of Bio-oil and Bio-char from Pyrolysis of Palm Oil Wastes, Bioenergy Res 6 (2013) 830–840. https://doi.org/10.1007/s12155-013-9313-8.
[178] K.P. Huber, G. Herzberg, Molecular Spectra and Molecular Structure, Springer US, 1979. https://doi.org/10.1007/978-1-4757-0961-2.
[179] Abdullah, M. Apriyanti, Sunardi, U.T. Santoso, A.B. Junaidi, D. Aditiya, U. Irawati, Pyrolysis of palm oil using zeolite catalyst and characterization of the boil-oil, Green Processing and Synthesis 8 (2019) 649–658. https://doi.org/10.1515/gps-2019-0035.
[180] R. Supriyanto, W. Simanjuntak, K.D. Pandiangan, R.T.M. Situmeang, M.Y. Ahmadhani, Chemical composition of liquid fuel produced by co-pyrolysis of sugarcane bagasse and sludge palm oil using zeolite-Y as catalyst, Oriental Journal of Chemistry 34 (2018) 1533–1540. https://doi.org/10.13005/ojc/340345.
[181] H.C. Allen, E.K. Plyler, L.R. Blaine, Infrared spectrum of carbonyl sulfide, J Chem Phys 26 (1957) 400–403. https://doi.org/10.1063/1.1743307.
[182] J. Asomaning, P. Mussone, D.C. Bressler, Thermal deoxygenation and pyrolysis of oleic acid, J Anal Appl Pyrolysis 105 (2014) 1–7. https://doi.org/10.1016/j.jaap.2013.09.005.
[183] J. Asomaning, P. Mussone, D.C. Bressler, Pyrolysis of polyunsaturated fatty acids, Fuel Processing Technology 120 (2014) 89–95. https://doi.org/10.1016/j.fuproc.2013.12.007.
[184] H. Yang, R. Yan, H. Chen, D.H. Lee, D.T. Liang, C. Zheng, Pyrolysis of palm oil wastes for enhanced production of hydrogen rich gases, Fuel Processing Technology 87 (2006) 935–942. https://doi.org/10.1016/J.FUPROC.2006.07.001.
[185] S. Bakshi, M.R. Rover, R.G. Smith, R.C. Brown, Conversion of Phenolic Oil from Biomass Pyrolysis into Phenyl Esters, (2022). https://doi.org/10.1021/acs.energyfuels.2c00769.
[186] E. Reizer, B. Viskolcz, B. Fiser, Formation and growth mechanisms of polycyclic aromatic hydrocarbons: A mini-review, Chemosphere 291 (2022). https://doi.org/10.1016/j.chemosphere.2021.132793.